PEARSALL, ELIZABETH A., Ph.D. Molecular Mechanisms of Mutant μ-Opioid Receptors Where Naloxone Acts as an Agonist (2013)
Directed by Dr. Patricia H. Reggio. 153 pp.

Pain management is often one of the most difficult aspects of treatment for patients suffering from acute or chronic pain. The mu-opioid receptor (MOR) agonist, morphine, and its derivatives are highly used in pain management strategies. However, these medications have many side effects including respiratory depression, gastrointestinal problems, as well as dependence and addiction liabilities. For these reasons, innovative new modalities for pain management continue to be needed. One new approach to the design of opioid therapies for chronic pain with reduced liabilities is a targeted-gene therapy strategy developed by the lab of Dr. Ping-Yee Law at the University of Minnesota. This strategy makes novel use of a MOR S4.54A mutant at which the classical opioid antagonist, naloxone, acts as a partial agonist. Targeted gene therapy studies using this mutant have shown that naloxone becomes an antinociceptive agent at the S4.54A mutant both *in vitro* and *in vivo*. Because expression of the mutant MOR is targeted to the spinal cord injection site region, systemic administration of naloxone results in antagonism of all other (native) MOR's. The reduced number of receptors activated in this paradigm results in no measurable dependence/addiction as seen with traditional mu agonists like morphine.

Despite the clear success of basing this strategy on the S4.54A MOR mutant, the origins of this unusual phenotype are not yet understood. It was therefore the overall goal of this dissertation to identify the molecular basis for the agonism of naloxone at this

novel S4.54A mutant. To this end, a model of the wild-type and S4.54A mu opioid receptor was developed and ligand docking studies were used to probe this model.

The opioid receptors, delta, kappa and mu, belong to the Class A subfamily of G-Protein Coupled Receptors (GPCRs). These are integral membrane proteins that possess seven transmembrane helices (TMHs) arranged to form a closed bundle with loops that extend both extracellularly and intracellularly. The N-terminus is extracellular and the C-terminus is intracellular. In recent years, X-ray crystallography studies have yielded structures of numerous GPCRs. In 2012, the nociception/orphanin FQ receptor and the mu, delta and kappa opioid receptor crystal structures were published. Prior to the release of the MOR crystal structure, we developed a homology model of WT MOR using the β2-AR crystal structure[2,3] as a template with substitutions for TMH 1, 2, 4 and 7 based on sequence divergences, as described in methods. This model was then used for studies of the MOR including analyzing the receptor for cholesterol and palmitoylaiton interactions as well as modeling a homodimer interface for the MOR based on experimental data.

In 2012, new models of WT MOR and the S4.54A/L mutants were developed using the MOR crystal structure. The conformational change in TMH4 that would be created upon the S4.54A mutation was examined using the simulated annealing/Monte Carlo method, Conformational Memories, and the result was incorporated into the model. The S4.54A mutant model was then used for naloxone docking studies using Glide. These studies revealed that in the crystal structure, Y3.34 forms a hydrogen bond with the sidechain of S4.54; however, in the S4.54A MT MOR, this interaction is broken as there

is no polar partner for Y3.34. The breaking of this interaction allows the extracellular end of TMH4 to kink away from TMH3 and towards TMH5, which leads to changes in the packing of the receptor binding pocket. In the wild type MOR, naloxone interacts with D3.32 and sits in close proximity to the binding pocket "toggle switch" residue, W6.48, restricting its movement. However, in the S4.54A MT MOR, naloxone sits higher in the binding pocket, away from W6.48 and interacts with D3.32 and E5.35. In this higher location, naloxone exerts no effect on W6.48, permitting W6.48 to assume an active state conformation. This shift in binding pocket location for naloxone may be the origin of naloxone's partial agonism in the S4.54A MOR mutant.

We also explored additional experimental data generated in Dr. Ping Law's lab for other mutations at the 4.54 locus. Mutating S4.54 to Phe or Gly results in the same phenotype as the S4.54A mutation. On the other hand, for Ile or Val mutants, naloxone behaves as in WT MOR. We propose that in the case of the S4.54 I / V, an increase in hydrophobic interactions between W4.50 and I/V4.54 allow TMH4 to maintain its wild type conformation. However, while the S4.54F is also able to increase hydrophobic interactions, its size prevents the helix from maintaining the wild type shape. In the S4.54L mutant, there is no increase in hydrophobic interactions and the orientation of the leucine gives rise to a straighter TMH4, as seen in the S4.54A MT MOR. The S4.54G mutant offers additional flexibility and a higher turn ratio, with 5 residues per turn in that region such that the extracellular end of TMH4 moves away from TMH3 and towards TMH5.

Additionally, Law and coworkers have published studies using a S4.54L/T7.44A/C7.47S triple mutant MOR that gives rise to naloxone acting as a full agonist.[4] While this gene therapy has been shown in cells and in spinal cord, the underlying mechanism is unknown. A triple mutant MOR model was developed and analyzed to determine the molecular mechanism for which naloxone acts as an agonist. The binding pocket for mu opioid ligands is formed by TMHs 3, 5 and 6 in the wild type receptor, as seen in the crystal structure with β-FNA[5] and in our glide dock of naloxone (see Chapter 3). As studied in the single mutant MOR, S4.54 is a lipid facing residue. Interestingly, both of the mutated residues on TMH7 (T7.44 and C7.47) in the triple mutant MOR also face lipid. We report here that the combination of the S4.54L mutation on TMH4 along with TMH7 face shift changes occur upon mutation of T7.44 and C7.47 produce overall packing changes that give rise to a different binding pocket than seen in the wild type or single mutant MORs. These changes result in naloxone's ability to fully activate the S4.54L/T7.44A/C7.47S MOR.

MOLECULAR MECHANISMS OF MUTANT μ-OPIOID RECEPTORS WHERE NALOXONE ACTS AS AN AGONIST

by

Elizabeth A. Pearsall

A Dissertation Submitted to
the Faculty of the Graduate School at
The University of North Carolina at Greensboro
in Partial Fulfillment
of the Requirements for the Degree
Doctor of Philosophy

Greensboro
2013

Approved by

_____
Committee Chair

APPROVAL PAGE

This dissertation written by Elizabeth A. Pearsall has been approved by the following committee of the Faculty of The Graduate School at The University of North Carolina at Greensboro.

Committee Chair _____

Committee Members _____

_____

_____

_____
Date of Acceptance by Committee

_____
Date of Final Oral Examination

ACKNOWLEDGEMENTS

This research was supported by NIH grant # DA023905.

TABLE OF CONTENTS

Page

CHAPTER

I. PALMITOYLATION AND MEMBRANE CHOLESTEROL STABILIZE μ-OPIOID RECEPTOR HOMODIMERIZATION AND G PROTEIN COUPLING 1

Introduction....1
Methods....3
Results....13
Discussion....36
Conclusions....39
References....41

II. COMPARISON OF THE MOR R HOMOLOGY MODEL AND THE MOR CRYSTAL STRUCTURE....46

Introduction....46
Methods....47
Results....51
Discussion....61
Conclusions....68
References....70

III. MOLECULAR DETERMINANTS FOR TARGETED GENE THERAPY μ-OPIOID RECEPTOR FOR MULTIPLE MUTANTS AT WHICH NALOXONE ACTS AS A PARTIAL AGONIST 75

Abstract....75
Introduction....76
Methods....79
Results....84
Discussion....97
Conclusions....106
References....107

IV. MOLECULAR STUDIES OF A S4.54l/T7.44A/C7.47S TRIPLE MUTANT MOR AT WHICH NALOXONE ACTS AS A FULL AGONIST 113

Introduction 113
Methods 114
Results 117
Discussion 128
Conclusions 135
References 137

V. PARAMETERIZATION DEVELOPMENT OF THE N-ALLYL TAIL OF NALOXONE 139

Introduction 139
Methods 140
Results & Discussion 146
Conclusions 152
References 153

APPENDIX A. BOND, ANGLE, AND TORSION PARAMETERS FOR NALOXONE 154

CHAPTER I

PALMITOYLATION AND MEMBRANE CHOLESTEROL STABILIZE μ-OPIOID RECEPTOR HOMODIMERIZATION AND G PROTEIN COUPLING

Hui Zheng[1,2,*], Elizabeth A. Pearsall.[3], Dow P. Hurst[3], Yuhan Zhang[1], Ji Chu[1], Yali Zhou[1], Patricia H. Reggio[3], Horace H. Loh[1] and Ping-Yee Law[1]

[1]Department of Pharmacology, University of Minnesota, Minneapolis, Minnesota 55455

[2]Stem Cell and Cancer Biology Group, Key Laboratory of Regenerative Biology, South China Institute for Stem Cell Biology and Regenerative Medicine, Guangzhou Institutes of Biomedicine and Health, Chinese Academy of Sciences, Guangzhou 510530, China

[3]Department of Chemistry and Biochemistry, Center for Drug Discovery, University of North Carolina, Greensboro, North Carolina 27402

Introduction

A cholesterol–palmitoyl interaction at C7.68(341) has been reported to occur in the crystallographic dimeric interface of transmembrane helix (TMH) 1 and Helix 8 in a β_2-adrenergic receptor (β_2-AR) crystal structure [3]. Because palmitoylation of the rhodopsin sub-family of G protein-coupled receptors (GPCR) has been universally reported, similar cholesterol–palmitoyl interactions may exist with other GPCRs. Palmitoylation is a covalent attachment of palmitic acid to cysteine residues of membrane proteins. Sequence alignment has identified cysteine residues in the carboxy termini as potential palmitoylation sites in about 78% of the 74 GPCRs examined [6]. However, these

cysteines are not the only palmitoylation sites. For example, although rat μ-opioid receptor (OPRM1) has two cysteines [C7.63(346) and C7.68(351)] in its C terminus, mutating these cysteines did not decrease the palmitoylation of OPRM1 [7], suggesting that C3.55(170) (the only other intracellular cysteine of rat OPRM1) may be the palmitoylation site. Similarly, V_{1A} vasopressin receptor also has palmitoylation sites outside its C terminus domain [8]. Normally, palmitoylation facilitates the membrane targeting and signaling of GPCRs [9]. For instance, palmitoylation-dependent receptor–G protein interaction is observed with both β_2-adrenergic receptor and M2 muscarinic acetylcholine receptor[10].

Although there is no definitive answer to how receptor palmitoylation contributes to GPCR signaling, the cholesterol–palmitoyl interaction at the β_2-AR crystallographic dimeric interface suggests that facilitation of homodimerization may be one possible scenario. Because of the enrichment of many GPCRs in lipid raft (cholesterol-rich) microdomains in cell membranes[11], cholesterol within such microdomains can be easily incorporated into the receptor dimer. In addition, because the interaction surface appears to be too small for the GPCR monomer to interact with G proteins[12], dimerization may facilitate G protein coupling. Actually, dimerization of many GPCRs, including OPRM1 and β_2-AR, regulates receptor signaling[13]. In the work described here, we tested the hypothesis that a specific cholesterol–palmitoyl interaction at the OPRM1 signaling complex may affect its signaling by facilitating homodimerization and G protein coupling.

Cholesterol, an important component of lipid raft microdomains on cell membrane, is critical for GPCR signaling[14]. The localization of some GPCRs in lipid raft

microdomains has been suggested to contribute to the downstream signaling [11]. For example, OPRM1 locates in the lipid raft microdomains on cell membrane in the absence of agonist [15]. Extracting cholesterol from the cells disrupts the entirety of lipid raft microdomains and inhibits the ability of OPRM1 to transducer signaling, such as morphine-induced adenylyl cyclase inhibition and ERK phosphorylation [15]. Thus if cholesterol-palmitoyl interaction could be identified in the interface of OPRM1 homodimer, the cholesterol and cholesterol-enriched lipid raft microdomains may be linked to the receptor palmitoylation during the regulation of receptor signaling. Especially, the receptor dimerization and G protein couple may also be involved, which can extend our understanding the mechanisms underlying GPCR signaling.

The palmitoylation site on OPRM1 was identified, and the ability of the cholesterol–palmitoyl interaction to contribute to receptor homodimerization, G protein coupling, and signaling was examined. In addition, a computational model of OPRM1 was developed to calculate the contribution of the cholesterol–palmitoyl interaction to the total interaction energy at the homodimer interface.

Methods

Palmitoylation Assay

The palmitoylation assay was carried out as reported by Drisdel et al. [16]. Briefly, receptor was immunoprecipitated with Protein G agarose beads. The beads were then sequentially incubated with 50 mM NEM to block free sulfhydryl groups, 1 M

hydroxylamine to remove thioester-linked palmitic acid, and 40 μM btn-BMCC to conjugate biotin to the depalmitoylated cysteines. To assess the receptor palmitoylation level, the amount of conjugated biotin was determined by immunoprecipitation and immunoblotting [15, 17]. Protein concentrations and receptor expression levels were measured to ensure that equal amounts of receptor were loaded in each lane of the gel.

Membrane Purification and Cholesterol Assay

Cells were homogenized in 0.32 M sucrose and 10 mM HEPES (pH 7.7). The crude lysate was then centrifuged at 1,000 x *g* for 10 min at 4°C, the supernatant was collected, and the pellet was re-homogenized. These processes were repeated until the pellet appeared translucent. The collected supernatant was centrifuged at 100,000 x *g* for 60 min at 4°C. The pellet was re-suspended and used to determine the cholesterol content in cell membranes. The results were normalized against cholesterol levels in cells under control condition.

Cholesterol concentrations were determined by using the Amplex Red Cholesterol Assay Kit (Invitrogen, Carlsbad, CA) on the cell membrane preparation following the instruction provided by the company.

To determine the amount of cholesterol associated with OPRM1 complex, a new method was used. Cell was treated with lysis buffer (50 mM Tris-HCl, pH 7.5, 150 mM NaCl, 0.25% sodium deoxycholate, 0.1% Nonidet P-40, 0.5% Triton X-100, 0.1% digitonin, 50 mM NaF, 1 mM dithiothreitol, 0.5 mM phenylmethylsulfonyl fluoride, 50 mM sodium pyrophosphate, 10 mM sodium vanadate, and 1X protease inhibitor cocktail;

Roche, Indianapolis, IN). The supernatants from the cells lysate was divided into three equal aliquots. These aliquots were used to perform co-immunoprecipitation with PBS (control), HA antibody (OPRM1 and C170A were tagged with HA, Convance, 1:1000), or FLAG antibody (Sigma, 1:1000). After antibody incubation, Protein G agarose (Invitrogen, Carlsbad, CA) was added for additional overnight incubation. The resulted agarose was used to determine the amount of precipitated cholesterol with Amplex Red Cholesterol Assay Kit (Invitrogen, Carlsbad, CA). The FLAG antibody was used as control antibody to exclude the possible influence from antibody usage. The higher amount of cholesterol precipitated by HA antibody compared with PBS or FLAG antibody reflects the cholesterol associated specifically with OPRM1 signaling complex. Although this method could not determine the cholesterol interact with receptor directly, but could detect the cholesterol specifically interacted with receptor signaling complex.

FRET (Fluorescence Resonance Energy Transfer)

CFP and YFP were fused to the C terminus of wild-type OPRM1 or the C170A mutant of OPRM1. YFPGαi2 has YFP inserted between residues 91 and 92 of Gαi2 [18]. Throughout the studies, all FRET values are expressed as the normalized net FRET by the following formula: I_{FRET} =[(I_{CFP}×CoA) – (I_{YFP}×CoB)] / [the square root of (I_{CFP}×I_{YFP})]. I_{FRET} is the fluorescence intensity when a CFP-YFP (excitation-emission) filter set is used, I_{CFP} is the fluorescence intensity when a CFP-CFP filter set is used, and I_{YFP} is the fluorescence intensity when a YFP-YFP filter set is used. CoA was determined in the cells transfected with only CFP constructs by the following formula: CoA= I_{FRET} /

I_{CFP}. CoB was determined similarly. Including "square root" in the formula eliminates the influence from the differential expression of CFP- and YFP-conjugated protein. Briefly, more than twenty individual regions on the cell membrane of a single cell were analyzed, and more than twelve individual cells were analyzed for each sample.

OPRM1 Binding Assay

The amounts of receptor on cell membrane and the affinity of agonists to receptors were determined by binding assay [19]. Briefly, purified cell membrane was incubated with [^{3}H]-diprenorphine and agonists/antagonists. After incubation, PEG8000 and NaCl were added to trapped the receptors on Whatman GF/B filters for final radioactive reading. Scatchard analyses were carried out to determine the level of wild-type or mutant OPRM1 expressed on cell membranes. To determine the affinities of various ligands, the cell membranes were incubated with 2 nM [^{3}H]-diprenorphine and various concentrations of morphine, naloxone, and CTOP (0.01 nM – 10 μM). These competition binding studies were analyzed with one- or two-site curve-fitting models in GraphPad 5.0.

Transient Transfection

The pCMV-shuttle vector (Stratagene) was used in current studies. cDNA of receptor, Gαi2 and their fluorescence-conjugated constructs were controlled by the CMV promoter. The transient transfection was performed with Lipofectamine 2000 (Invitrogen)

following the instruction provided by the company. Cells were allowed to rest for 24 hours before further treatment.

Assays based on antibodies

Immunoblotting and co-immunoprecipitation assays were performed as described previously [17]. The same Confocal Imager used for FRET was used to analyze colocalization. The adenylyl cyclase inhibition was measured as previously reported [15]. ERK phosphorylation was determined by immunoblotting [17].

Colocalization studies were performed as reported previously [15]. Briefly, cells were cultured on poly-lysine-coated coverslip in six-well plates. After transient transfection and various treatments, cells were fixed with 2% formaldehyde for 30 min. HA antibody, Flag antibody, and Gαi2 antibody were used as primary antibody (1:1000). The confocal images were captured with a BD CARV II Confocal Imager and a Leica DMIRE2 fluorescence microscope. Colocalization of the fluorescence pixels was calculated with IPlab 4.0 software (BD Biosciences-Bioimage) and the following formula: $2 \times N_{yellow} / (N_{red} + N_{green})$. N represents the number of pixels with fluorescence intensity over a pre-defined threshold.

Model development of the OPRM1 homodimer

A computational model of the OPRM1 inactive state was first developed using a β_2-AR crystal structure template [3] with two major modifications. First, the TMH 7/elbow/Hx8 region of the β_2-AR was replaced with that of the adenosine A_{2A} crystal

structure [20] because the "elbow region" between TMH7 and the C terminus Helix 8 contains only two residues (P7.57 D7.58). This results in an elbow region of β_2-AR that is stretched. The OPRM1 would not have a similar conformation since it has three elbow residues (D7.57 E7.58 N7.59). We therefore used in the OPRM1 model, the elbow conformation in the A_{2A} crystal structure [20] which also has three residues.

Second, the Monte Carlo/simulated annealing technique CM [21] was used to study the conformations of three OPRM1 TMHs with important sequence divergences from the β_2-AR template: TMH2 (P2.58 OPRM1 vs. P2.59 β_2-AR), TMH4 (P4.59 OPRM1 vs. P4.60 β_2-AR), and TMH6 (CWTP OPRM1 vs. CWLP β_2-AR).

The CM technique explores the low free energy conformations possible for a helix of interest using Monte Carlo simulated annealing. The method of CM, developed by Guarnieri and Wilson [22] and extended by Guarnieri and Weinstein [23], efficiently and completely explores the dihedral conformational space of a molecule, independent of the dihedral conformation of the initial molecular structure. The CM method combines Monte Carlo exploration of the dihedral angle space with simulated annealing (MC/SA) to determine the range of values that each dihedral angle is capable of exploring in a broad temperature range. The CM method has been expanded to allow the variation of of bond angles in addition to dihedral angles [21]. In the CM calculations reported here, the backbone dihedrals of each helix were set to the standard φ (-63°) and ψ (-41.6°) for transmembrane helices. Our established protocol is to allow all torsion angles to vary ±10°, and to allow a larger variation of ±50° in regions containing flexible areas. These flexible areas are regions where there are known helix bending residues such as prolines,

glycines, serines and/or threonines [24]. The OPRM1 TMH regions considered flexible were the following: TMH2: region of i (P2.58) to i-4 (T2.54); TMH4 region of i (P4.59) to i-4 (A4.55) and TMH6 region of i (P6.50) to i-4 (V6.46). Individual bond angles were allowed to vary ±8°. The CM calculation is performed in two phases, an exploratory phase and a biased annealing phase. In the exploratory phase, a random walk is used to first identify the region of conformational space most probable for each torsion angle and bond angle. The initial temperature for each run was 3000 K with 50,000 Monte Carlo steps applied to each torsion or bond angle variation with cooling in 18 steps to a final temperature of 310 K. Each step consists of varying two dihedral angles and one bond angle chosen at random from the entire set of variable angles. The torsion angles and bond angles are randomly picked at each temperature and each move is accepted or rejected using the Metropolis criterion [25]. Accepted conformations in the Exploratory Phase are used to create "memories" of torsion angles and bond angles that were accepted. This information provides a map of the accessible conformational space of each TMH as a function of temperature. In the biased annealing phase, the only torsion angle and bond angle moves attempted are those that would keep the angle in the "populated conformational space" mapped at 310K in the exploratory phase. The biased annealing phase for the calculations reported here began at 749.4 K with cooling to 310 K in 7 steps. 105 structures were output at 310 K. The output from each TMH study was superimposed on the corresponding template helix in the β2-AR template that had been mutated to the sequence of the OPRM1. A helix was selected for inclusion in the revised

OPRM1 that fit in the bundle with no van der Waals overlaps with residues on other TMHs.

The CM helices chosen for substitution into the TMH bundle had the following helix bend angles, wobble angles, and face shifts: TMH2 (35.2°, -105.8°, 40.3°), TMH4 (14.8°, -126.1°, 25.9°), and TMH6 (30.6°, -129.9°, 45.6°). Extracellular and intracellular loops were then added using MODELLER v8.2 [26]. Energy minimizations were performed using Macromodel and the OPLS2005 all-atom force field (version 9.8, Schrödinger, LLC, New York, NY). A distance-dependent dielectric, 8.0 Å extended nonbonded cutoff, 20.0 Å electrostatic cutoff, and 4.0 Å hydrogen bond cutoff were used.

The palmitoyl was then added to C3.55(170), and a cholesterol was docked between palmitoylated C3.55(170) and TMH3. Interactive docking studies in Maestro (version 9.1, Schrödinger, LLC, New York, NY) were used to orient two OPRM1/cholesterol protomers at the symmetric TMH4 interface of mouse dark state rhodopsin [27]. In this orientation, the OPRM1 protomers form an interface analogous to that shown by Guo and co-workers to characterize the inactive state homodimer interface of the dopamine D2 receptor [1]. This interface in OPRM1 involves N4.41, I4.44, C4.48, I4.51, A4.55, and P4.59 on each protomer. In the resultant dimer, cholesterol is packed up against the TMH4 interface and TMH3. The palmitoyl at C3.55(170) is packed against the cholesterol and TMH5, blocking cholesterol from leaving the interface. The energy of the OPRM1 homodimer complex was minimized using the same force field, dielectric, and cutoffs as described above. In the first stage of the calculation, Polak-Ribier conjugate gradient minimization was employed until a gradient of 0.1 kcal/mol·A^2

was reached. A force constant of 250 kcal/mol was used on the loop backbone atoms. All charged residues in the loop regions and at the ends of the TMHs that face toward lipid head groups were mutated to neutral forms. Non-moving fixed atom restraints were applied to the C-alpha atoms of TMH3 in both protomers, restraining the protomers from moving apart. The protocol was repeated with TMH3 non-moving fixed restraints removed.

Macromodel was used to output the pair-wise interaction energy (van der Waals and coulombic) for a given pair of atoms. The nonbonded interactions are represented in OPLS2005 as implemented in Macromodel through Coulomb and Lennard-Jones terms interacting between sites centered on nuclei. Thus, the intermolecular interaction energy between molecules a and b is given by the sum of interactions between the sites on the two molecules [28] as represented in the equation below:

$$\Delta E_{ab} = \sum_{i}^{on\,a} \sum_{j}^{on\,b} \left(q_i q_j e^2 / r_{ij} + A_{ij} / r_{ij}^{12} - C_{ij} / r_{ij}^{6} \right)$$

a and b are collected by Macromodel as atom sets representing all atoms of a single residue for a and all atoms of a nearby residue for b. The residue represented by a is evaluated separately against all residues within a 7.0Å radius of residue a. With Cholesterol A defined as Group 1 and with all of the atoms of any residue within 7.0 Å of Protomers A or B defined as Group 2, the pair-wise interaction energies were calculated. The interaction energy at the homodimer interface was calculated as the sum of the interaction energies between Protomers A and B at the homodimer interface plus the

interaction energy of Cholesterol A with Protomer B and the interaction energy of Cholesterol B with Protomer A. The close interaction and steric bulk of Protomer A's TMH4 with Protomer B's TMH4 blocked Cholesterols A and B from interacting with each other. The palmitoyls could not interact with each other for the same reason.
This additional information has been added to the Materials and Methods section.

Statistic methods

Experiments were repeated at least four times (more than twelve individual cells for image analysis). Data were analyzed and compared by one-way ANOVA with Dunnett-test as post-hoc test for comparisons, or by two-way ANOVA with Bonferroni-test as post-hoc test. Error bars and "*" presented the standard deviations and significant changes ($p<0.05$), respectively.

List of Abbreviations

The following abbreviations are used: 2-BP, 2-bromopalmitate; β2-AR, β2-adrenergic receptor; btn-BMCC, 1-biotinamido-4- [4′-(maleimidomethyl) cyclohexane carboxamido] butane; CM: Conformational Memories; CTOP, Cys2-Tyr3-Orn5-Pen7-amide; GM1, monosialotetrahexosylganglioside; GPCR, G protein-coupled receptor; NEM, N-ethylmaleimide; OPRM1, μ-opioid receptor; TMH, transmembrane helix; TR, transferrin receptor; VDW, van der Waals.

Results

Cys^{170} is the palmitoylation site of OPRM1

Wild-type HEK293 cells (HEK) and HEKOPRM1 cells (HEK cells heterologously expressing OPRM1 with HA spliced at the amino terminus) were used to validate the palmitoylation assay [16]. The HA-tagged receptor were precipitated with HA antibody and Protein G agarose. The following procedures were used to determine receptor palmitoylation: 1) The free sulfhydryl groups in precipitated receptor were blocked with N-ethylmaleimide (NEM). 2) The palmitoylated cysteine was and hydrolyzed with hydroxylamine. 3) Biotin was conjugated to the de-palmitoylated cysteines in the immunoprecipitated receptor with btn-BMCC (1-biotinamido-4- [4′-(maleimidomethyl) cyclohexane carboxamido] butane). The amounts of biotin linked to the receptor were determined by immunoblotting.

Intensive biotin labeling was detected in HEKOPRM1 cells, but not in HEK cells, suggesting that the detected palmitoylation is specific to OPRM1 (Fig. 1.1a, Lanes 1-2). Since NEM was used to blocked the free sulfhydryl groups, the immunoreactivity of biotin increased when the NEM step was omitted (Fig. 1.1a, Lane 4). In addition, the immunoreactivity of biotin decreased when hydroxylamine step was omitted (Fig. 1.1a, Lanes 5), and no biotin was detected when btn-BMCC was not used (Fig. 1.1a, Lanes 6), suggesting that the assay is suitable for detecting the palmitoylation of OPRM1.

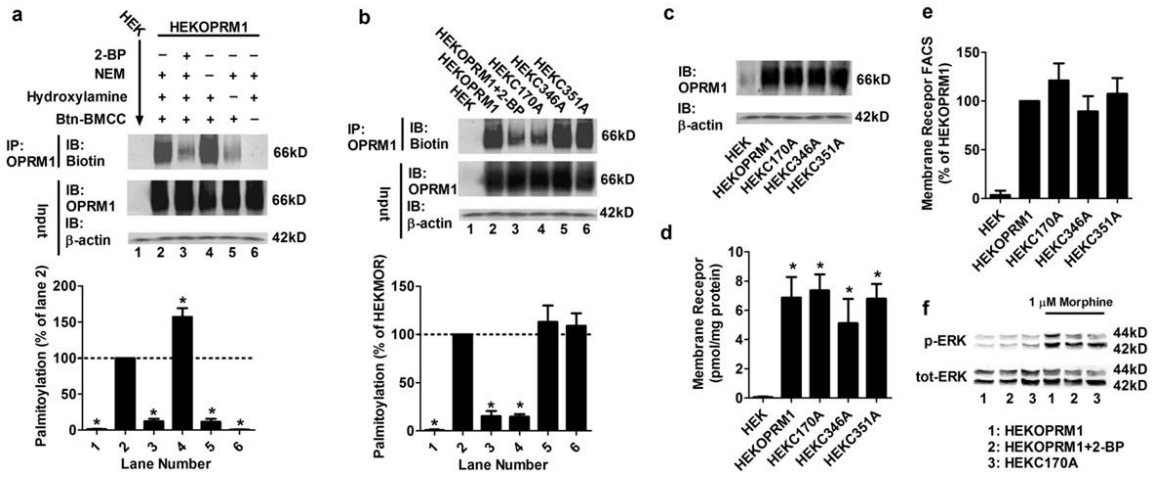

Figure 1.1. Cys^{170} is the palmitoylation site of OPRM1. (a) Palmitoylation assays were performed in HEK and HEKOPRM1 cells. The amounts of palmitoylated receptor were normalized against that in HEKOPRM1 (Lane 2). 50 μM 2-BP was used to treat HEKOPRM1 for 12 h (Lane 3). Individual steps (treatment with NEM, hydroxylamine, or btn-BMCC) were omitted to validate the assay (Lanes 4-6). (b) The palmitoylation assay was performed in HEK, HEKOPRM1, HEKOPRM1 treated with 50 μM 2-BP for 12 h, HEKC170A, HEKC346A, and HEKC351A cells. The amounts of palmitoylated receptor were normalized against that in HEKOPRM1 (Lane 2). (c-e) Membrane receptor levels were determined with immunoblotting (c), binding assay (d), and FACS (e). (f) HEKOPRM1, HEKOPRM1 treated with 50 μM 2-BP for 12 hr, and HEKC170A cells were treated with 1 μM morphine for 5 min. Phosphorylated ERK and total-ERK were determined by immunoblotting. One-way ANOVA with Dunnett-test as post-hoc test was used for analysis. The error bars and "*" presented the standard deviations and significant changes ($p<0.05$, $n>3$), respectively.

To confirm the assay used can detect the palmitoylation specifically, 2-bromopalmitate (2-BP), a palmitoylation inhibitor, was used to block all the palmitoylation. A low level of receptor palmitoylation was observed when HEKOPRM1 cells were pretreated with the 2-BP for 12 h (Fig. 1.1a, Lane 3), which also suggests the detected palmitoylation is on OPRM1. Since palmitoylation is important for the cell functions, prolonged treatment or high concentration of 2-BP will affect cell viability.

Thus in the current study the treatment time and concentration of 2-BP were determined empirically so as to inhibit receptor palmitoylation and to have minimal effect

on cell viability. Thus the current 2-BP treatment paradigm did not block receptor palmitoylation totally.

Mutating the two conserved cysteine residues [C8.53(346) and C8.58(351)] in the C terminus of OPRM1 does not affect palmitoylation [7]. Thus the only other intracellular cysteine, C3.55(170), should be the putative palmitoylation site. To confirm this hypothesis, these three cysteines were mutated to alanine individually, and the mutants were stably expressed in HEK cells to obtain HEKC170A, HEKC346A, and HEKC351A. Although C170A is difficult to stably express in CHO cells [7], we successfully expressed a high level of C170A in the cell membrane of HEK cells, possibly due to the differences between cell lines and poly-L-lysine used during the cell culture. As shown in Fig. 1.1b, Lanes 2 and 5-6, similar amounts of palmitoylated receptor were detected in HEKOPRM1, HEKC346A, and HEKC351A cells. Furthermore, the amount of palmitoylated receptor in HEKC170A cells was similar to that in 2-BP-pretreated HEKOPRM1 cells (Fig. 1.1b). Therefore, it is reasonable to suggest that C3.55(170) but not C8.53(346) or C8.58(351) was the palmitoylation site of OPRM1.

Immunoblotting indicated that the overall receptor expression levels were similar in these cell lines (Fig. 1.1c), and a [^{3}H]-diprenorphine saturation binding assay with isolated cell membranes indicated that there was no difference in the amounts of receptors in the cell membranes. HEK, HEKOPRM1, HEKC170A, HEKC346A, and HEKC351A cells have membrane receptor expressed at 0.06±0.05, 6.87±1.14, 7.36±1.10, 5.12±1.67, and 6.80±1.61 pmol/mg protein respectively (Fig. 1.1d). To further confirm that there is no difference in the amounts of membrane receptor in these cell lines,

antibody against the HA-tag was used for FACS analysis (Fig. 1.1e). Since the HA was tagged in the N-terminal of receptors and the cell membrane was not disrupted during the analysis, the results obtained from FACS assay should represent the actual amounts of membrane receptor. Thus there was no difference in membrane receptor levels, it is reasonable to conclude that C3.55(170) is the major palmitoylation site of OPRM1. For the sake of consistency, "OPRM1" is used for the wild-type OPRM1, "C170A" is used for the palmitoylation-deficient mutant, and "receptor" indicates both the wild type and mutants in subsequent studies described here.

In addition, agonist treatment did not affect receptor palmitoylation when morphine and fentanyl were used to challenge the HEKOPRM1 cells (data not shown). Since the current studies focused on how receptor palmitoylation influenced receptor signaling, the effects of agonists on receptor palmitoylation or other subsequent observations were not discussed in depth.

Receptor palmitoylation stabilizes morphine-induced signaling and receptor-Gαi2 coupling

To determine the influence of palmitoylation on receptor signaling, morphine-induced adenylyl cyclase inhibition and ERK phosphorylation were monitored. Morphine-induced adenylyl cyclase inhibition is defined by the ability of morphine to inhibit the forskolin-induced increase in the intracellular cAMP level. Morphine-induced ERK phosphorylation was analyzed by calculating the percentage increase of phosphorylated ERK when compared to basal level.

Table 1.1. Palmitoylation did not affect the binding of agonists

		HEKOPRM1	HEKC170A
Relative Affinities			
239 Morphine	**K_H (nM)**	2.8±0.56	2.2±0.42
	K_L (nM)	155±27	123±31
Naloxone	**K_I (nM)**	5.1±0.71	6.2±1.2
CTOP	**K_I (nM)**	11±1.4	9.5±2.1

The affinities of receptor for ligands were determined in HEKOPRM1 and HEKC170A cells using agonist binding assay. One-site (K_I: naloxone and CTOP) or two-site (K_H and K_L: morphine) curve-fitting models were used in the analyses with GraphPad Prism 5.0. . Data were analyzed by one-way ANOVA with post-hoc Dunnett's test. Standard deviations are provided, and "*" represents significant changes ($p<0.05$).

As summarized in Table 1.1, no difference in the affinities for ligands [morphine, naloxone, and Cys^2-Tyr^3-Orn^5-Pen^7-amide (CTOP)] was detected between OPRM1 and C170A. For example, the K_I of CTOP was 11±1.4 nM in HEKOPRM1 cells, and was 9.5±2.1 nM in HEKC170A cells (Table I). In addition, the expression levels of OPRM1 and C170A in the cell membrane were similar (Fig. 1.1c-e). However, morphine induced less signaling in HEKC170A than in HEKOPRM1 cells. The ability of morphine to induce adenylyl cyclase inhibition in HEKC170A was about 75% of that in HEKOPRM1, when the maximum inhibition was analyzed (Table 2). The ability to induce ERK phosphorylation in HEKC170A was about 69% of that in HEKOPRM1 (Table 2 and Fig. 1.1f). In addition, morphine induced receptor signaling in 2-BP-treated HEKOPRM1

cells as did in HEKC170A cells (Table 2 and Fig. 1.1f). Thus palmitoylation blockage impairs receptor signaling induced by morphine.

Table 1.2. Palmitoylation impaired morphine-induced receptor signaling

		HEKOPRM1	HEKOPRM1 +2-BP	HEKC170A
Morphine-Induced Signaling				
AC Inhibition	**K_I (nM)**	9.3±0.89	15±1.2*	14±1.3*
	Max. Inh. (%)	84±2.8	56±5.1*	63±4.3*
pERK	**(% of basal)**	239±10	154±10*	164±12*

The percentage inhibition of forskolin-induced cAMP increase by various concentrations of morphine was analyzed with GraphPad Prism 5.0. The results are presented as the maximum inhibition (Max. Inh.) and the IC50 values (K_I). ERK phosphorylation was indicated by the amount of phosphorylated ERK after 5 min of treatment with 1 μM morphine (Blots were provided in Fig. 1f). The amount of total ERK and the results under control condition were used for normalization. Experiments were repeated at least four times. Data were analyzed by one-way ANOVA with post-hoc Dunnett's test. Standard deviations are provided, and "*" represents significant changes ($p<0.05$).

Both signaling events monitored above are mediated via Gαi2 [15]; thus, the effect of receptor palmitoylation on Gαi2 coupling was investigated. The colocalization between receptor and Gαi2 in HEKOPRM1 was more obvious than in HEKC170A cells, when the immunoreactivity of OPRM1 and Gαi2 on the cell membrane was analyzed (Fig. 1.2a). Similar observations were noted in the co-immunoprecipitation experiments (Fig. 1.2b and 1.2c). When Gαi2 antibody was used to perform co-immunoprecipitation, the amount of OPRM1 co-immunoprecipitated with Gαi2 was larger than that of C170A. When HA antibody was used to immunoprecipitate the receptor, more Gαi2 was co-immunoprecipitated with OPRM1 than with C170A. Thus the interaction between Gαi2 and C170A is weaker than that between Gαi2 and OPRM1.

The interaction between receptor and Gαi2 was investigated further with FRET analysis. The normalized net FRET between CFPOPRM1 and YFPGαi2 was much higher than that between CFP and YFP, suggesting that OPRM1 and Gαi2 were in proximity of each other, ≤ 10 nm. The FRET analysis was performed on the cell membrane to exclude the possible influence from the intracellular expression of fluorescence constructs. The normalized net FRET between CFPOPRM1 and YFPGαi2 was higher than that between CFPC170A and YFPGαi2 (Fig. 1.2d). Because 1) the expressions of the fluorescence constructs, like CFPOPRMA1 and YFPGαi2, were kept to the similar levels by titrating the amounts of plasmids used for transfection; 2) immunoblotting was also used to monitor the expression during the studies, and 3) overall fluorescence intensities were determined prior to FRET and colocalization studies, the FRET difference supports the conclusion that blockage of receptor palmitoylation in the C170A mutant impairs Gαi2 coupling.

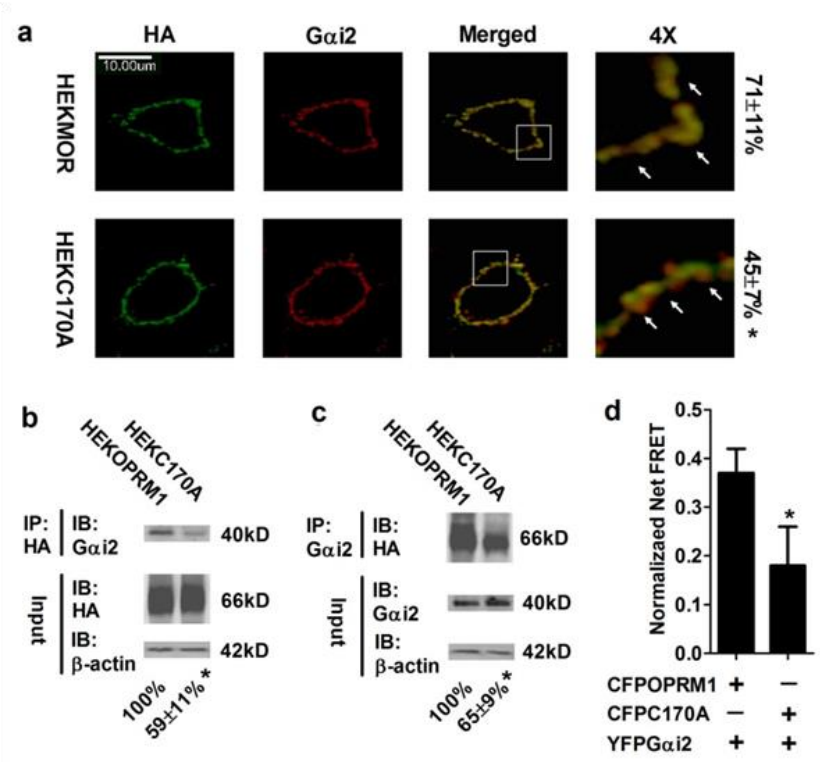

Figure 1.2. Palmitoylation contributes to Gαi2 coupling. (a) The colocalization between HA-tagged receptor and Gαi2 was determined in HEKOPRM1 and HEKC170A cells. Images were analyzed as described in *Methods*. (b) Anti-HA antibody was used to precipitate receptors in HEKOPRM1 and HEKC170A cells. Gαi2 precipitated with receptors was quantified and normalized to that in HEKOPRM1cells. (c) Co-immunoprecipitation was performed with Anti-Gαi2 antibody, and the precipitated receptor was quantified. (d) CFPMOR or CFPC170A was transfected into HEK cells with YFPGαi2. FRET analysis was performed. Two-tailed student t-test was used. Error bars and "*" represent the standard deviations and significant changes ($p<0.05$, $n>3$ for b and c; $n>10$ for a and d), respectively. IP, immunoprecipitation; IB, immunoblotting

The YFP/CFP tagged receptors had similar functions as FLAG- and HA-tagged. Morphine-induced adenylyl cyclase inhibition in the cells transiently expressed these receptor constructs with similar K_Is: 9.8±1.1 nM (HA-tagged OPRM1), 10.7±1.4 nM

(FLAG-tagged OPRM1), 8.9±1.2 nM (CFPOPRM1), and 9.5±0.8 nM (YFPOPRM1). Thus the FRET experiment could indicate the function characteristics of receptors.

Receptor palmitoylation facilitates homodimerization and subsequent Gαi2 coupling

The possible contribution of OPRM1 palmitoylation to homodimerization was investigated by performing FRET analysis between CFPOPRM1/CFPC170A and YFPOPRM1/YFPC170A. As indicated in Fig. 1.3a, the normalized net FRET between CFPOPRM1 and YFPOPRM1 was 0.49±0.03, whereas it was 0.07±0.02 between CFPC170A and YFPC170A in the cell membrane. In addition, when the HEK cells were co-transfected with CFPOPRM1 and YFPC170A or with CFPC170A and YFPOPRM1, the normalized net FRETs were 0.30±0.05 and 0.27±0.05, respectively. The colocalization and co-immunoprecipitation assays between HAOPRM1/HAC170A and FLAGOPRM1/FLAGC170A confirmed the results of the FRET assay (Fig. 1.3b and 1.3c). In summary, colocalization, co-immunoprecipitation, and FRET studies suggest that the amount of OPRM1-OPRM1 homodimer is larger than the amount of OPRM1-C170A dimer, and the amount of OPRM1-C170A dimer is larger than that of C170A-C170A homodimer, when similar levels of receptors are expressed. It is reasonable, therefore, to suggest that the ability of C170A to form a homodimer is lower than that of OPRM1.

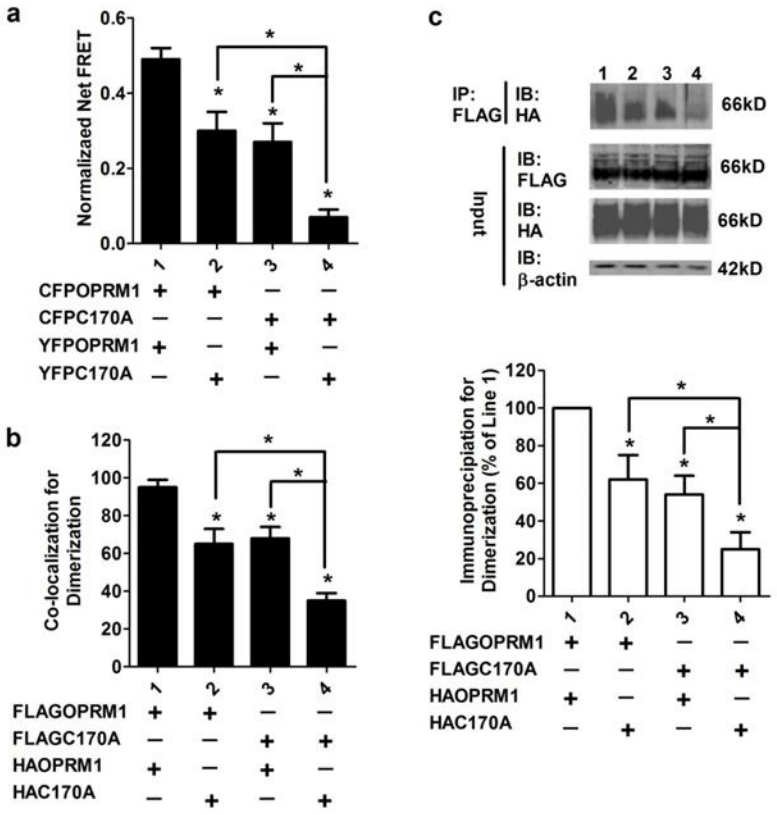

Figure 1.3. Palmitoylation stabilizes homodimerization. (a) FRET analysis was performed after transfecting combinations of CFPOPRM1/CFPC170A and YFPOPRM1/YFPC170A into HEK cells. (b-c) FLAGOPRM1 /FLAGC170A and HAOPRM1/HAC170A were transfected into HEK cells. The colocalization between FLAG-tagged receptor and HA-tagged receptor was determined in (b). The amounts of HA-tagged receptor precipitated with Flag-tagged receptor were normalized against the amount of HAOPRM1 precipitated with FLAGOPRM1 and summarized in (c). One-way ANOVA with Dunnett-test as post-hoc test was used for analysis. The error bars and "*" presented the standard deviations and significant changes ($p<0.05$, $n>3$), respectively

Because the amounts of homodimer decreased sequentially from Lane 1 to Lane 4 in Fig. 1.3c, we used FRET analysis to determine if the decrease affected receptor–Gαi2 coupling (Fig. 1.4a). We transiently transfected YFPGαi2 with either CFPOPRM1 or CFPC170A into HEKOPRM1 and HEKC170A cells. Two caveats in these experiments were considered so as to ensure the success of the studies: 1) HEKOPRM1 and

HEKC170A cells expressed similar amounts of membrane receptors; 2) transient transfection of CFPOPRM1 and CFPC170A was tightly controlled to reach the similar expression levels.

If receptor palmitoylation affects Gαi2 coupling, a similar sequential decrease in receptor–Gαi2 coupling should be observed between OPRM1 homodimer, OPRM1-C170A dimer and C170A homodimer. As indicated in Fig. 4a, the normalized net FRET between CFPOPRM1 and YFPGαi2 was greater than that between CFPC170A and YFPGαi2 in both HEKOPRM1 and HEKC170A cells. The normalized net FRET between CFPOPRM1 and YFPGαi2 as well as between CFPC170A and YFPGαi2 was greater in HEKOPRM1 than in HEKC170A. These results suggest a positive correlation between the receptor palmitoylation and Gαi2 coupling.

This correlation could be explained by two mechanisms. One possible explanation is that the homodimers affinity for Gαi2 is much higher than the monomer's affinity for Gαi2; this mechanism is supported by a previous report [12]. A second explanation is that the C170A monomer's affinity for Gαi2 is much lower than the OPRM1 monomer's affinity for Gαi2. If the second mechanism was the dominant one, the FRET between transiently transfected CFPC170A and YFPGαi2 should be smaller in HEKOPRM1 cells than in HEKC170A cells, because OPRM1's higher affinity for YFPGαi2 would result in a higher competition for Gαi2 in HEKOPRM1 than in HEKC170A.

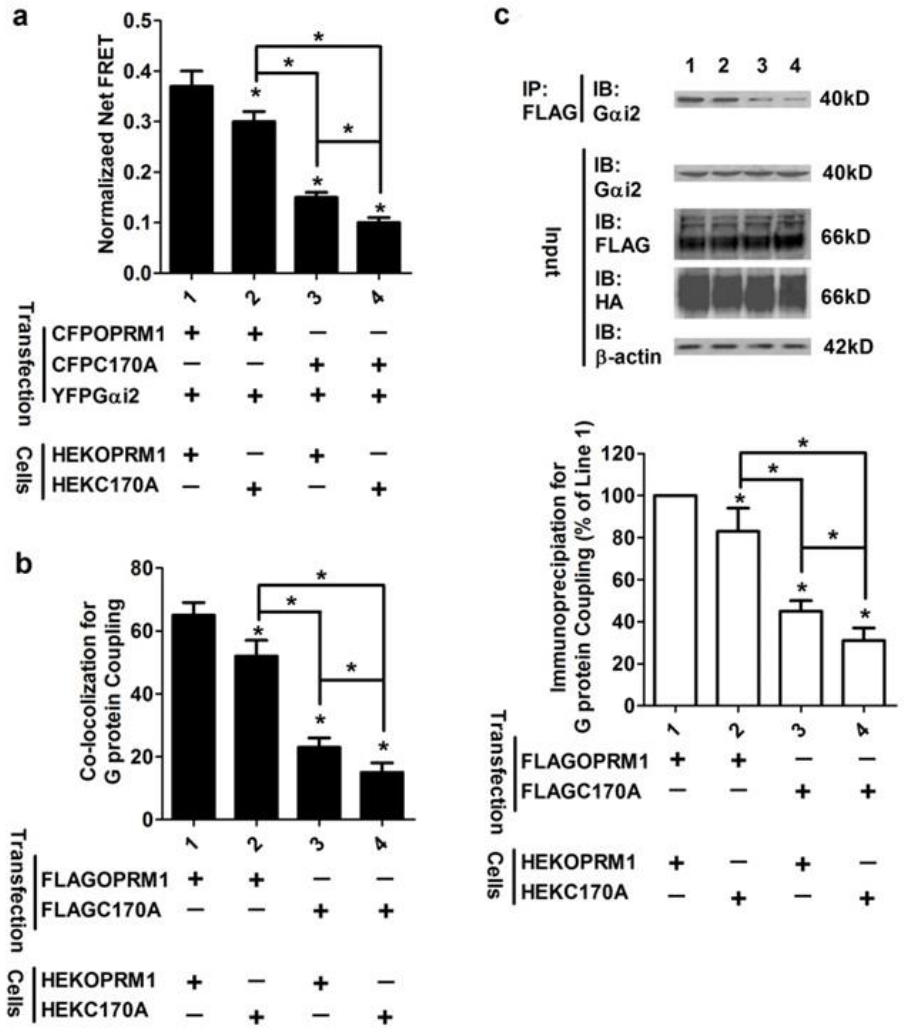

Figure 1.4. Palmitoylation stabilizes Gαi2 coupling. (a) The FRET between CFPOPRM1 and YFPGαi2 and the FRET between CFPC170A and YFPGαi2 were determined in HEKOPRM1 and HEKC170A cells. (b-c) Colocalization between FLAGOPRM1 and Gαi2 (or FLAGC170A and Gαi2) was compared in HEKOPRM1 and HEKC170A cells after transfection (b). The amounts of Gαi2 precipitated with FLAGOPRM1 and FLAGC170A in the two cell lines were compared in (c). The amount of Gαi2 precipitated with FLAGOPRM1 in HEKOPRM1 cells was used for normalization. One-way ANOVA with Dunnett-test as post-hoc test was used. The error bars and "*" presented the standard deviations and significant changes ($p<0.05$, $n>3$), respectively.

However, the FRET analysis produced the opposite result: FRET between CFPC170A and YFPGαi2 was higher in HEKOPRM1 cells than in HEKC170A cells

(Fig. 1.4a). These observations suggest that the reduced receptor dimerization in the absence of palmitoylation leads to decreased Gαi2 coupling. Additional colocalization and co-immunoprecipitation studies further support this hypothesis (Fig. 1.4b and 1.4c). These results indicate a correlation between receptor homodimerization and Gαi2 coupling.

Receptor palmitoylation facilitates cholesterol association in the receptor signaling complex

Although it still requires further investigation to explore the contribution of receptor dimerization to G protein coupling, receptor palmitoylation facilitating receptor dimerization and G protein coupling was established above. In order to determine the detailed mechanisms underlying these phenomena, the observed interaction between cholesterol and palmitoyl group in the crystal structure of β_2-AR [3] was utilized. To determine the existence of similar cholesterol-palmitoyl interaction in OPRM1 complex, the cholesterol exists in the receptor complex should be quantified first. Because the direct detection of the cholesterol within the homodimer requires the purification of the receptor to homogeneity, and there is no guarantee that the cholesterol–receptor association will stay intact during purification, we instead examined the amount of cholesterol incorporated into the receptor signaling complex.

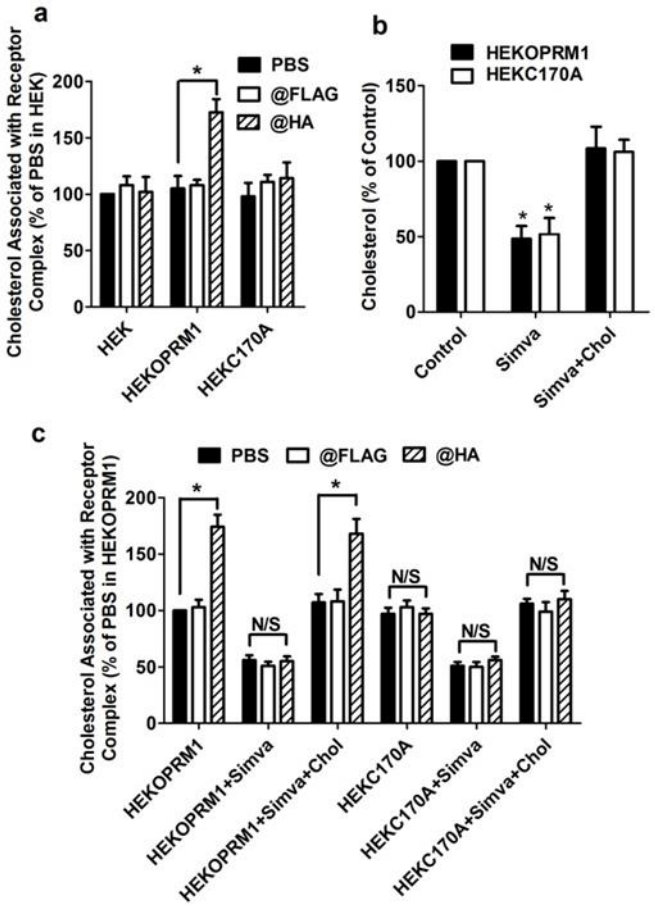

Figure 1.5. Palmitoylation facilitates cholesterol association. (a) Cholesterol associated with receptor complex was determined in HEK, HEKOPRM1, HEKC170A cells. The amount of cholesterol precipitated with PBS in HEK cells was used for normalization. (b-c) HEKOPRM1 and HEKC170A cells were treated with PBS (Control), 0.5 μM simvastatin (Simva), or 0.5 μM simvastatin with 20 ng/ml cholesterol (Simva+Chol) for 12 h. Membrane cholesterol contents were determined in (b) as described in *Materials and Methods*. Cholesterol association with receptor complex was determined in (c). One-way ANOVA with Dunnett-test (b) or two-way ANOVA with Bonferroni's test (a, c) was used. The error bars and "*" presented the standard deviations and significant changes ($p<0.05$, $n>3$), respectively. IP, immunoprecipitation; IB, immunoblot; N/S, no significance.

A new method was used to determine cholesterol association with receptor complex. HA-antibody was used to precipitate the HA-tagged receptor. If cholesterol did associate with receptor complex specifically, larger amount of cholesterol should be precipitated by HA antibody when compared to the immunoprecipitation with no antibody. To avoid the possible influence from the usage of antibody, FLAG antibody (no protein was tagged FLAG in current paradigm) was used as control antibody.

Cholesterol association with the receptor signaling complex was indicated by the additional amount of cholesterol precipitated by HA antibody compared with that

precipitated by a control antibody. The extensive washing with lysis buffer containing Triton X-100 and digitonin ensured the removal of cholesterol that was nonspecifically associated with the receptor signaling complex. With this procedure, HA antibody precipitated more cholesterol in HEKOPRM1 cells than FLAG antibody or PBS did. Since receptor was HA tagged at the N-terminal, the detected cholesterol in precipitated receptors should be the cholesterol associated with receptor signaling complex. As control experiments, in HEK cells, the two antibodies and PBS precipitated similar amounts of cholesterol (Fig. 1.5a). These results suggest that this assay can detect the cholesterol associated with the receptor signaling complex.

Decreased cholesterol association was also noted in HEKC170A cells (Fig. 1.5a). The amount of cholesterol precipitated with HA antibody was similar to that precipitated with FLAG antibody, suggesting the mutation on C3.55(170) contributes to the cholesterol association. Although the assay could not distinguish between cholesterol that associates with the receptor directly and cholesterol that associates with other proteins within the signaling complex, receptor palmitoylation appears to regulate the amount of cholesterol that associates with the complex.

Cholesterol association facilitates homodimerization and G*αi*2 coupling

The cholesterol-palmitoyl interaction has been suggested in the β2-AR crystal structure. Receptor palmitoylation was demonstrated to facilitate receptor dimerization and G protein coupling from Fig. 1.2 to Fig. 1.4, thus it is possible that cholesterol has the same functions. To determine the contribution of cholesterol association to receptor

signaling, simvastatin, an HMG-CoA reductase inhibitor was used to treat the cells. Receptor dimerization and G protein coupling was assayed with FRET, co-localization, and immunoprecipitation.

After treating HEKOPRM1 cells with 0.5 μM simvastatin for 12 h, the cellular cholesterol content decreased on the cell membrane. The decreases in cholesterol content could be prevented by the inclusion of 20 ng/ml cholesterol during the simvastatin treatment (Fig. 1.5b). As expected, simvastatin treatment also induced a decrease in cholesterol level on the membrane of HEKC170A cells (Fig. 1.5b).

How cholesterol depletion influenced its association to receptor signaling complex was accessed. Simvastatin treatment decreased the association of cholesterol to receptor complex, which could be prevented by including 20 ng/ml cholesterol in the culture medium (Fig. 1.5c). Simvastatin not only decreased the amount of cholesterol precipitated in the "PBS" group, but also impaired the ability of HA antibody to precipitate more cholesterol than FLAG antibody. Since cholesterol association was not detected in the HEKC170A cells, simvastatin treatment had no effect in these cells (Fig. 1.5c).

Simvastatin decreased the cellular cholesterol content, the FRET assay was then used to determine whether cholesterol content affect receptor dimerization and G protein couping. The normalized net FRET between CFPOPRM1 and YFPOPRM1 in simvastatin-treated HEK cells was decreased and could be reversed by inclusion of cholesterol during the simvastatin treatment (Fig. 1.6a). A similar simvastatin-mediated decrease was also observed with CFPOPRM1 and YFPGαi2 and could also be reversed

by the inclusion of cholesterol during the simvastatin treatment (Fig. 1.6b). However, the cholesterol depletion induced by simvastatin did not affect the homodimerization (Fig. 1.6a) and G protein coupling of C170A (Fig. 1.6b). Therefore, the presence of cholesterol within the receptor signaling complex is critical for receptor homodimerization and Gαi2 coupling.

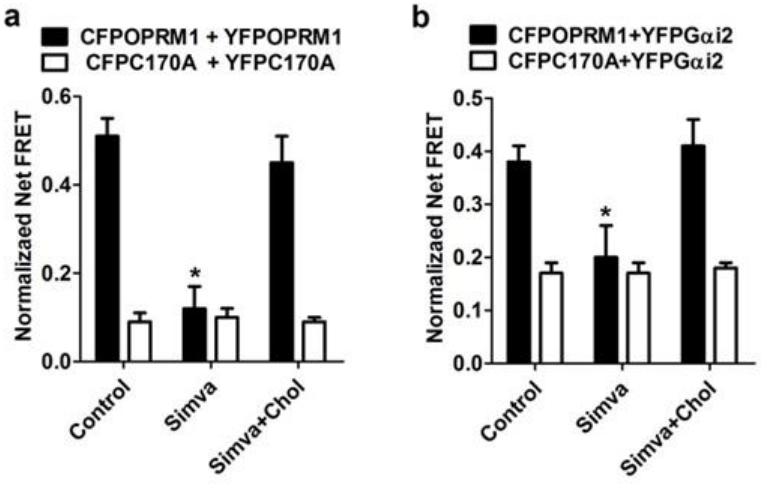

Figure 1.6. Reducing cellular cholesterol affects homodimerization and G protein coupling (a) HEK cells were transfected with CFPOPRM1 and YFPOPRM1 or transfected with CFPC170A and YFPC170A for 24 h. These cells were than treated with with PBS (Control), 0.5 μM simvastatin (Simva), or 0.5 μM simvastatin with 20 ng/ml cholesterol (Simva+Chol) for 12 h. The FRET was analyzed to determine the amount of homodimer. (b) HEK cells were transfected with CFPOPRM1 and YFPGαi2 or transfected with CFPC170A and YFPGαi2 for 24 h. These cells were than treated as in (a), G protein coupling was determined with FRETassay. One-way ANOVA with Dunnett-test was used. The error bars and "*" presented the standard deviations and significant changes ($p<0.05$, $n>3$), respectively.

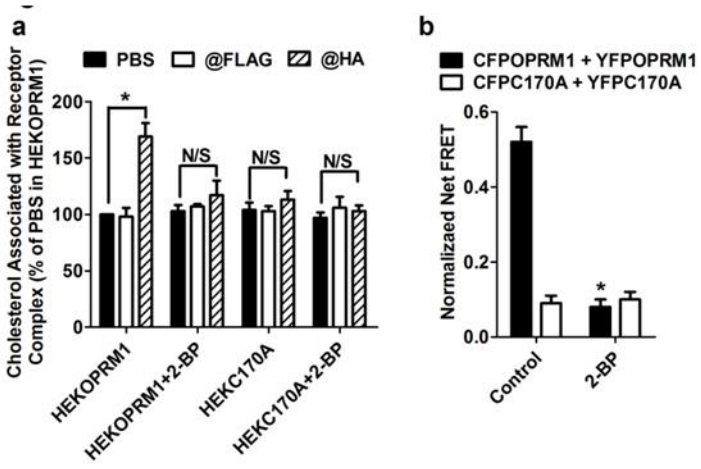

Figure 1.7. Palmitoylation inhibitor impairs homodimerization and cholesterol association. (a) HEKOPRM1 or HEKC170A cells were treated with 50 μM 2-BP or vehicle for 12 hours, the cholesterol associated with receptor complex was measured. (b) HEK cells were transfected with CFPOPRM1 and YFPOPRM1 or transfected with CFPC170A and YFPC170A for 24 hours. 50 μM 2-BP or vehicle was used to treat the cells for additional 12 hours. FRET was then determined. Two-way ANOVA with Bonferroni-test (a) or student t-test (b) was used. Error bars and "*" presented the standard deviations and significant changes ($p<0.05$, $n>3$), respectively.

The relationship between receptor palmitoylation, cholesterol association, and receptor dimerization was further illustrated by incubating cells with the palmitoylation inhibitor 2-BP. A decrease in the cholesterol associated with the OPRM1 signaling complex was also observed after 2-BP treatment (Fig. 1.7a). Due to the inhibitory effect of palmitoylation blockage on Gαi2 membrane targeting [29], the influence of 2-BP on Gαi2 coupling was not investigated. Reduction in the normalized net FRET between CFPOPRM1 and YFPOPRM1 was also seen after 2-BP treatment (Fig. 1.7b). In addition, 2-BP treatment did not affect the cholesterol association with C170A or the homodimerization of C170A, since palmitoylation blockage in C170A already impaired these two function to the basal levels (Fig. 1.7).

Computational modeling suggests that palmitoyl–cholesterol interaction stabilizes the OPRM1 homodimer

Modeling studies were used to confirm that a specific cholesterol interaction with palmitoylated C3.55(170) may enhance the interactions at the homodimer interface of OPRM1. The OPRM1 model developed for the modeling studies reported here is a homology model that uses the β_2-AR crystal structure as a template [2]. As mentioned in *Materials and Methods* the OPRM1 has two TMHs that differ in the position of helix deforming residues from the template β_2-AR (TMH2: P2.58 OPRM1 vs. P2.59 β_2-AR and TMH4: P4.59 OPRM1 vs. P4.60 β_2-AR). Our Conformational Memories calculations revealed that the location of P2.58 in OPRM1 causes the pitch of TMH2 to change after the proline such that residue 2.60 faces into the binding pocket. This same residue position in the β_2-AR resides in the TMH2/3 interface. These results from Conformational Memories (CM) are consistent with the conformation of TMH2 in the CXCR4 crystal structure. CXCR4 also has a Pro at 2.58) [30]. The TMH4 region from 4.53 to 4.58 is SSAIGLP in OPRM1. CM calculations showed that the presence of the G2.56 so close to P2.58 causes a wider turn in TMH4 than is seen in β_2-AR. The net result is that the EC end of TMH4 leans more towards TMH5. One result of this change is the lipid exposure of residue 4.59, a key residue in the TMH4 dimer interface, see below. These two key helix changes, along with changes in helix packing due to these changes distinguish the OPRM1 binding pocket (and lipid face) from that of β_2-ARThe detailed modeling procedures are described in *Materials and Methods*. Fig. 1.8a illustrates the position of cholesterol relative to the palmitoyl and the TMH bundle. Due to the extreme

tilt of TMH3 in the TMH bundle, the intracellular end of TMH3 (orange) is between the intracellular ends of TMH4 (yellow) and TMH5 (cyan). This position of TMH3 allows the cholesterol to pack between the C3.55(170) palmitoyl and TMH4. Fig. 1.8b provides an extracellular view of the final energy-minimized OPRM1 homodimer. In the resultant dimer, cholesterol is packed up against the TMH4 interface and TMH3. The palmitoyl at C3.55(170) is packed against the cholesterol with TMH5, blocking cholesterol from leaving the interface. Table III provides a summary of the resultant interaction energies for the palmitoylated OPRM1 homodimer/cholesterol complex. It is clear here that the major energetic contributions to the interaction energies between the protomers are van der Waals (VDW) energies.

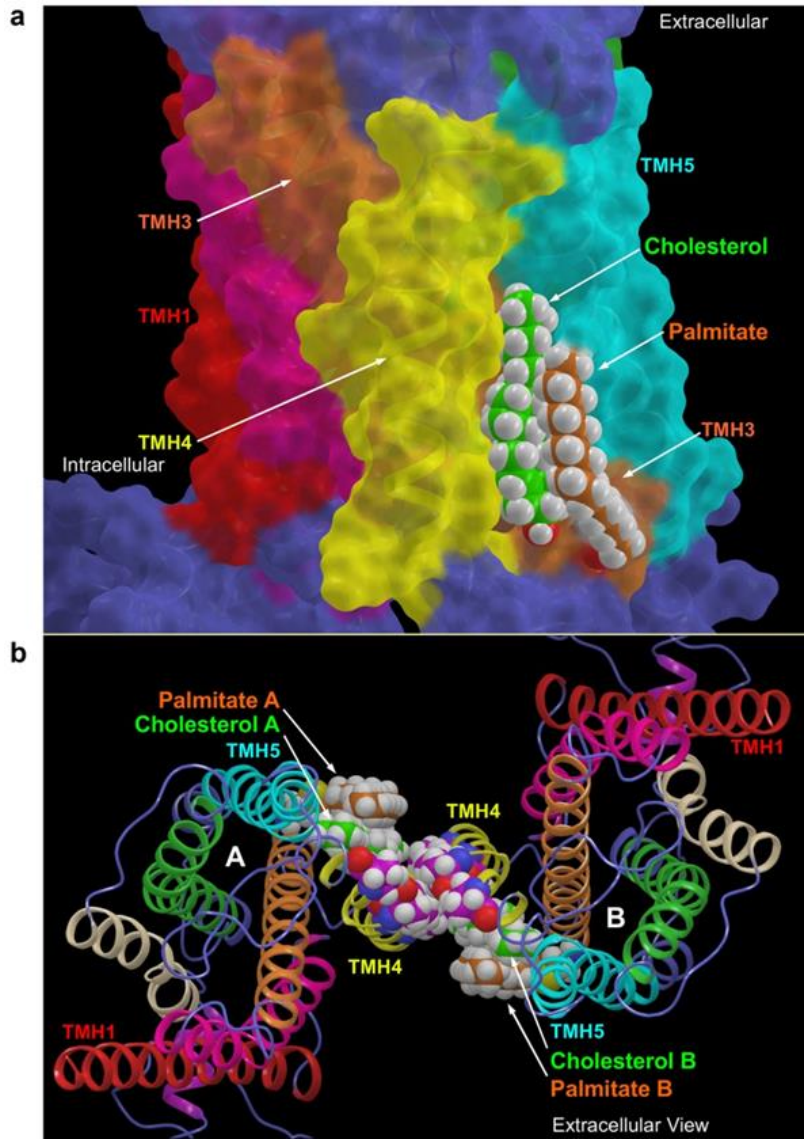

Figure 1.8. Computational modeling of the OPRM1 homodimer interface. (a) This figure illustrates the position of cholesterol relative to the palmitoyl and the OPRM1 TMH bundle. The view is from lipid looking toward TMH4 (yellow). The OPRM1 model is displayed in molecular surface view, with cholesterol (green) and palmitoyl (orange) contoured at their van der Waals radii. TMH3and TMH5 are in orange and cyan, respectively. (b) This figure illustrates an extracellular view of Protomers A and B forming the OPRM1 homodimer TMH4 interface. Residues that form the interface (N4.41, I4.44, C4.48, I4.51, A4.55, and P4.59) are contoured at their van der Waals radii and colored magenta. Also contoured at their van der Waals radii are the palmitoyls (orange) and cholesterols (green). In this arrangement, cholesterols associated with one protomer also interact with the opposite protomer.

The homodimer interface residues with VDW contributions are N4.41, I4.44, C4.48, I4.51, and I4.56, with a total energy of -14.76 kcal/mol. The cholesterol associated with Protomer A interacts with Protomer B residues R4.40, N4.41, K4.43, I4.44, and V4.47, contributing an additional -2.44 kcal/mol, and the cholesterol associated with Protomer B contributes an additional -2.39 kcal/mol similarly. Thus, the total cholesterol interactions (-4.83 kcal/mol) contribute 24.7% to the total interaction energy at the homodimer interface (-19.59 kcal/mol), suggesting that interaction between cholesterol and palmitoyl facilitates OPRM1 homodimerization.

Table 1.3. Homodimer Interface Interaction Energies

Interaction Energies	Coulombic kcal/mol	VDW kcal/mol	Total kcal/mol
	Protomer A, B		
T4.38	-0.01	-0.03	-0.04
P4.39	0.08	-0.02	0.06
R4.40	0.30	-0.31	-0.01
N4.41	-0.32	-1.06	-1.38
I4.44	-0.02	-3.56	-3.58
I4.45	0.09	-1.22	-1.13
V4.47	-0.06	-0.24	-0.31
C4.48	0.11	-1.49	-1.38
W4.50	0.03	-0.02	0.01
I4.51	0.18	-2.77	-2.58
L4.52	0.03	-0.11	-0.08
S4.54	0.03	-0.06	-0.03
A4.55	0.21	-2.11	-1.90
I4.56	0.11	-2.42	-2.32
G4.57	-0.03	0.00	-0.04
P4.59	0.01	-0.07	-0.06
	0.74	-15.50	**-14.76**
Cholesterol A, Protomer B	0.07	-2.52	-2.44
Cholesterol B, Protomer A	0.10	-2.49	-2.39
	0.17	-5.01	**-4.83**
Total kcal/mol	0.91	-20.51	**-19.59**

Residues in bold are residue positions shown to be involved in the TMH4 homodimer inactive state interface of the dopamine D2 receptor [1].

Discussion

In summary, a cholesterol–palmitoyl interaction was suggested to facilitate homodimerization and G protein coupling. This conclusion was further supported by computational models of the OPRM1 homodimer: palmitoyl linked to C3.55(170) can trap cholesterol at the interface of OPRM1 homodimer, which subsequently stabilizes the homodimerization. C3.55 is highly conserved in the Class A Rhodopsin GPCRs, especially in the families like Peptide, Opsin, Olfactory, Thyrotropin-releasing hormone and Melatonin [31]. C3.55(130) on melatonin type 1 receptor contributes to G protein activation [32]. The critical roles played by the homologous residues in G protein coupling/activation have also been confirmed with m5 muscarinic receptor, α_{1b}-adrenergic receptor, AT1 angiotensin receptor, and interleukin-8 receptor as summarized in the GPCRDB [31]. Although the palmitoylation of the other two opioid receptor, δ-opioid receptor and κ-opioid receptor, has not been reported yet, the palmitoylation site in OPRM1 is conserved in the other two opioid receptors, C3.55(151) in δ-opioid receptor and C3.55(161) in κ-opioid receptor. The location of δ-opioid receptors in cholesterol-rich lipid raft and its heterodimer formed with OPRM1 suggested the possible involvement of the palmitoylation on C3.55 in its signaling [33].

The palmitoylation inhibitor 2-BP decreased the normalized net FRET between CFPOPRM1 and YFPOPRM1 to the level of that between CFPC170A and YFPC170A (Fig. 1.3a and Fig. 1.7b). 2-BP also decreased the cholesterol association with signaling complex (Fig. 1.7a). The influences of 2-BP on receptor signaling and G protein coupling

were not determined, because of its inhibitory effect on the membrane targeting of the highly palmitoylated G proteins [29]. Since the effects of 2-BP were consistent with the effects of the C3.55(170) mutation, any conformational changes other than depalmitoylation are not significant in current observations.

The dimerization of GPCRs, including the higher order oligomeric state of rhodopsin, has been reported for a long time [27, 34]. The interface of monomer GPCR has been suggested to be too small for G protein coupling [12]. However, the interaction between GPCR monomer and G protein still can not be excluded. The FRET between CFPC170A and YFPC170A was about 13% of that between CFPOPRM1 and YFPOPRM1 (Fig. 1.3a), whereas the FRET between CFPC170A and YFPGαi2 was about 28% of that between CFPOPRM1 and YFPGαi2 (Fig. 1.4a). This difference suggests that the receptor monomer can still interact with Gαi2, though with a lower affinity than the homodimer.

In the β_2-AR crystal structure, cholesterols are found situated at the intracellular side of the TMH1-TMH4 bundles [3]. Thus, it is probable that localization of OPRM1 within cholesterol- enriched domains such as lipid rafts regulates the cholesterol content within the receptor complex and receptor signaling. Therefore, the cholesterol-enriched lipid raft microdomain may be essential for the ability of the cholesterol–palmitoyl interaction to stabilize receptor homodimerization and G protein coupling.

C3.55(170) palmitoylation affected the amount of cholesterol associated with signaling complex. As reported previously, Gαi2 anchors OPRM1 to the lipid raft

microdomains. Thus by facilitating Gαi2 coupling, cholesterol associated with OPRM1 increases the percentage of receptor in lipid raft microdomains.

The modeling studies reported here show that the C3.55(170) palmitoylation site is located very near the Class A GPCR inactive homodimer interface identified by Guo and co-workers for dopamine D2 receptor [35]. For an OPRM1 homodimer formed at this interface, the cholesterol associated with C3.55(170) is ideally placed to contribute to the total energy of interaction for the homodimer. As Lambert discusses in his recent review [36], the interaction energies at the homodimer interface are likely weak but sufficient to promote dimer formation transiently. We report here that the enthalpic component of the interaction between OPRM1 homodimers is -14.76 kcal/mol and that the presence of cholesterols at the OPRM1 homodimer interface raises the total interaction enthalpy to -19.59 kcal/mol. This modest interaction energy is derived predominantly from VDW interactions, as would be expected for the hydrophobic residues, as well as the hydrophobic cholesterols in the homodimer interface. By identifying a consensus cholesterol binding motif in the TMH2-TMH4 region that predicts cholesterol binding for 44% of human class A receptors, Hanson and co-workers suggest that specific sterol binding is important to the structure and stability of many GPCRs [37]. However, this consensus motif is not present in OPRM1 and does not involve C3.55.

In summary, both experimental data and computational models delineate a cascade from cholesterol–palmitoyl interaction to receptor homodimerization and then to G protein coupling/activation. Conceivably, by regulating cholesterol–palmitoyl interaction, either by the control of cholesterol metabolism or receptor palmitoylation, the stability of

GPCR homodimers is altered, leading to the uncoupling of G protein. In this respect, the cellular cholesterol content, specifically the cholesterol associated with the receptor, represents an additional target through which the signaling of GPCRs can be regulated.

Conclusions

C3.55(170) is the palmitoylation site of OPRM1

OPRM1 is highly palmitoylated. The C3.55(170) has been suggested to be the palmitoylation site indirectly with the fact that the only other two cysteines [C7.63(346) and C7.68(351)] are not the palmitoylation site [7]. Our current studies directly proved that C3.55(170) was the palmitoylation site, for the first time

Cholesterol-palmitoyl interaction can be identified in OPRM1 complex

Cholesterol-palmitoyl interaction has been identified both in the β_2-AR crystal structure [3] and in the OPRM1 in current studies. Although it is not the first time to identify cholesterol-palmitoyl interaction in GPCR, our studies suggested that such interaction may be observed in the signaling complexes of many GPCRs.

Cholesterol-palmitoyl interaction contributes to OPRM1 signaling by facilitating receptor homodimerization and G protein coupling

Our studies reported the contributions of cholesterol-palmitoyl interaction to receptor signaling for the first time. In addition, by the using the different assays,

including FRET, the mechanism underlying these contributions were illustrated. Understanding this mechanism provided additional information on receptor homodimerization and G protein coupling.

Computational modeling of OPRM1 homodimer supported the conclusions listed above

To support the conclusions mentioned above, a computational model of OPRM1 homodimer was generated basing on the structure of other relevant GPCRs. The computational model suggested that cholesterol-palmitoyl interaction provide addition energy to stabilize the homodimer, which was consistent with our other observations.

References

1. Guo, W.; Shi, L.; Filizola, M.; Weinstein, H.; Javitch, J. A., Crosstalk in G protein-coupled receptors: changes at the transmembrane homodimer interface determine activation. *Proc Natl Acad Sci U S A* **2005,** *102* (48), 17495-500.

2. Rasmussen, S. G.; Choi, H. J.; Rosenbaum, D. M.; Kobilka, T. S.; Thian, F. S.; Edwards, P. C.; Burghammer, M.; Ratnala, V. R.; Sanishvili, R.; Fischetti, R. F.; Schertler, G. F.; Weis, W. I.; Kobilka, B. K., Crystal structure of the human beta2 adrenergic G-protein-coupled receptor. *Nature* **2007,** *450* (7168), 383-7.

3. Cherezov, V.; Rosenbaum, D. M.; Hanson, M. A.; Rasmussen, S. G.; Thian, F. S.; Kobilka, T. S.; Choi, H. J.; Kuhn, P.; Weis, W. I.; Kobilka, B. K.; Stevens, R. C., High-resolution crystal structure of an engineered human beta2-adrenergic G protein-coupled receptor. *Science* **2007,** *318* (5854), 1258-65.

4. Claude-Geppert, P. A.; Liu, J.; Solberg, J.; Erickson-Herbrandson, L. J.; Loh, H. H.; Law, P. Y., Antagonist efficacy in MORS196L mutant is affected by the interaction between transmembrane domains of the opioid receptor. *J Pharmacol Exp Ther* **2005,** *313* (1), 216-26.

5. Manglik, A.; Kruse, A.; Kobilka, T.; Thian, F. S.; Mathiesen, J.; Sunahara, R.; Pardo, L.; Weis, W. I.; Kobilka, B. K.; Granier, S., Crystal Structure of the Mu-Opioid receptor bound to a morphinan antagonist. *Nature* **2012**.

6. Probst, W. C.; Snyder, L. A.; Schuster, D. I.; Brosius, J.; Sealfon, S. C., Sequence alignment of the G-protein coupled receptor superfamily. *DNA Cell Biol* **1992,** *11* (1), 1-20.

7. Chen, C.; Shahabi, V.; Xu, W.; Liu-Chen, L. Y., Palmitoylation of the rat mu opioid receptor. *FEBS Lett* **1998,** *441* (1), 148-52.

8. Hawtin, S. R.; Tobin, A. B.; Patel, S.; Wheatley, M., Palmitoylation of the vasopressin V1a receptor reveals different conformational requirements for signaling, agonist-induced receptor phosphorylation, and sequestration. *J Biol Chem* **2001,** *276* (41), 38139-46.

9. Escriba, P. V.; Wedegaertner, P. B.; Goni, F. M.; Vogler, O., Lipid-protein interactions in GPCR-associated signaling. *Biochim Biophys Acta* **2007,** *1768* (4), 836-52.

10. (a) O'Dowd, B. F.; Hnatowich, M.; Caron, M. G.; Lefkowitz, R. J.; Bouvier, M., Palmitoylation of the human beta 2-adrenergic receptor. Mutation of Cys341 in the carboxyl tail leads to an uncoupled nonpalmitoylated form of the receptor. *J Biol Chem* **1989,** *264* (13), 7564-9; (b) Hayashi, M. K.; Haga, T., Palmitoylation of muscarinic acetylcholine receptor m2 subtypes: reduction in their ability to activate G proteins by mutation of a putative palmitoylation site, cysteine 457, in the carboxyl-terminal tail. *Arch Biochem Biophys* **1997,** *340* (2), 376-82.

11. Chini, B.; Parenti, M., G-protein coupled receptors in lipid rafts and caveolae: how, when and why do they go there? *J Mol Endocrinol* **2004,** *32* (2), 325-38.

12. Milligan, G.; Canals, M.; Pediani, J. D.; Ellis, J.; Lopez-Gimenez, J. F., The role of GPCR dimerisation/oligomerisation in receptor signalling. *Ernst Schering Found Symp Proc* **2006,** (2), 145-61.

13. Franco, R.; Casado, V.; Cortes, A.; Ferrada, C.; Mallol, J.; Woods, A.; Lluis, C.; Canela, E. I.; Ferre, S., Basic concepts in G-protein-coupled receptor homo- and heterodimerization. *ScientificWorldJournal* **2007,** *7*, 48-57.

14. Barnett-Norris, J.; Lynch, D.; Reggio, P. H., Lipids, lipid rafts and caveolae: their importance for GPCR signaling and their centrality to the endocannabinoid system. *Life Sci* **2005,** *77* (14), 1625-39.

15. Zheng, H.; Chu, J.; Qiu, Y.; Loh, H. H.; Law, P. Y., Agonist-selective signaling is determined by the receptor location within the membrane domains. *Proc Natl Acad Sci U S A* **2008,** *105* (27), 9421-6.

16. Drisdel, R. C.; Alexander, J. K.; Sayeed, A.; Green, W. N., Assays of protein palmitoylation. *Methods* **2006,** *40* (2), 127-34.

17. Zheng, H.; Loh, H. H.; Law, P. Y., {beta}-Arrestin-Dependent {micro}-Opioid Receptor-Activated Extracellular Signal-Regulated Kinases (ERKs) Translocate to Nucleus in Contrast to G Protein-Dependent ERK Activation. *Mol Pharmacol* **2008,** *73* (1), 178-90.

18. Monika, F.; Leonore, T.; Martin, J. L.; Moritz, B., G Protein Activation without Subunit Dissociation Depends on a Gai-specific Region. *J Biol Chem* **2005,** *280*, 24584-90.

19. Chu, J.; Zheng, H.; Loh, H. H.; Law, P. Y., Morphine-induced mu-opioid receptor rapid desensitization is independent of receptor phosphorylation and beta-arrestins. *Cell Signal* **2008,** *20* (9), 1616-24.

20. Jaakola, V. P.; Griffith, M. T.; Hanson, M. A.; Cherezov, V.; Chien, E. Y.; Lane, J. R.; Ijzerman, A. P.; Stevens, R. C., The 2.6 angstrom crystal structure of a human A2A adenosine receptor bound to an antagonist. *Science* **2008,** *322* (5905), 1211-7.

21. Whitnell, R. M.; Hurst, D. P.; Reggio, P. H.; Guarnieri, F., Conformational memories with variable bond angles. *J Comput Chem* **2008,** *29* (5), 741-52.

22. Guamieri, F.; Wilson, S. R., Conformational Memories and a Simulated Annealing Program That Learns: Application to LTB4. . *J Comp Chem* **1995,** *16*, 648-653.

23. Guamieri, F.; Weinstein, H., Conformational Memories and the Exploration of Biologically Relevant Peptide Conformations: An Illustration for the Gonadotropin-Releasing Hormone. . *J Amer Chem Soc* **1996,** *118*, 5580-5589.

24. Visiers, I.; Braunheim, B. B.; Weinstein, H., Prokink: a protocol for numerical evaluation of helix distortions by proline. *Protein Eng* **2000,** *13* (9), 603-6.

25. Konvicka, K.; Guarnieri, F.; Ballesteros, J. A.; Weinstein, H., A proposed structure for transmembrane segment 7 of G protein-coupled receptors incorporating an asn-Pro/Asp-Pro motif. *Biophys J* **1998,** *75* (2), 601-11.

26. Sali, A.; Blundell, T. L., Comparative protein modelling by satisfaction of spatial restraints. *J Mol Biol* **1993,** *234* (3), 779-815.

27. Liang, Y.; Fotiadis, D.; Filipek, S.; Saperstein, D. A.; Palczewski, K.; Engel, A., Organization of the G protein-coupled receptors rhodopsin and opsin in native membranes. *J Biol Chem* **2003,** *278* (24), 21655-62.

28. Kostenis, E.; Martini, L.; Ellis, J.; Waldhoer, M.; Heydorn, A.; Rosenkilde, M. M.; Norregaard, P. K.; Jorgensen, R.; Whistler, J. L.; Milligan, G., A highly conserved glycine within linker I and the extreme C terminus of G protein alpha subunits interact cooperatively in switching G protein-coupled receptor-to-effector specificity. *J Pharmacol Exp Ther* **2005,** *313* (1), 78-87.

29. Ross, E. M., Protein modification. Palmitoylation in G-protein signaling pathways. *Curr Biol* **1995,** *5* (2), 107-9.

30. Wu, B.; Chien, E. Y.; Mol, C. D.; Fenalti, G.; Liu, W.; Katritch, V.; Abagyan, R.; Brooun, A.; Wells, P.; Bi, F. C.; Hamel, D. J.; Kuhn, P.; Handel, T. M.; Cherezov, V.; Stevens, R. C., Structures of the CXCR4 Chemokine GPCR with Small-Molecule and Cyclic Peptide Antagonists. *Science* **2010,** *330* (6007), 1066-71.

31. Horn, F.; Bettler, E.; Oliveira, L.; Campagne, F.; Cohen, F. E.; Vriend, G., GPCRDB information system for G protein-coupled receptors. *Nucleic Acids Res* **2003,** *31* (1), 294-7.

32. Kokkola, T.; Salo, O. M.; Poso, A.; Laitinen, J. T., The functional role of cysteines adjacent to the NRY motif of the human MT1 melatonin receptor. *J Pineal Res* **2005,** *39* (1), 1-11.

33. (a) Andre, A.; Gaibelet, G.; Le Guyader, L.; Welby, M.; Lopez, A.; Lebrun, C., Membrane partitioning of various delta-opioid receptor forms before and after agonist activations: the effect of cholesterol. *Biochim Biophys Acta* **2008,** *1778* (6), 1483-92; (b)

Law, P. Y.; Erickson-Herbrandson, L. J.; Zha, Q. Q.; Solberg, J.; Chu, J.; Sarre, A.; Loh, H. H., Heterodimerization of mu- and delta-opioid receptors occurs at the cell surface only and requires receptor-G protein interactions. *J Biol Chem* **2005,** *280* (12), 11152-64.

34. Davies, A.; Gowen, B. E.; Krebs, A. M.; Schertler, G. F.; Saibil, H. R., Three-dimensional structure of an invertebrate rhodopsin and basis for ordered alignment in the photoreceptor membrane. *J Mol Biol* **2001,** *314* (3), 455-63.

35. Guo, W.; Shi, L.; Javitch, J. A., The fourth transmembrane segment forms the interface of the dopamine D2 receptor homodimer. *J Biol Chem* **2003,** *278* (7), 4385-8.

36. Lambert, N. A., GPCR dimers fall apart. *Sci Signal* **2010,** *3* (115), pe12.

37. Hanson, M. A.; Cherezov, V.; Griffith, M. T.; Roth, C. B.; Jaakola, V. P.; Chien, E. Y.; Velasquez, J.; Kuhn, P.; Stevens, R. C., A specific cholesterol binding site is established by the 2.8 A structure of the human beta2-adrenergic receptor. *Structure* **2008,** *16* (6), 897-905.

CHAPTER II

COMPARISON OF THE MOR R HOMOLOGY MODEL AND THE MOR CRYSTAL STRUCTURE

Introduction

The opioid receptors, delta, kappa and mu, belong to the Class A subfamily of G-Protein Coupled Receptors (GPCRs). GPCRs are integral membrane proteins with seven transmembrane helices (TMHs) arranged to form a closed bundle with loops that extend both extracellularly and intracellularly. The N-terminus is extracellular and the C-terminus is intracellular, but begins with a short helix (called Helix 8) that follows the end of TMH7, but runs parallel to the membrane. Until recently, the only Class A GPCR x-ray crystal structure available was that of rhodopsin.[1] After 2007, the field exploded starting with x-ray structures became available for the carazolol bound beta-2-adrenergic (β 2-AR),[2,3] and followed quickly by the β1 adrenergic receptor (β1-AR),[4,5] the adenosine A2A receptor,[6,7] the CXCR4 receptor,[8] the dopamine D3 receptor,[9] the histamine H1 receptor,[10] and the S1P1 receptor.[11] In 2012, the nociception/orphanin FQ receptor[12] and the mu[13], delta[14] and kappa[15] opioid receptor crystal structures were published.

Prior to the release of the MOR crystal structure, the best way to determine receptor structure was to build a homology model using one of the known structures as a template model. Therefore, in preliminary work, an inactive, R state MOR computational

model was built using the β2-AR crystal structure[2,3] as a template with substitutions for TMH 1, 2, 4 and 7 based on sequence divergences, as described in methods. This model was then used for studies of the MOR including analyzing the receptor for cholesterol and palmitoylaiton interactions as well as modeling a homodimer interface for the MOR based on experimental data.[16] The work described herein compares the inactive state MOR model with the antagonist bound MOR crystal structure.

Methods

Construction of the initial MOR R state model

Initially a homology model of the MOR was built using the β2-adrenergic receptor crystal structure (2rh1) as the template. The model was constructed by first aligning the mu sequence with that of the β2-AR template using the highly conserved Class A GPCR sequence motifs (TMH3 E/DRY; TMH6 CWXP; TMH7 NPXXY) or highly conserved residues (N1.50, D2.50, W4.50, P5.50) as the alignment guides. The structure of the template was mutated to the corresponding mu residues using Maestro (Schrodinger 2006). Mu receptor helices that diverged from the template structure in the location of helix deforming residues such as prolines or glycines were then identified. The conformations possible for such helices (TMH2, TMH4 and TMH6) were studied using Conformational Memories[17,18] (described below) and an appropriate substitute helix was incorporated into the model. The TMH7 / helix 8 region was modeled using the adenosine A2A crystal structure[6] based on the fact that the mu opioid and adenosine

A2A receptors have two residues in the elbow region of TMH7, whereas the β2-AR only has one residue in the elbow region. Extracellular and intracellular loops as well as the N- and C- termini were added using Modeller.[19, 20, 21] A short, 5ns molecular dynamics simulation of the resultant model in a POPC bilayer was performed using NAMD.[22] The output was analyzed and was compared to the initial MOR model to determine any significant changes.

After building the initial MOR model, new crystal structures were released that provided additional information about receptor structure. A new sequence alignment using the CXCR4[8] and dopamine D3[9] crystal structures was completed. Changes to the initial model were made on TMH 1, 2, 6, and 7 based on the MD output and the new information from the CXCR4 and dopamine D3 receptor crystal structures. Extracellular and intracellular loops were added to the revised model (specifics described below) using Modeller.[19-21] The N- and C- termini were preserved from the original model and minimally adjusted such that there were no overlaps with the new receptor.

Specific Changes to Original MOR Model

TMHs 1 and 7**:** Using N1.50 as the alignment guide for TMH1 and P7.50 as the guide for TMH7, the sequence alignment was studied. Originally, the β2-AR TMH1 was used for the MOR model since rhodopsin has a proline in TMH1 and the MOR does not. In the original model, the adenosine A2A TMH7/Hx 8 region was used as the template of the MOR model since there are two residues in the elbow region of the mu opioid receptor and the adenosine receptor, but only one residue in the β2-AR. Upon further

examination of the CXCR4 and dopamine D3 structures, it was determined that the dopamine D3 receptor would be a better match for the MOR model based on receptor packing between TMH1 and TMH7 as there were packing issues using the Adenosine A2A TMH7 and β2-AR TMH1.

TMH2: The alignment for TMH2 centered upon the conserved D2.50 residue seen in Class A GPCRs. Additionally, there is a proline at position 2.58 or 2.59 in most Class A GPCRs. In the initial model, Conformational Memories was used to determine a structure for TMH2 since the MOR has a P2.58 whereas the β2-AR has a P2.59. Upon the release of the CXCR4 crystal structure, we decided to use TMH2 from it since it also had a P2.58. The sequence was mutated and superimposed onto the template structure and incorporated into the revised MOR model.

TMH6: In the initial model Conformational Memories was used to select an appropriate TMH6 for the wild type inactive state MOR model. The improvement to the model was obtained by incorporating the information from the short MD simulation. The MD simulation showed that at the extreme extracellular end of TMH6, K6.58 had rotated to the outside of the bundle rather than pointing directly into the bundle and binding pocket. An evaluation of published mutations studies showed that K6.58 was not likely to be pointed into the receptor. Therefore, in the revised model of the MOR, the CM TMH6 was used however; the backbone dihedral values of P6.50-V6.61 were adjusted to match the TMH6 from the MD simulation.

Extracellular and Intracellular Loops

Extracellular (EC) and intracellular (IC) loops were added to the MOR R model using Modeller.[19-21] Each of the three extracellular and intracellular loops was varied in the presence of the transmembrane receptor region. To preserve the binding pocket, the naloxone/MOR R complex was used as the model to which the loops were added. MODELLER is a Monte Carlo technique described by Fiser et al. in 2000 that uses a template library of possible side chain conformations from the Protein Data Bank for all amino acids. Using the CHARMM force field, each loop is varied and assigned an objective function ranking value. The objective function is based on steric interactions and hydrogen bonding of each possible conformation. The 250 loops with the lowest objective function were used for further analysis.

Restraints were put on the EC2 loop of the MOR such that the conserved disulfide bridge between C3.25 and a cysteine in the EC2 loop was intact as seen in the crystal structures of rhodopsin,[1] the β2-AR,[2-3] β1-AR,[4] adenosine A2A,[6] CXCR4[8] and dopamine D3[9] receptors. Additionally, an EC2 loop was selected for the MOR model with a Cβ-Cβ distance between D218 in the EC2 and H7.36 consistent with experimental data which show a zinc binding site between the two residues.[23] In each of the Class A GPCRs mentioned herein, the second residue after the cysteine in the EC2 loop that participates in the disulfide bridge points down into the transmembrane bundle and was therefore one of the criterion in selecting the EC2 loop. After examination of the CXCR4 EC2 loop[8] and the MOR sequence, it was decided that the last four residues of the MOR EC2 loop

(trp-tyr-trp-glu) were likely a helical extension of the extracellular portion of TMH5 in the MOR and was modeled as such.

Lacking structural information about the remaining five loops, Modeller output was assessed to ensure that each loops structurally made sense, e. g. hydrophobic residues close to the lipid bilayer were pointing into the receptor rather than directly positioned in water. The N and C termini were added 14 residues at a time with the last 3 residues of the previous section being allowed to vary with the 14 residues of the new section. Due to the length of the MOR N-terminus and the associated problems of correct simulation of long peptide segments, the first 39 residues of the MOR N-terminus were truncated, which has been shown experimentally to retain full activity.[24]

Results

Comparison of the Transmembrane Region

To compare the MOR Model and the MOR crystal structure[13], the model was superimposed onto the crystal structure using the X.50 residue Cα in each helix (N1.50, D2.50, R3.50, W4.50, P5.50, P6.50, and P7.50). The two receptors were then analyzed and important similarities and differences were observed. As shown in Figure 2.1 from an extracellular view point, the MOR Model (dark purple) and the MOR crystal structure (magenta) overlay very similarly. The intracellular region has been colored gray in both structures and the loops removed for clarity.

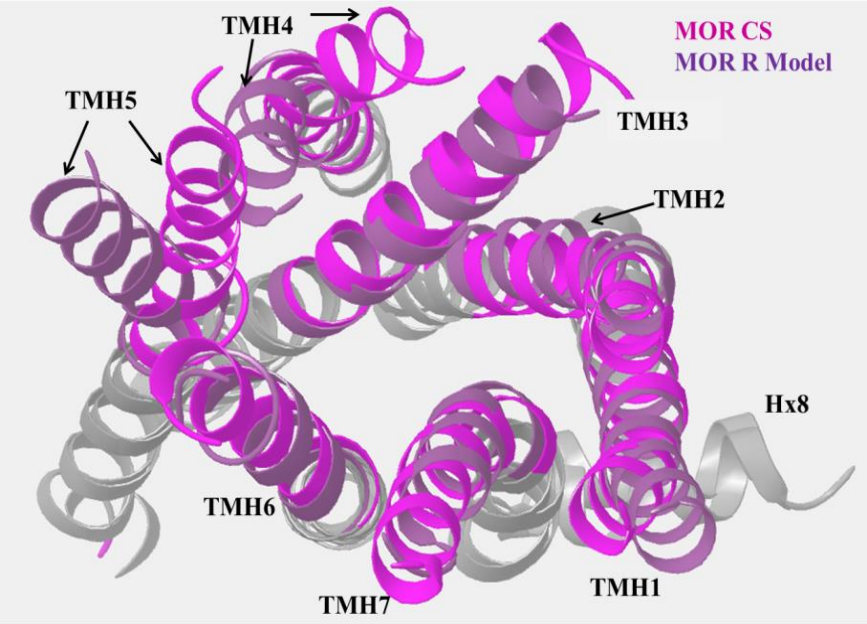

Figure 2.1. An extracellular view of the MOR model (dark purple) superimposed with the MOR crystal structure (magenta). Significant differences include the EC ends of TMH 4 and 5. Loops have been removed and the intracellular portions colored gray for clarity.

As shown, TMH 1, 2, 6 and 7 overlay very nicely in the superimposed image of the MOR CS and the MOR R Model. There is a slight shift in the extreme extracellular end of TMH1, which can be seen in a view from lipid in Figure 2.2a. Additionally, there is a small difference in the extracellular end of TMH3, which is due to the EC2 loop in the MOR crystal structure. TMH4 and TMH5 have large differences in the extracellular end between the MOR Model and the MOR crystal structure, as shown in Figures 2.1 and 2.2b.

Figure 2.2a, shows TMH5, TMH6, TMH7 and TMH1 of the MOR crystal structure (magenta) and MOR R model (purple) in a side view from lipid. As shown, there is a slight different in the extreme extracellular end of TMH1. TMH5 is pulled

back further in the MOR R model than in the crystal structure at the extracellular end, after P5.50. Both TMH6 and TMH7 are identical in the model and in the crystal structure. In the MOR model, we added an additional helical turn at the extracellular end of TMH6, as described in Methods, based on a 5ns MD simulation. This additional turn is seen in the MOR crystal structure, validating the MD simulation output structure.

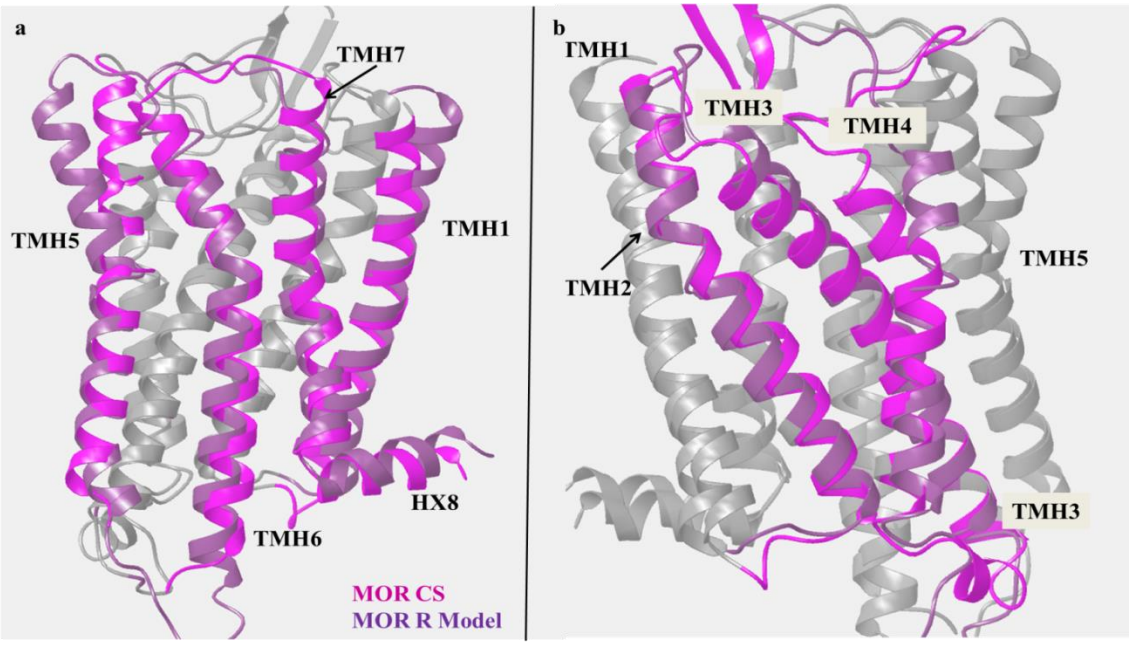

Figure 2.2. Views from lipid of each side of the MOR CS and MOR R Model superimposed. 2a shows TMH5, 6, 7 and 1 with the crystal structure in magenta and the MOR R model in purple. 2b shows TMH2, 3 and 4 in the same color scheme.

Figure 2.2b shows TMH2, TMH3 and TMH4 in the same color scheme. As illustrated, it can be seen that TMH2 in the MOR model and the MOR crystal structure are identical matches and that TMH3 is extremely similar, the only exception being the extreme extracellular end of the helix. In the MOR crystal structure, the EC2 loop pushes

the extracellular portion of TMH3 away from the bundle, which is the difference between the crystal structure TMH3 and the MOR model TMH3.

The largest difference between the MOR crystal structure and the MOR R model is that of TMH4, seen in Figure 2.2b. Using Conformational Memories, TMH4 was modeled starting from a perfect alpha helical helix. The helix selected for the model was believed to bend into the receptor between TMH3 and TMH5, as seen in many crystal structures.

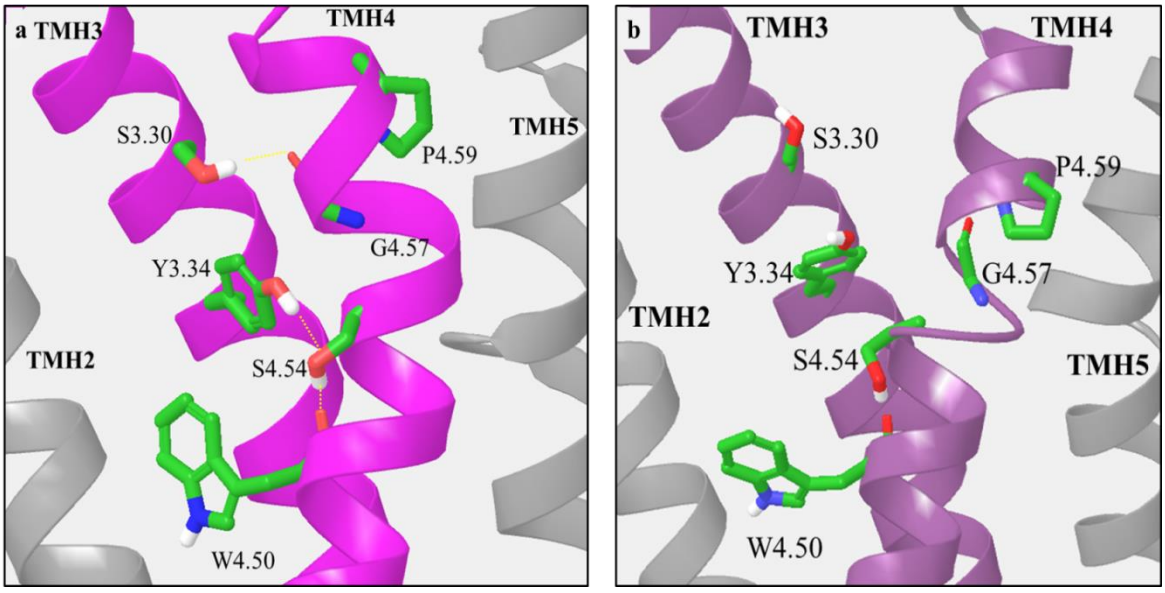

Figure 2.3. Intrahelical TMH3 / TMH4 hydrogen bonding network residues seen from lipid. 3a. shows the intact hydrogen bonding network comprised of S3.30, Y3.34, G4.57, S4.54 and W4.50 in the MOR crystal structure. 3b. Residues involved in the TMH3 / TMH4 hydrogen bonding network in the MOR model showing the network is broken.

However, in the published MOR crystal structure, that was not the case and TMH4 kinked backwards and bent towards TMH3 at the extracellular end. Upon examination of

the crystal structure, an intrahelical hydrogen-bonding network between TMH3 and TMH4 became clear, as shown in Figure 2.3.

The TMH3 / TMH4 hydrogen bonding network in the MOR crystal structure (Figure 2.4a) is comprised of S3.30, Y3.34, G4.57, and S4.54. Here the lipid facing Y3.34 hydroxyl interacts with the polar sidechain of S4.54 and S3.30 forms a hydrogen bond with the backbone carbonyl of G4.57. Also, S4.54 forms a hydrogen bond with the backbone carbonyl of W4.50. This network pulls TMH4 towards TMH3 and away from TMH5. The P4.59 provides additional kinking of TMH4 at the extreme extracellular end of TMH4. In the MOR R model (Figure 2.3b) the hydrogen bonding network is broken. While S4.54 is interacting with the backbone carbonyl of W4.50, neither Y3.34 nor S3.30 is interacting with residues on TMH4.

Previously published work shows that C3.55 is the palmitoylation site on the MOR[16] (see Chapter 1). The same work also shows that cholesterol is located in the same vicinity of the palmitate and that cholesterol is in fact needed for maximal signaling and dimerization of the mu opioid receptor. In the MOR model, we modeled the palmitate and a cholesterol molecule in a cavity formed by the intracellular transmembrane region of TMH 3, 4 and 5, consistent with experimental data. In Figure 2.4, the MOR model (right, dark purple) and the crystal structure (left, magenta) are shown along with residues Y3.51 and C3.55. The MOR crystal structure did not have any cholesterol or the palmitoylation site crystallized with the receptor.[13] As shown, in the MOR model, Y3.51 is behind C3.55 and the palmitate side chain towards TMH5. However, in the crystal structure, it can be seen that Y3.51 is blocking access to C3.55.

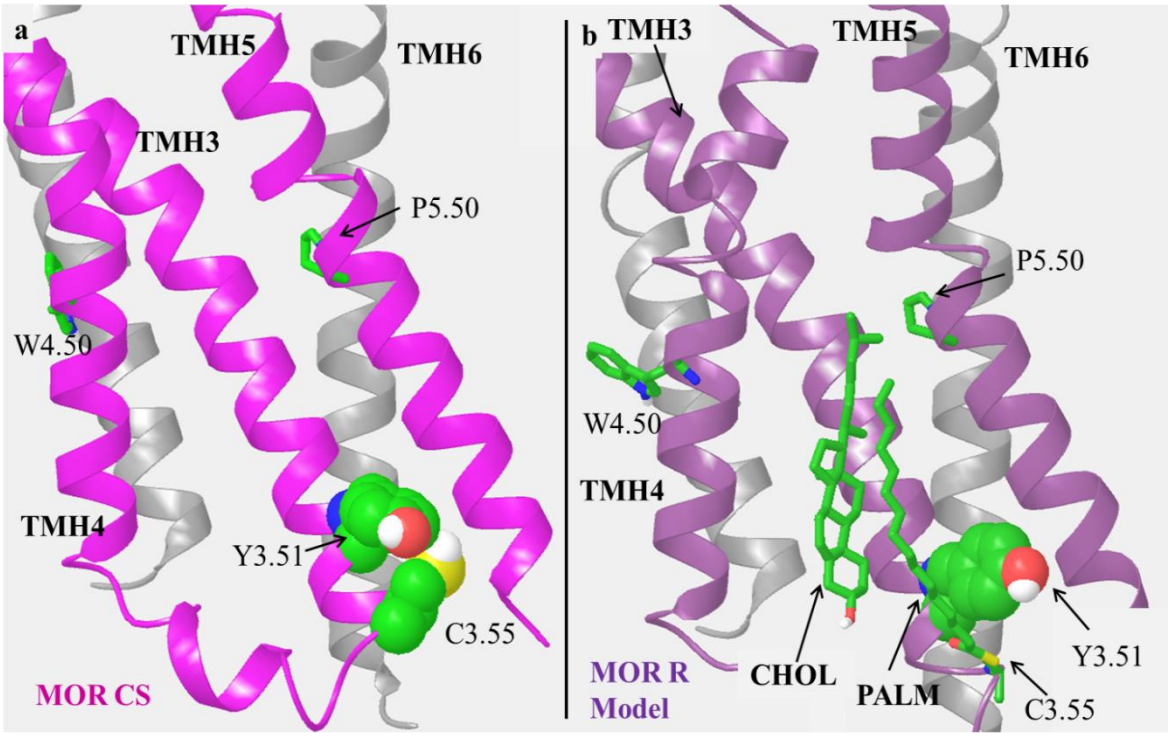

Figure 2.4. A view from lipid showing the palmitoylation site, C3.55 of the MOR crystal structure (4a) and the MOR R Model (4b). In the crystal structure, access to C3.55 is blocked by Y3.51 and the intracellular end of TMH4 is wound tightly. However, in the MOR R Model, Y3.51 is behind C3.55. The palmitate is attached and the cholesterol has been docked. W4.50 and P5.50 have been displayed for reference purposes.

Comparison of the Loop Region

Predicting loop regions can be very difficult since they generally have no set structure and are flexible in their water like environment. The MOR model was comprised of an N-terminus, C-terminus and all three extracellular and intracellular loops. The MOR crystal structure was crystalized without the N or C termini, and had a T4 lysozyme fused to the IC3 loop, which was partially missing.

The most significant loop is the EC2 loop. The MOR does exhibit the conserved disulfide bridge between a cysteine in the EC2 loop and C3.25, as seen in many Class A GPCRs. We selected an EC2 loop for the MOR model also using the criterion that the

second residue after the disulfide cysteine (a leucine) is pointing down into the binding pocket. In every Class A GPCR crystal structure thus far, the second residue after the disulfide cysteine has pointed into the bundle, regardless of the residue and its charge. This residue varies widely from isoleucine in rhodopsin and opsin, to a phenylalanine in the beta adrenergic receptors and an arginine in the CXCR4 receptor. The MOR crystal structure proves no different; the leucine, two residues after the disulfide bridge in the E2 loop, is pointing down into the binding pocket. The EC2 loop in the crystal structure also has a parallel beta sheet before the disulfide bridge. This beta sheet is seen in other receptors, like rhodopsin, but not necessarily the same residues. Unlike the MOR model, the EC2 loop in the crystal structure is pushed back and out towards TMH3 such that the center of the receptor is uncovered and open. While this is unusual, this behavior is also seen in the CXCR4 crystal structure.

Two other loops have differences between the MOR model and the crystal structure. The IC2 loop in the MOR crystal structure has a helical portion, which is unlike many other crystal structures. Also, the C-terminal portion of the EC3 loop is helical and forms a helical extension at the top of TMH7. In many of the available crystal structures (rhodopsin, adenosine A2A and CXCR4), there is a helical extension of the intracellular end of TMH6 from the IC3 loop. In the MOR model, this six residue extension was added. The MOR crystal structure has an intracellular TMH 6 helical extension, consistent with the model. However, the extension in the crystal structure is only three residues, not the six that were modeled. It is impossible to know for sure based on this structure if the extension should be three or six residues, or possibly none at

all since the T4 lysozyme was fused to the IC3 loop and could be perturbing the structure in this area.

Dimer Interface of the MOR Crystal Structure and MOR Model

The dimer interface in the inactive MOR was predicted to be along the TMH4 / TMH5 interface, as discussed in the previous chapter based on experimental information on the dopamine D2 receptor.[25] The residues on TMH4 involved in this dimer interface are N4.41, I4.44, C4.48, I4.51, A4.55 and P4.59, shown in Figure 2.5. The cholesterol bound to protomer A interacts with R4.40, N4.41, K4.43, I4.44 and V4.47 on protomer B. Likewise the cholesterol on protomer B interacts with residues on protomer A. Thus dimer interface is enhanced by the palmitate attached to C3.55 and presence of cholesterol. In the MOR model dimer interface, the cholesterol is packed between intracellular TMH3 and TMH4 and the palmitoyl group on C3.55 and is unable to leave the interface.

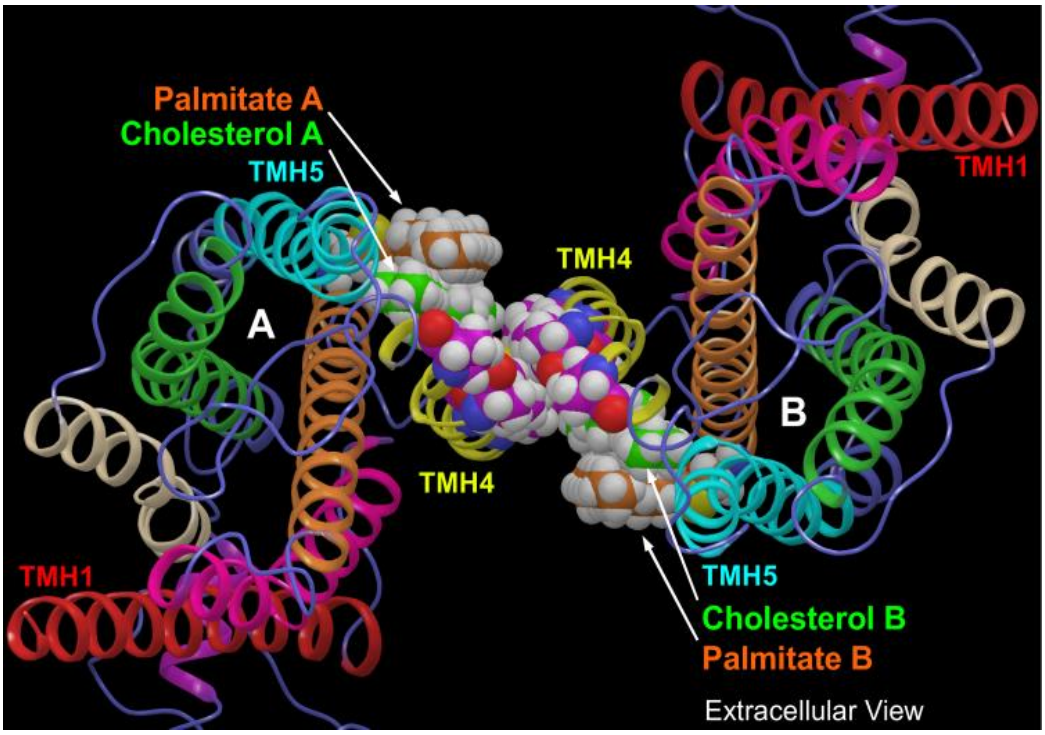

Figure 2.5. An extracellular view of the MOR model dimer interface. The residues on TMH4 involved in the interface are N4.41, I4.44, C4.48, I4.51, A4.55 and P4.59. The palmitate has been added to C3.55 on each protomer, as has the cholesterol. The cholesterol is locked in position by the intracellular end of TMH3 and the palmitate group.

The MOR was crystallized with two dimer interfaces, TMH5 / TMH6 and a TMH 1/TMH7/Hx interface.[13] The TMH5 / TMH6 dimer interface is the same interface seen in the CXCR4 crystal structure,[8] and was reported to be much stronger than the TMH1/TMH7/Hx8 interface in the MOR crystal structure paper. Figure 2.6 is an extracellular view of the TMH5/TMH6 crystallized dimer interface of the MOR. Protomer A is on the right, with TMH5 and TMH6 shown in blue ribbon and Protomer B is on the left with TMH5 and TMH6 shown in lime ribbon. In each protomer, TMH4 is red and TMH7 is magenta and other helices are gray.

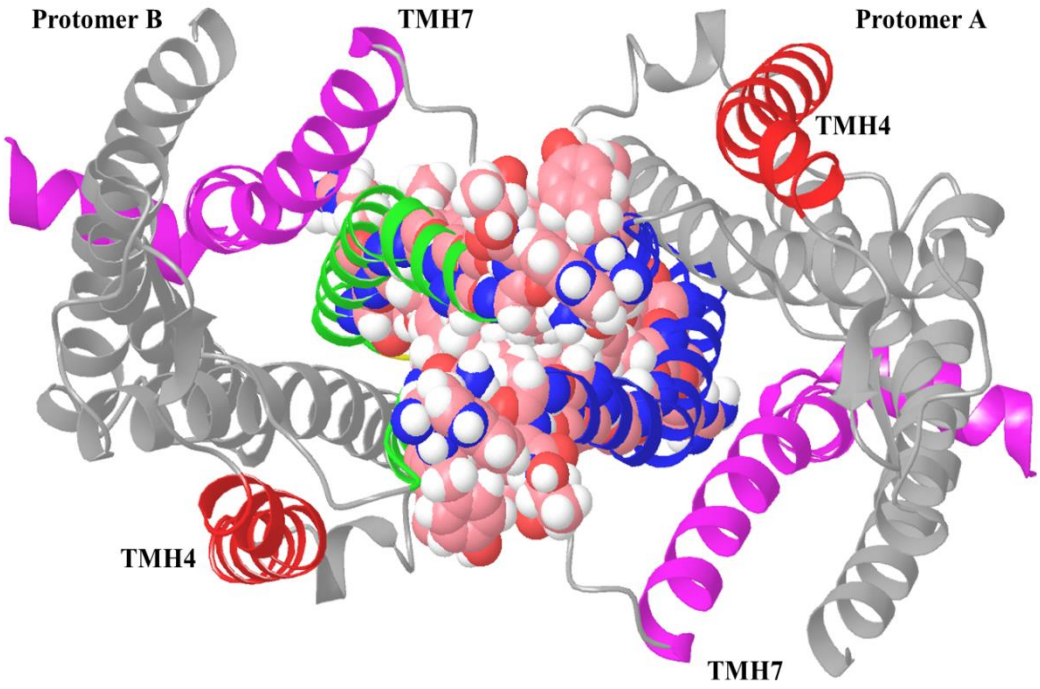

Figure 2.6. An extracellular view of the crystallized MOR TMH5/TMH6 dimer interface. TMH5/6 of Protomer A is shown in blue ribbon, and TMH5/6 of Protomer B is shown in lime ribbon. Residues involved are shown in pink.

The residues involved in the reported dimer interface on TMH5 includeY5.33, N5.36, L5.37, I5.40, F5.43, I5.44, F5.47, I5.48, V5.51, L5.52, T5.55, Y5.58, M5.61, I5.62, and L5.63. The TMH6 residues in the dimer interface include T6.34, R6.35, L6.38, I6.45, T6.49, I6.53, I6.56, I6.57, L6.60, and I6.61.[13] Additionally, the crystallized dimer interface includes residues on the T4 lysozyme, which was fused to the IC3 loop of both protomers.

Discussion

Transmembrane Region Comparison

TMH1 & TMH7: The MOR model was completed using TMH1 and TMH7 from the dopamine D3 receptor[9] instead of using the β2-AR template.[2-3] The β2-AR has only one residue in the elbow region, while the MOR has two residues and thus the placement of helix 8 would have been incorrect had the β2-AR TMH7 been used. Additionally, the β2-AR has a W7.40, which prevents TMH1 from packing closely to TMH7. While the dopamine D3 receptor has this same W7.40, it has a different orientation of the residue and allows for much better packing of the TMH1 / TMH7 interface. Although TMH1 bends in slightly at the extracellular end in the MOR crystal structure, TMH1 and TMH7 were almost identical between the MOR model and MOR crystal structure, as shown in Figure 2.3a. In the MOR crystal structure, TMH7 does have an additional ½ turn at the extracellular end, formed by the last three residues of the EC3 loop.

TMH2: In the initial MOR R model, Conformational Memories was used to determine a suitable TMH2 since the β2-AR template structure has a P2.59 but the MOR has a P2.58. The CM output helix showed that residue 2.60 would face into the binding pocket of the MOR, whereas in the β2-AR, this residue faces the TMH2/TMH3 interface. By using the CXCR4 crystal structure[8] TMH2 instead for the MOR model, we were able to use a known helix with similar characteristics to the MOR TMH2 in our model. Compared with the crystal structure, TMH2 of the MOR model was virtually perfect in both shape and special position within the receptor (see Figure 2.2b).

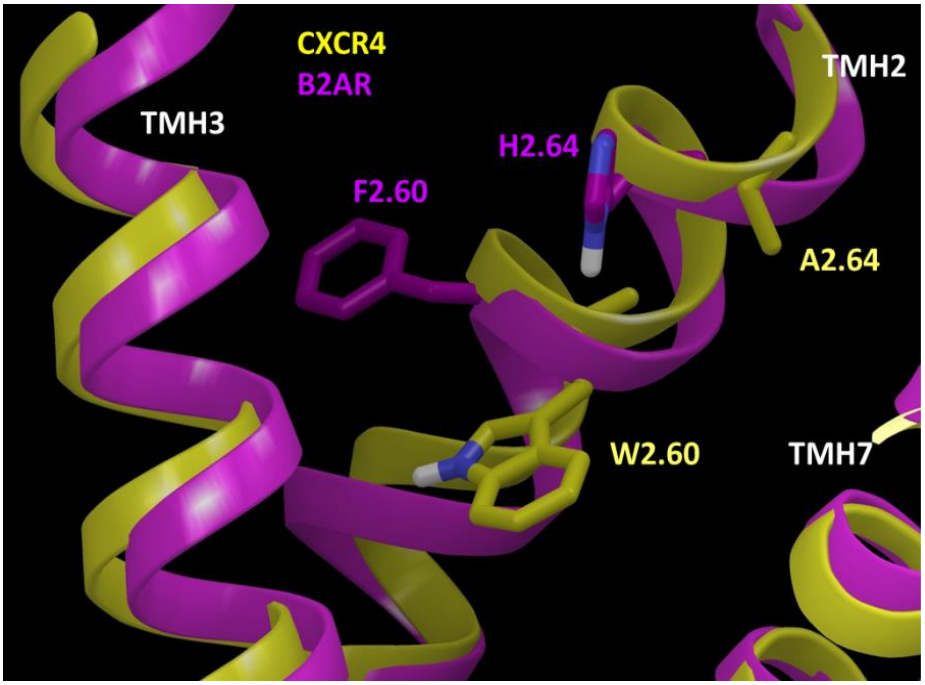

Figure 2.7. A view of TMH2 looking through TMH6 of the β2-AR (purple) and CXCR4 (yellow) superimposed crystal structures. As shown, the Cα residues of 2.60 and 2.64 change greatly due to a P2.59 (β2-AR) vs. a P2.58 (CXCR4).

TMH2 of the β2-AR and CXCR4 receptors was superimposed and the residue location changes due to a proline can be seen in Figure 2.7. As depicted, W2.60 in the CXCR4 crystal structure faces into the binding pocket, while F2.60 in the β2-AR faces towards TMH3. Additionally, A2.64 in CXCR4 faces TMH7; however H2.64 in the β2-AR is rotated away from TMH7 and towards TMH3.

The CXCR4 and MOR also have a T2.56, 2 residues prior to the P2.58, which face lipid. In the CXCR4 crystal structure, T2.56 undertakes a g- conformation.[8] Thus, it was determined that in the MOR, this residue was likely in a g- conformation and that using the CXCR4 crystal structure TMH2 was a valid option. The CXCR4 crystal

structure also validates work by Ballesteros and colleagues in 2000 showing that a lipid facing serine or threonine can be in a g- conformation to satisfy its hydrogen bond.[26]

TMH3: In the MOR model, TMH3 was not pushed back at the extracellular end, as it is in the MOR crystal structure[13] (see Figure 2.2b). This pushback in the MOR crystal structure is due to the conformation of the EC2 loop, which leaves the extracellular portion of the receptor open by forcing the end of TMH3 outwards. Although this portion of TMH3 is different, the relative position of the helix in the bundle as well as D3.32, a ligand binding residue was seamless upon superimposition. The position of D3.32 is important for both ligand binding as well as for a D3.32/Y7.43 interaction. This interaction is seen in many Class A GPCR crystal structures, including the β1-AR,[4] β2-AR,[2-3] dopamine D3,[9] and the histamine H1[27] receptors. This interaction was incorporated into the MOR model, and is also seen in the MOR crystal structure.

TMH4 and TMH5: The largest difference between the MOR model and the MOR crystal structure was the extracellular positioning of TMH4 and TMH5, as shown in Figures 2.1 and 2.2. The TMH4 selected from the Conformational Memories output for the MOR model incorporated the belief that S4.54 could be in a g- conformation. This conformation combined with G4.57 and P4.59 produced an additive effect in the TMH4 in the model such that TMH4 bent into the bundle between TMH3 and TMH5. Due to this bend into the bundle, the P5.50 allowed TMH5 to be pushed back at the extracellular end, as seen in Figure 2.3. The crystallized conformation of TMH4 in the MOR shows that S4.54 is in a g+ conformation and is involved in an intrahelical hydrogen bonding network with TMH3. This network was not able to be predicted based on the crystal

structures or mutation data available at the time of its development. In the TMH3/TMH4 hydrogen bonding network, the lipid facing Y3.34 hydroxyl interacts with the polar sidechain of S4.54 and S3.30 forms a hydrogen bond with the backbone carbonyl of G4.57.

In the CXCR4 crystal structure,[8] the EC end of TMH5, coming off the EC2 loop has an extra helical turn formed by the last four residues of the EC2 loop, Asp-Leu-Trp-Val. In the MOR sequence, the corresponding residues are Trp-Tyr-Trp-Glu. Based on the CXCR4 crystal structure and the similarity in the EC2 loops of the CXCR4 and MOR, we modeled this additional helical turn at the EC end of TMH5. This additional turn is seen in the MOR crystal structure and aids in validating the MOR model.

TMH6: Class A GPCRs have a conserved CWXP motif in TMH6. In the β2-AR, the region is CWLP, while in the MOR, the region is CWTP. While the leucine and threonine residues are both beta-branching residues, the threonine is slightly smaller and has more flexibility than the leucine. Therefore, we employed the Conformational Memories technique to determine a plausible structure for TMH6 in the MOR model. As seen in Figures 2.1 and 2.2a, the TMH6 in our model superimposes perfectly with the TMH6 in the MOR crystal structure.

Conformation of Specific Residues in the Inactive State Receptor

The structural characteristics that define the GPCR inactive (R) and active (R*) states have been deduced primarily from biophysical studies of rhodopsin and the β2-AR receptor. In the inactive or off state (R), the intracellular (IC) end of TMH6 is bent

towards TMH3 and a salt bridge between R3.50 and E/D6.30 on the intracellular side of the TMH bundle forms an "ionic lock". In the activated state, TMH6 undergoes a conformational change, straightening in the highly conserved CWXP hinge region.[28, 29, 30, 31, 32, 33] This results in the intracellular ionic lock breaking as TMH3 and TMH6 move away from each other.[34] Previous studies have shown that while the MOR does not form an "ionic lock" at the exact same location as rhodopsin, it does form a strong hydrogen bond between R3.50 and T6.34[35] that serves the same purpose for MOR. The R3.50 and T6.34 interaction is indeed present in the μ-opioid crystal structure with antagonist β-FNA present.[13]

The ionic lock in the MOR comprised of R3.50 and T6.34, was incorporated into the MOR Model. In Class A GPCR crystal structures, the ionic lock has not been intact in any structure except for the MOR crystal structure when a T4 lysozyme has been fused to the IC3 loop between TMH5 and TMH6. While the ionic lock was intact in the MOR structure, it is possible that the T4 lysozyme has perturbed the structures of the intracellular portions of TMH5 and TMH6 in other receptors, and possibly the MOR, due to its size and proximity to the receptor.

The change from the inactive to active states also results in changes within the ligand binding pocket. In the R state, a tryptophan residue in the CWXP motif on TMH6, W6.48, adopts a $g+$ χ^1 dihedral angle. This conformation in rhodopsin is due to the close proximity of the beta-ionone ring of rhodopsin's covalently bound ligand, 11-cis-retinal to W6.48, such that the tryptophan is locked in place.[36,37,1] W6.48 is part of the highly conserved TMH6 CWXP motif and has been identified as important for GPCR activation

through early mutagenesis studies. A recent x-ray crystal structure of a constitutively active rhodopsin mutant suggests that when rhodopsin is activated and undergoes the isomerization of 11-cis retinal to all-trans-retinal, the beta-ionone ring is shifted 4.3Å towards the cleft between TMH5 and TMH6 and W6.48 is released from its locked position. The indole group of W6.48 moves 3.6Å away from its ground-state position as a consequence of rhodopsin activation[38] and W6.48 undergoes a change in its $\chi 1$ angle from *g+* → *trans*.[39] Although this change is not seen in recent activated GPCR crystal structures, it is possible that such a change is transient and therefore not captured in the crystalline state. In fact, in molecular dynamics simulations of cannabinoid CB2 receptor activation by its endogenous ligand, we observed such a transient change in W6.48.[40] Likewise, a rotameric change of W6.48 has been documented to occur in microsecond long molecular dynamics simulations[12] of the β-2 adrenergic receptor in complex with the Gs protein.

We modeled the W6.48 in the MOR in the inactive, g+ conformation. The MOR was crystallized with β-FNA, a covalently bound antagonist.[13] In the MOR crystal structure, W6.48 is indeed in the g+ conformation. Upon superimposition, not only are the backbone residues of TMH6 in the MOR model and the MOR crystal structure seamless, but the conformation and relative position of W6.48, both backbone and sidechain, are seamless as well.

MOR Dimer Interface

Experimental studies (Chapter 1) suggest that both cholesterol and palmitoylation of the MOR facilitates MOR homodimer formation and signaling of the MOR.[16] These studies also show that the palmitoylation site of the MOR is located at C3.55, not the C-terminus as seen in most Class A GPCRs. This palmitoylation site may be conserved in the DOR and KOR, as they both have the conserved C3.55, but experimental studies of both receptors are needed to verify this palmitoylation site. Using the MOR model described herein as well as the experimental data for cholesterol and MOR palmitoylation, a possible MOR homodimer interface was modeled (Figure 2.5). This interface is equivalent to the one experimentally shown in the dopamine D2 receptor by Guo and collogues.[25] In the MOR, the dimer interface involves N4.41, I4.44, C4.48, I4.51, A4.55 and P4.59. In the dimer, cholesterol is packed against TMH3 and TMH4 and locked in place by the palmitoyl attached to C3.55 and TMH5.

The MOR crystal structure shows two different dimer interfaces, TMH5/TMH6 interface showing in Figure 2.6 and a TMH1/TMH7/helix 8 interface.[13] The TMH5/TMH6 dimer interface in the MOR is the same as the dimer interface seen in the CXCR4 crystal structures; however the MOR dimer interface involves more residues with better packing than the CXCR4 dimer interface. The residues involved in the reported dimer interface of the MOR on TMH5 include Y5.33, N5.36, L5.37, I5.40, F5.43, I5.44, F5.47, I5.48, V5.51, L5.52, T5.55, Y5.58, M5.61, I5.62, and L5.63. The TMH6 residues in the MOR dimer interface include T6.34, R6.35, L6.38, I6.45, T6.49, I6.53, I6.56, I6.57, L6.60, and I6.61.

The MOR was crystallized with a T4 lysozyme fused to the intracellular 3 (IC3) loop region of the receptor. In the TMH5/TMH6 dimer interface, the T4 lysozymes of both protomers are in close proximity and interact with each other. Johnston and Filizola presented work at the Biophysical Society Conference in 2013 on the stability of the dimer interfaces in the MOR.[41] Using umbrella sampling molecular dynamics calculations, they were able to show that the TMH5/TMH6 dimer interface in the MOR was favored over the TMH1/TMH7/helix 8 dimer interface. The calculated free energy of dimerization of the TMH5/TMH6 interface was -11.8kcal/mol while the TMH1/TMH7/helix 8 interface was -4.1kcal/mol. Additionally, it was shown in simulations with the MOR homodimer and T4 lysozyme, the two MOR protomers could be pulled apart easily but that the T4 lysozyme maintained a strong interaction. The T4 lysozyme interactions were substantial enough to cause a distortion in the membrane. Thus, it cannot be ruled out that the TMH5/TMH6 dimer interface in the MOR is initiated by the T4 lysozymes, not by the transmembrane MOR protomers. Cross-linking studies are needed to aid in the determination of the physiological homodimer interface in the MOR.

Conclusions

The validity of computational homology modeling of GPCRs has been an area of debate in many circles. However, our MOR model comparison with the MOR crystal structure helps to validate the usefulness and accuracy of homology modeling. The

inactive state MOR model was very similar to the antagonist bound MOR crystal structure. The ionic lock, D3.32/Y7.43 interaction and locations of helices relative to the receptor as a whole were seen in both the MOR model and the MOR crystal structure. The ability of lipid facing serines and threonines to undertake a g- conformation was confirmed with the conformation of 11 transmembrane serines/threonines in the MOR crystal structure in a g- conformation including T2.56. Although the extracellular ends of TMH4 and TMH5 were different from the crystal structure, the underlying intrahelical hydrogen bonding network causing these changes could not be predicted based on known crystal structures. Overall, homology modeling is a good tool to keep in the toolbox for determining GPCR structure.

References

1. Palczewski, K.; Kumasaka, T.; Hori, T.; Behnke, C. A.; Motoshima, H.; Fox, B. A.; Le Trong, I.; Teller, D. C.; Okada, T.; Stenkamp, R. E.; Yamamoto, M.; Miyano, M., Crystal structure of rhodopsin: A G protein-coupled receptor. *Science* **2000,** *289* (5480), 739-45.

2. Rasmussen, S. G.; Choi, H. J.; Rosenbaum, D. M.; Kobilka, T. S.; Thian, F. S.; Edwards, P. C.; Burghammer, M.; Ratnala, V. R.; Sanishvili, R.; Fischetti, R. F.; Schertler, G. F.; Weis, W. I.; Kobilka, B. K., Crystal structure of the human beta2 adrenergic G-protein-coupled receptor. *Nature* **2007,** *450* (7168), 383-7.

3. Cherezov, V.; Rosenbaum, D. M.; Hanson, M. A.; Rasmussen, S. G.; Thian, F. S.; Kobilka, T. S.; Choi, H. J.; Kuhn, P.; Weis, W. I.; Kobilka, B. K.; Stevens, R. C., High-resolution crystal structure of an engineered human beta2-adrenergic G protein-coupled receptor. *Science* **2007,** *318* (5854), 1258-65.

4. Warne, T.; Serrano-Vega, M. J.; Baker, J. G.; Moukhametzianov, R.; Edwards, P. C.; Henderson, R.; Leslie, A. G.; Tate, C. G.; Schertler, G. F., Structure of a beta1-adrenergic G-protein-coupled receptor. *Nature* **2008,** *454* (7203), 486-91.

5. Moukhametzianov, R.; Warne, T.; Edwards, P. C.; Serrano-Vega, M. J.; Leslie, A. G.; Tate, C. G.; Schertler, G. F., Two distinct conformations of helix 6 observed in antagonist-bound structures of a beta1-adrenergic receptor. *Proceedings of the National Academy of Sciences of the United States of America* **2011,** *108* (20), 8228-32.

6. Jaakola, V. P.; Griffith, M. T.; Hanson, M. A.; Cherezov, V.; Chien, E. Y.; Lane, J. R.; Ijzerman, A. P.; Stevens, R. C., The 2.6 angstrom crystal structure of a human A2A adenosine receptor bound to an antagonist. *Science* **2008,** *322* (5905), 1211-7.

7. Carroll, I.; Thomas, J. B.; Dykstra, L. A.; Granger, A. L.; Allen, R. M.; Howard, J. L.; Pollard, G. T.; Aceto, M. D.; Harris, L. S., Pharmacological properties of JDTic: a novel kappa-opioid receptor antagonist. *Eur J Pharmacol* **2004,** *501* (1-3), 111-9.

8. Wu, B.; Chien, E. Y.; Mol, C. D.; Fenalti, G.; Liu, W.; Katritch, V.; Abagyan, R.; Brooun, A.; Wells, P.; Bi, F. C.; Hamel, D. J.; Kuhn, P.; Handel, T. M.; Cherezov, V.; Stevens, R. C., Structures of the CXCR4 Chemokine GPCR with Small-Molecule and Cyclic Peptide Antagonists. *Science* **2010,** *330* (6007), 1066-71.

9. Chien, E. Y.; Liu, W.; Zhao, Q.; Katritch, V.; Han, G. W.; Hanson, M. A.; Shi, L.; Newman, A. H.; Javitch, J. A.; Cherezov, V.; Stevens, R. C., Structure of the human dopamine d3 receptor in complex with a d2/d3 selective antagonist. *Science* **2010,** *330* (6007), 1091-5.

10. T., S., Structure of the human histamine H1 receptor complex with doxepin. *Nature* **2011,** *475*, 65-70.

11. Rasmussen, S. G.; DeVree, B. T.; Zou, Y.; Kruse, A. C.; Chung, K. Y.; Kobilka, T. S.; Thian, F. S.; Chae, P. S.; Pardon, E.; Calinski, D.; Mathiesen, J. M.; Shah, S. T.; Lyons, J. A.; Caffrey, M.; Gellman, S. H.; Steyaert, J.; Skiniotis, G.; Weis, W. I.; Sunahara, R. K.; Kobilka, B. K., Crystal structure of the beta2 adrenergic receptor-Gs protein complex. *Nature* **2011,** *477* (7366), 549-55
.

12. Lynch, D.; Hurst, D.; Romo, T.; Grossfield, A.; Reggio, P.; Pitman, M., Characterizing the Motion of W6.48 in the Active State of a GPCR. *2012 Biophysical Society Meeting Abstracts. Biophysical Journal* **2012,** *Supplement* (Abstract).

13. Manglik, A.; Kruse, A.; Kobilka, T.; Thian, F. S.; Mathiesen, J.; Sunahara, R.; Pardo, L.; Weis, W. I.; Kobilka, B. K.; Granier, S., Crystal Structure of the Mu-Opioid receptor bound to a morphinan antagonist. *Nature* **2012**.

14. Granier, S.; Manglik, A.; Kruse, A. C.; Kobilka, T. S.; Thian, F. S.; Weis, W. I.; Kobilka, B. K., Structure of the delta-opioid receptor bound to naltrindole. *Nature* **2012,** *485* (7398), 400-4.

15. Wu, H.; Wacker, D.; Mileni, M.; Katritch, V.; Won Han, G., Structure of the human kappa opioid receptor in complex with JDTic. *Nature* **2012**.

16. Zheng, H.; Pearsall, E. A.; Hurst, D. P.; Zhang, Y.; Chu, J.; Zhou, Y.; Reggio, P. H.; Loh, H. H.; Law, P. Y., Palmitoylation and membrane cholesterol stabilize mu-opioid receptor homodimerization and G protein coupling. *BMC Cell Biol* **2012,** *13*, 6
.

17. Konvicka, K.; Guarnieri, F.; Ballesteros, J. A.; Weinstein, H., A proposed structure for transmembrane segment 7 of G protein-coupled receptors incorporating an asn-Pro/Asp-Pro motif. *Biophys J* **1998,** *75* (2), 601-11
.

18. Whitnell, R. M.; Hurst, D. P.; Reggio, P. H.; Guarnieri, F., Conformational memories with variable bond angles. *J Comput Chem* **2008,** *29*, 741-752.

19. Fiser, A.; Do, R. K.; Sali, A., Modeling of loops in protein structures. *Protein Sci* **2000,** *9* (9), 1753-73.

20. Marti-Renom, M. A.; Stuart, A. C.; Fiser, A.; Sanchez, R.; Melo, F.; Sali, A., Comparative protein structure modeling of genes and genomes. *Annu Rev Biophys Biomol Struct* **2000,** *29*, 291-325.

21. Sali, A.; Blundell, T. L., Comparative protein modelling by satisfaction of spatial restraints. *J Mol Biol* **1993,** *234* (3), 779-815.

22. Phillips, J. C.; Braun, R.; Wang, W.; Gumbart, J.; Tajkhorshid, E.; Villa, E.; Chipot, C.; Skeel, R. D.; Kale, L.; Schulten, K., Scalable Molecular Dynamics with NAMD. *J. Comp. Chem.* **2005,** *26*, 1781-1802.

23. Fowler, C. B.; Pogozheva, I. D.; LeVine, H., 3rd; Mosberg, H. I., Refinement of a homology model of the mu-opioid receptor using distance constraints from intrinsic and engineered zinc-binding sites. *Biochemistry* **2004,** *43* (27), 8700-10.

24. Chaturvedi, K.; Shahrestanifar, M.; Howells, R., Mu opioid receptor: role for the amino terminus as a determinant of ligand binding affinity. *Molecular Brain Research* **2000,** *76*, 64-72.

25. Guo, W.; Shi, L.; Javitch, J. A., The fourth transmembrane segment forms the interface of the dopamine D2 receptor homodimer. *J Biol Chem* **2003,** *278* (7), 4385-8.
26. Ballesteros JA, D. X., Olivella M, Haaksma EE and Pardo L, Serine and Threonine Residues Bend Alpha-Helices in the chi(1) = g- conformation. *Biophys J* **2000,** *79* (5), 2754-60.

27. Shimamura, T.; Shiroishi, M.; Weyand, S.; Tsujimoto, H.; Winter, G.; Katritch, V.; Abagyan, R.; Cherezov, V.; Liu, W.; Han, G. W.; Kobayashi, T.; Stevens, R. C.; Iwata, S., Structure of the human histamine H1 receptor complex with doxepin. *Nature* **2011,** *475* (7354), 65-70.

28. Farrens, D. L.; Altenbach, C.; Yang, K.; Hubbell, W. L.; Khorana, H. G., Requirement of Rigid-Body Motion of Transmembrane Helicies for Light-Activation of Rhodopsin. *Science* **1996,** *274*, 768-770.

29. Ghanouni, P., Steenhuis, JJ., Farrens D and Kobilka, B., Agonist Induced conformational Changes in the G-Protein Coupling Domain of the Beta-2-Adrenergic Receptor. *Proc Natl Acad Sci* **2001,** *98* (11), 5997-6002.

30. Javitch, J. A.; Fu, D.; Liapakis, G.; Chen, J., Constitutive activation of the beta2 adrenergic receptor alters the orientation of its sixth membrane-spanning segment. *J Biol Chem* **1997,** *272* (30), 18546-9.

31. Jensen, A. D.; Guarnieri, F.; Rasmussen, S. G.; Asmar, F.; Ballesteros, J. A.; Gether, U., Agonist-induced conformational changes at the cytoplasmic side of transmembrane segment 6 in the beta 2 adrenergic receptor mapped by site-selective fluorescent labeling. *J Biol Chem* **2001,** *276* (12), 9279-90.

32. Lin, S. W.; Sakmar, T. P., Specific tryptophan UV-absorbance changes are probes of the transition of rhodopsin to its active state. *Biochemistry* **1996,** *35* (34), 11149-59.

33. Nakanishi, J.; Takarada, T.; Yunoki, S.; Kikuchi, Y.; Maeda, M., FRET-based monitoring of conformational change of the beta2 adrenergic receptor in living cells. *Biochem Biophys Res Commun* **2006,** *343* (4), 1191-6
.

34. Ballesteros, J. A.; Jensen, A. D.; Liapakis, G.; Rasmussen, S. G.; Shi, L.; Gether, U.; Javitch, J. A., Activation of the beta 2-adrenergic receptor involves disruption of an ionic lock between the cytoplasmic ends of transmembrane segments 3 and 6. *J Biol Chem* **2001,** *276* (31), 29171-7.

35. Huang, P.; Visiers, I.; Weinstein, H.; Liu-Chen, L. Y., The local environment at the cytoplasmic end of TM6 of the mu opioid receptor differs from those of rhodopsin and monoamine receptors: introduction of an ionic lock between the cytoplasmic ends of helices 3 and 6 by a L6.30(275)E mutation inactivates the mu opioid receptor and reduces the constitutive activity of its T6.34(279)K mutant. *Biochemistry* **2002,** *41* (40), 11972-80.

36. Li J, E. P., Burghammer M, Villa C and Schertler GF, Structure of Bovine Rhodopsin in a Trigonal Crystal Form. *J Mol Biol* **2004,** *3443* (5), 1429-38
.

37. Okada, T.; Fujiyoshi, Y.; Silow, M.; Navarro, J.; Landau, E. M.; Shichida, Y., Functional role of internal water molecules in rhodopsin revealed by X-ray crystallography. *Proc Natl Acad Sci U S A* **2002,** *99* (9), 5982-7.

38. Standfuss, J.; Edwards, P. C.; D'Antona, A.; Fransen, M.; Xie, G.; Oprian, D. D.; Schertler, G. F., The structural basis of agonist-induced activation in constitutively active rhodopsin. *Nature* **2011,** *471* (7340), 656-60.

39. Shi, L.; Liapakis, G.; Xu, R.; Guarnieri, F.; Ballesteros, J. A.; Javitch, J. A., Beta2 adrenergic receptor activation. Modulation of the proline kink in transmembrane 6 by a rotamer toggle switch. *J Biol Chem* **2002,** *277* (43), 40989-96.

40. Hurst, D. P.; Grossfield, A.; Lynch, D. L.; Feller, S.; Romo, T. D.; Gawrisch, K.; Pitman, M. C.; Reggio, P. H., A lipid pathway for ligand binding is necessary for a cannabinoid G protein-coupled receptor. *J Biol Chem* **2010,** *285* (23), 17954-64.

41. Johnston, J., Filizola M, On the relative stability of dimeric interfaces of the mu opioid receptor inferred from recent crystallographic studies. *Biophysical Journal Supplement* **2013,** *Abstract Issue*.

CHAPTER III

MOLECULAR DETERMINANTS FOR TARGETED GENE THERAPY μ-OPIOID RECEPTOR FOR MULTIPLE MUTANTS AT WHICH NALOXONE ACTS AS A PARTIAL AGONIST

Abstract

A targeted gene therapy strategy has recently been reported that makes novel use of a μ-opioid receptor (MOR) S4.54A mutant at which the classical opioid antagonist, naloxone, becomes a partial agonist.[1,2,3] Despite the clear success of basing this strategy on the S4.54A MOR mutant, the origins of this unusual phenotype are not yet understood. Therefore, the goal of the work reported here was to identify the molecular basis for the agonism of naloxone at this novel S4.54A mutant. To this end, we used the recent x-ray crystal structure of the MOR to create a WT MOR model into which naloxone was docked using Glide (Schrodinger, 2011). The crystal structure was also used to create a homology model of the S4.54A mutant MOR. The conformational change in TMH4 that would be created upon the S4.54A mutation was examined using the simulated annealing/Monte Carlo method, Conformational Memories, and the result was incorporated into the model. The S4.54A mutant model was then used for naloxone docking studies using Glide. These studies revealed that in the crystal structure, Y3.34

forms a hydrogen bond with the sidechain of S4.54; however, in the S4.54A MT MOR, this interaction is broken as there is no polar partner for Y3.34. The breaking of this interaction allows the extracellular end of TMH4 to kink away from TMH3 and towards TMH5, which leads to changes in the packing of the receptor binding pocket. In the wild type MOR, naloxone interacts with D3.32 and sits in close proximity to the binding pocket "toggle switch" residue, W6.48, restricting its movement. However, in the S4.54A MT MOR, naloxone sits higher in the binding pocket, away from W6.48 and interacts with D3.32 and E5.35. In this higher location, naloxone exerts no effect on W6.48, permitting W6.48 to assume an active state conformation. This shift in binding pocket location for naloxone may be the origin of naloxone's partial agonism in the S4.54A MOR mutant.

Introduction

Pain management is often one of the most difficult aspects of treatment for patients suffering from acute or chronic pain. The mu-opioid receptor (MOR) agonist, morphine, and its derivatives are highly used in pain management strategies. However, these medications have many side effects including respiratory depression, gastrointestinal problems as well as dependence and addiction liabilities. For these reasons, innovative new modalities for pain management continue to be needed.

One new approach to the design of opioid therapies for chronic pain with reduced liabilities is a targeted-gene therapy strategy developed by the lab of Dr. Ping-Yee Law at

the University of Minnesota. This strategy makes novel use of a MOR S4.54A mutant at which the classical opioid antagonist, naloxone, acts as a partial agonist.[1,2,3] Targeted gene therapy studies using this mutant have shown that naloxone becomes an antinociceptive agent at the S4.54A mutant both *in vitro* and *in vivo*.[1,2,3] Because the targeted strategy produces expression of the mutant MOR only in and around the spinal cord injection site region, systemic administration of naloxone results in agonism in this region, but antagonism at all other (native) MORs. The reduced number of receptors activated in this paradigm results in no measurable dependence/addiction as seen with traditional mu agonists like morphine.[1] Despite the clear success of basing this strategy on the S4.54A MOR mutant, the origins of this unusual phenotype are not yet understood. It is therefore the goal of this paper to identify the molecular basis for the agonism of naloxone at this novel S4.54A mutant.

The opioid receptors, delta, kappa and mu, belong to the Class A subfamily of G-Protein Coupled Receptors (GPCRs). In the past few years, x-ray crystal structures of Class A GPCRs have increasingly become available. These include rhodopsin[4,5,6] (Rho), meta-rhodopsin II[7], the β2-adrenergic receptor (β2-AR),[8,9,10,11,12] the β1 adrenergic receptor (β1-AR),[13,14] the adenosine A2A receptor,[15,16] the CXCR4 receptor,[17] the dopamine D3 receptor,[18] the histamine H1 receptor,[19] S1P1 receptor[12], the nociception/orphanin FQ receptor[20] and the mu[21], delta[22] and kappa[23] opioid receptors. The mu opioid receptor structure shows that residue S4.54 is part of a small network of interactions in the TMH3/TMH4 region of the receptor (see Figure 3.1). This network includes residues S3.30, Y3.34, S4.54 and G4.57. Here the lipid facing Y3.34 hydroxyl

interacts with the polar sidechain of S4.54 and S3.30 forms a hydrogen bond with the backbone carbonyl of G4.57. In the work reported here, we take advantage of the availability of the MOR crystal structure to develop a homology model of the S4.54A mutant and explore the altered binding profile of naloxone in this mutant. We find here the S4.54A phenotype has its origins in the loss of the Y3.34—S4.54 interaction seen in the WT MOR crystal structure.

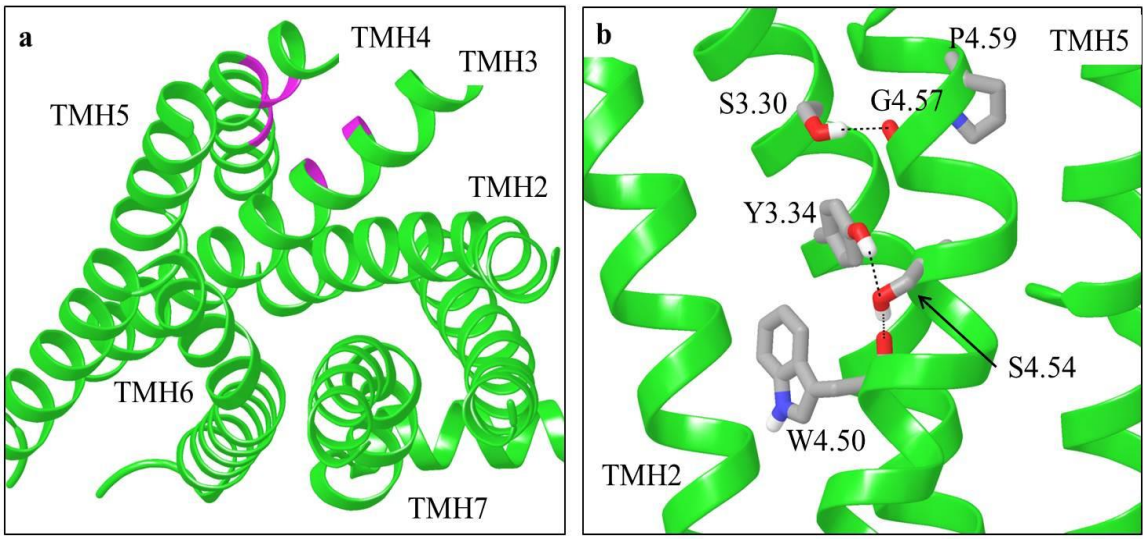

Figure 3.1. Hydrogen bonding network in the WT MOR receptor (lime). 1a. An extracellular view of the MOR with the backbone in lime and the location of residues on TMH3 and TMH4 that form a hydrogen bonding network. 1b. A view from lipid showing each of the residues in the TMH3/TMH4 hydrogen bonding network. S3.30 forms a hydrogen bond with the backbone carbonyl of G4.57. The hydroxyl of Y3.34 forms a hydrogen bond with the polar sidechain of S4.54 which also forms a bond with the backbone of W4.50.

We also report herein new experimental data for additional S4.54 mutants who also share the unique phenotype seen in the S4.54A[3,24,1,2] and S4.54L[25] MT MOR in which naloxone becomes a partial agonist as previously reported. Mutating S4.54 to both a phenylalanine and a glycine share the unusual phenotype seen in the S4.54A and S4.54L MT MOR. Interestingly, when S4.54 is mutated to isoleucine or valine, naloxone

maintains the same activity as seen in the wild type MOR. We propose that in the case of the S4.54 I / V, an increase in hydrophobic interactions between W4.50 and I/V4.54 allow TMH4 to maintain its wild type conformation. However, while the S4.54F is also able to increase hydrophobic interactions, its size prevents the helix from maintaining the wild type shape. In the S4.54L mutant, there is no increase in hydrophobic interactions and the orientation of the leucine gives rise to a straighter TMH4, as seen in the S4.54A MT MOR. The S4.54G mutant offers additional flexibility and a higher turn ratio, with 5 residues per turn in that region such that the extracellular end of TMH4 moves away from TMH3 and towards TMH5.

Methods

Xenopus oocyte electrophysiology

Mutations of Ser4.54 into various amino acid mutants were carried by cloning rat MOR into the pAlter vector and site-directed mutagenesis carried out as described by the manufacturer (*pAlter-Sites I in vitro Mutagenesis System, Promega*). cRNAs of wild type and mutant MOR, and GIRK1 channel (*a gift from Dr. Henry Lester)*[26] were prepared for injection by the *in vitro* transcription kit mMessage mMachine (Ambion, Inc). 1-3 ng of cRNAs of each GIRK1 and various MOR in 50 nl were injected into the vegetal pole of the oocytes as described previously[27]. After injection, oocytes were incubated in ND-96 (96 mM NaCl, 2 mM KCl, 1 mM $MgCl_2$, 1.8 mM $CaCl_2$ and 5 mM HEPES, pH7.4) supplemented with 2.5 mM sodium pyruvate and 5.0% heat-inactivated horse serum (*Life*

Technologies/GIBCO). 3-8 days after injection, oocytes were placed in a 100 µl recording chamber and were perfused at a rate of 0.5 ml/min with ND-96. The standard 2-electrode voltage-clamp recordings were performed at room temperature using a Dagan TEV-200 Voltage Clamp/Amplifier.[28] Oocytes with transmembrane potentials more negative than -40 mV were chosen for voltage-clamping at -80 mV. After oocytes were clamped at -80 mV, the perfusion buffer was changed to a high K^+ buffer (2 mM NaCl, 96 mM KCl, 1 mM $CaCl_2$, 5 mM HEPES, pH 7.4) for K^+ current recordings and drug addition. Drugs were applied for 0.25-1 min in high K^+ buffer. Each oocyte was exposed to only one concentration of opioid ligand. Statistical significance was determined using Statview for Macintosh (*Abacus*).

Measurement of forskolin-stimulated intracellular [^{3}H]cAMP production

Measurement of intracellular [^{3}H]cAMP production was carried out as described previously.[29] Briefly, CHO cells stably expressing wild type or mutant MOR were grown to confluency in 24-well plates in DMEM medium supplemented with 10% fetal calf serum and 1 mg/ml G418. 24 hours prior to the assay, media was changed and on the day of the assay, the intracellular cAMP pools were labeled by incubating the cells in DMEM media supplemented with 15.3 mM NaCl, 29.3 mM $NaHCO_3$, 40 µCi/10 ml of [^{3}H]adenine (20 Ci/mmole, Amersham) and 0.5 mM isobutylmethylxanthine (IBMX) for 1 hr at 37^0C, 10% CO_2. Afterwards, DMEM media was removed, and to each well, 0.5 ml of KRHB pH7.4 buffer containing 0.5 mM IBMX, 10 µM forskolin and various drugs at 1 µM was added. Cells were then incubated at 37ºC for 15 min. The reaction

was terminated by the addition of 50 µl of 3.3 N perchloric acid. [^{32}P]cAMP standard (3000-5000 cpm/well) was added, and [^{3}H]cAMP was separated from other radioactive nucleotides by Dowex and alumina column chromatrography as described previously discussed.[30] Radioactivity was determined by scintillation counting with a Beckman 5000 counter.

Creation of WT MOR Model and Docking of Naloxone

We designed a WT MOR model for the studies herein using the recently published MOR crystal structure[21] complexed with β-FNA, a covalently bound antagonist. Using Maestro (Schrodinger, 2011), hydrogen's were added to the crystal structure and β-FNA was removed. Glide (Schrodinger, 2011) was used to ascertain the binding region for naloxone employing D3.32 as a hydrogen bond interaction site. The dock with the best Glide score was evaluated and compared to the S4.54A MT MOR model.

Conformational Memories (CM) Technique for Calculating the Mutant TMH4s S4.54A/I/L/V/F/G

We explored the TMH4 conformational results of each mutation using the CM technique.[31,32] The CM method uses multiple Monte Carlo/simulated annealing random walks employing the CHARMM force field. An alpha helical TMH with the WT hMOR sequence was used as a starting point for these calculations. Each mutant was subsequently run using the same initial structure followed by a 1 step minimization to

alleviate backbone clashes from the newly inputted residue. The region of I4.51 to P4.59, with S4.54 mutated to the appropriate residue was considered the flexible region in these calculations. Backbone φ and ψ torsions in regions of interest were allowed to vary ±50°, while all other backbone torsion angles were allowed to vary ±10°. Side chain torsions were allowed to vary ±180° for the alanine and glycine mutants. For each of the leucine, isoleucine, valine and phenylalanine mutant TMH4, four runs were performed: 1) All side chain torsions were allowed to vary ±180°, 2) All side chain torsions were allowed to vary ±180° except the χ1 dihedral of 4.54 which was held in 2) *gauche*+ (-60°), 3) *gauche*- (+60°) and 4) *trans* (180°). In all runs, bond angles were allowed to vary ±8° except for the C–S–C angles that were allowed to vary ±15°. From each run, there were 120 output TMH4 conformers generated in a distance-dependent dielectric at 310 K. The CM output helices were subsequently evaluated in the context of the MOR TMH bundle and an appropriate helix was chosen for substitution into the MOR model (see next section).

Construction of the TMH Region of the S4.54A MT MOR and Ligand Docking

The recently reported MOR WT x-ray crystal structure[21] was used to create a homology model of the S4.54A mutant MOR. The MOR crystal structure was pulled apart 2Å in each direction from the center of the bundle. The selected S4.54A CM output helix was superimposed onto TMH4 of the crystal structure using the Cα atoms from R4.40 to W4.50. The transmembrane regions of the resultant S4.54A MOR model were energy minimized to allow the TMHs pack such that there were no large gaps. A 500

step energy minimization was performed using the OPLS2005 all atom force field in Macromodel 9.1 (Schrodinger, 2006), employing a distance-dependent dielectric with extended cutoffs. The backbone phi/psi dihedrals of the TMHs were constrained with a force of 500kJ/mol to preserve their geometries. The output structure from the 4th iteration of the minimization was selected as the model for the S4.54A MT MOR by comparing the TMH regions of the mutant and wild type receptors to ensure that the TMH region of the mutant receptor was not over-packed. Naloxone was docked in the resultant S4.54A model using Glide (Schrodinger 2006) with D3.32 as the primary interaction site for the ligand. The dock with the best Glide score was used for further study.

To preserve the general shape of the loop regions seen in the crystal structure, four of the loops from the crystal structure (EC2/IC3 excluded) were added to the S4.54A model. Due to the differences in the extracellular region of TMH4, MODELLER v9.1.[33,34,35] was used to add the EC2 loop. Restraints were added to the MODELLER run such that the disulfide bond with C3.25 and the beta sheet regions were preserved. The IC3 loop was not resolved in the crystal structure therefore; MODELLER was used to determine a likely loop conformation. Once the loops were added, naloxone was re-docked in the full model using Glide. The dock with the best Glide score was used for the final S4.54A MOR/naloxone complex model.

The resultant WT MOR/naloxone and S4.54A MOR/naloxone complexes were compared in order to investigate at the molecular level, the possible origins of naloxone's partial agonist behavior in the S4.54A MT MOR.

Results

S4.54 A Conformational Memories Results

The biased Monte Carlo/simulated annealing technique, Conformational Memories[31- 32] was used here to explore the conformational consequences of the S→A mutation at position 4.54 in the MOR. Figure 3.2 shows the CM output for the S4.54A TMH4 superimposed using the Cα atoms of residues R4.40 to W4.50 on TMH4 in the WT MOR. The most striking differences between the CM output and WT MOR TMH4 was that the extracellular ends of the S4.54A CM output helices were bent towards TMH5 rather than towards TMH3 as seen in the WT MOR crystal structure. The TMH4 chosen for use in the S4.54A mutant receptor model is colored magenta in Figure 3.2, while TMH4 of the WT MOR crystal structure is colored yellow. Prokink[36] was used to determine the bend, wobble, and face shift angles of these two helices.

The WT TMH4 measured 33.6°, -47.5°, and 152.4°, while the S4.54A MT TMH4 measured 31.5°, 128.9°, and 57.2°, respectively. Figures 3.3a and 3.3b illustrate the key differences between WT MOR TMH4 (lime) and the chosen S4.54A MT TMH4 (magenta). Figure 3.3a shows an extracellular view of the WT MOR and MT MOR with TMH4 in the top left hand corner. As shown, the extracellular end of TMH4 moves in the S4.54A MT MOR. In Figure 3.3b the view is from within the TMH bundle looking from TMH1 towards TMHs3-5. The large shift in the extracellular end of TMH4 is evident here. Using the locations of A4.64 and M4.61 as guides, we found that the Cα atom of A4.64 moves 7.1 Å and the Cα of M4.61 moves 5.7 Å

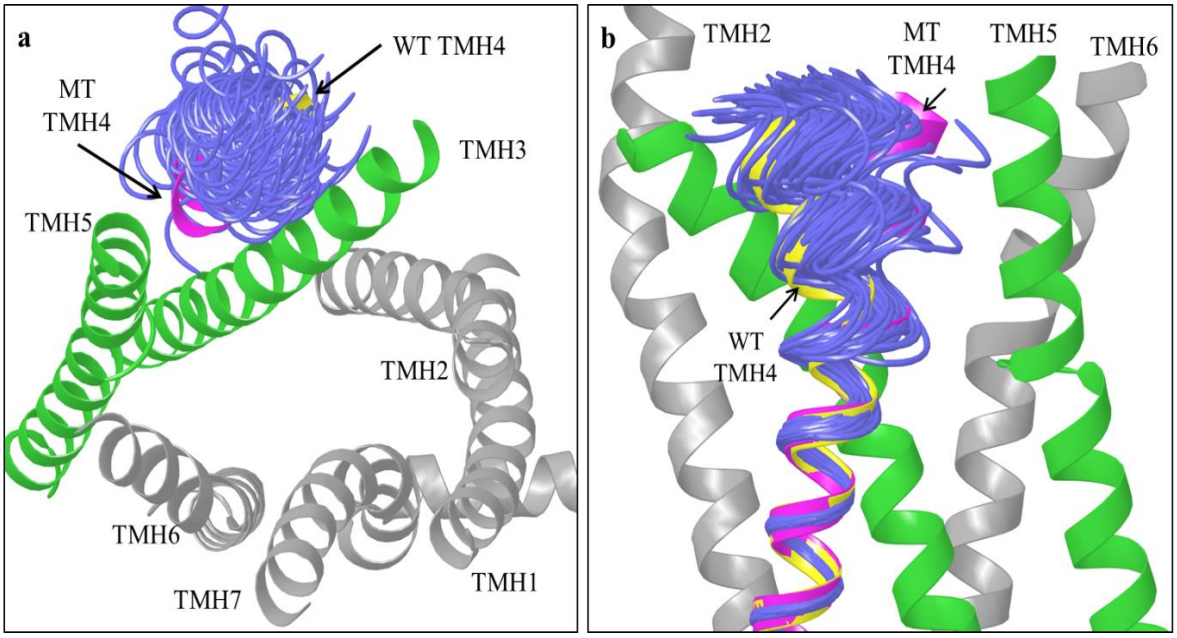

Figure 3.2. Conformation Memories (CM) output of S4.54A MT TMH4. An extracellular view (2a) and a view from lipid (2b) showing the WT MOR in gray, with TMH3 and TMH5 in lime and WT TMH4 in yellow. The CM output is shown in blue tube representation and the S4.54A MT TMH4 selected is shown in magenta.

Creation of S4.54A Mutant Model

A homology model of the S4.54A MT MOR was developed using the recently published mu-opioid crystal structure (PDB Code: 4DKL)[21] and the results of the Conformational Memories studies of TMH4 in the S4.54A mutant. Once the S4.54A MT MOR was completed, the transmembrane regions were superimposed onto the WT MOR crystal structure using the most conserved residue in each respective helix. The superimposed receptors are shown in Figure 3.3a, with the WT MOR in lime and the MT MOR in magenta. Here it is clear that there were no large backbone changes from the WT to the MT MOR model, except for the extracellular region of TMH4, at the top of the figure. There was some slight movement in the extracellular end of TMH5 which can be

attributed to the change in conformation of TMH4 in the S4.54A MT MOR. Additionally, there was some slight movement at the extracellular ends of TMH1 and TMH7, but these movements were not found to be significant.

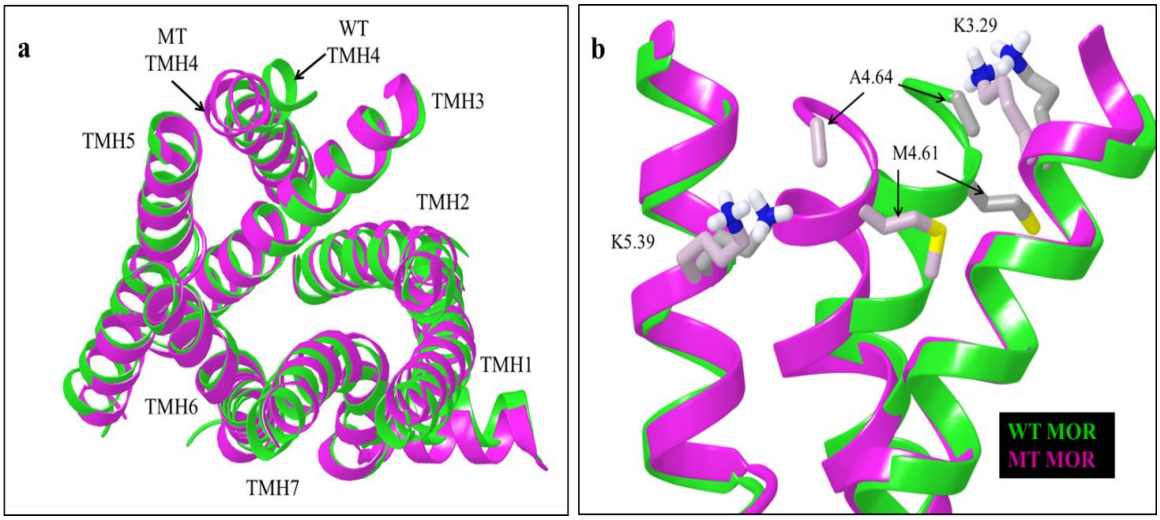

Figure 3.3. A comparison of the WT MOR (lime) and S4.54A MT MOR (magenta) models. 3a. An extracellular view of the two receptors superimposed using the most conserved residue in each helix. There are no large backbone changes in the S4.54A MT MOR except for the extracellular end of TMH4. 3b. A view inside the bundle from TMH1 looking towards the TMH3, 4, 5 region of the WT and S4.54A MT MORs. K3.29, M4.64, A4.61 and K5.39 are shown in the WT MOR (gray residues) and the S4.54A MT MOR (pink residues) to quantitate the changes of TMH4 in the WT MOR and the S4.54A MT MOR. The Cα of M4.61 and A4.64 moved 5.6Å and 7.1Å, respectively.

To quantitate the movement of TMH4 relative to TMHs 3 and 5, the following pairs of distances were measured in both the WT MOR and MT MOR (Table 1): K3.26-A4.64, K3.26-M4.61, K5.39-A4.64, and K5.39-M4.61. These residues can be seen in Figure 3.3b, where the WT is shown in lime and the MT model is shown in magenta. As shown, the last helical residue of TMH4, A4.64 moves away from TMH3 and towards TMH5 based on the measurements in the models. M4.61 displays the same movement, which is consistent with the Prokink[37] data in Figures 3.3a and 3.3b where there is a large

change in both the wobble and face shift angles of the WT TMH4 as compared to the S4.54A MT TMH4.

Table 1.1. Cα distances of select residues on TMHs 3, 4 and 5 in the WT MOR and the S4.54A MT MOR

DISTANCE MEASURED all are Cα	WT MOR (Å)	S4.54A MT MOR (Å)
M4.61--K3.26	4.963	8.611
A4.64--K3.26	5.136	10.712
M4.61--K5.39	15.618	11.399
A4.64--K5.39	15.538	10.145

The hydrogen bonding network seen in the MOR crystal structure (Figure 3.1), is not intact in the S4.54A MT MOR model. Although Y3.34 and A4.54 are close enough to make the hydrogen bond seen in the WT MOR, the Ala does not have a polar group for Y3.34 to interact with. Additionally, in the WT MOR, Cα S3.30 is only 4.6Å from the backbone carbonyl of G4.57; however in the S4.54A MT MOR, the Cα of S3.30 is 7.3Å from the backbone carbonyl of G4.57. The difference between S3.30 and G4.57 (See Figure 3.3b) is consistent with the Prokink data and measurements in Table 3.1.

Naloxone Docking Studies

WT MOR**:** The MOR was crystalized with Beta-FNA, a covalently bound antagonist. This antagonist was removed from the crystal structure in order to explore

naloxone's binding site at the WT MOR. Glide (Schrodinger, 2011) was used to identify docking poses for naloxone (yellow) in the WT MOR and the dock with the best score (-8.948) was chosen, as shown in Figure 3.4a. Shown in Figure 3.4a, both the crystallized ligand, β-FNA (cyan) and naloxone (yellow) form an electrostatic interaction with D3.32 (gray), consistent with experimental data.[38] It can be seen in Figure 3.4a that naloxone and β-FNA occupy the same binding pocket and same general location inside the receptor. Naloxone sits slightly lower in the binding pocket than β-FNA. This is likely due to the fact that naloxone does not have a covalent attachment to the receptor and can orient itself to optimize its binding, whereas β-FNA is locked into position by its covalent attachment at K5.39 (gray). The N-allyl of naloxone and the n-methylcyclopropyl of β-FNA sit in close proximity to W6.48 (gray). The driving interaction for naloxone in this dock is with the electrostatic interaction with D3.32; however naloxone also has significant Van-der-Waals (VDW) interactions with Y3.34, M3.36 and W6.48. The charged nitrogen of naloxone is 9.0Å away from the C-alpha carbon of W6.48 in the WT MOR (Figure 3.4a). In this position, the alkaloid fused ring system of naloxone would restrict movement W6.48 (see Figure 3.5a).

S4.54A Mutant**:** Glide was also used to identify a binding site for naloxone in the S4.54A MT MOR model. The dock with the best score (-7.240) was chosen (Figure 3.4b). In this docked position, naloxone (sea green) sits higher in the binding pocket compared to naloxone in the WT MOR (yellow) (see Figure 3.4c). Naloxone still has its primary electrostatic interaction with D3.32 (pink) here in the S4.54A MT MOR; however, naloxone also picks up a hydrogen bond with E5.35 (pink) which is not seen in

the WT MOR. In the MT MOR, naloxone maintains VdW interactions with Y3.34 and M3.36, but loses the interactions with W6.48 seen in the WT MOR. The charged nitrogen of naloxone is 12.1Å away from the C-alpha carbon of W6.48 in the MT MOR while only 9.0Å away in the WT MOR.

While the alkaloid fused ring system of naloxone restricts movement of W6.48 in the WT MOR (Figure 3.5a), it does not restrict movement of W6.48 in the S4.54A MT MOR (Figure 3.5b-d). Shown in space filling representation in Figure 3.5b, it can be seen that naloxone has rotated and shifted towards the extracellular part of the receptor in the S4.54A MT MOR model. This movement permits W6.48 conformational freedom in the binding pocket (see Figure 3.5b-d).

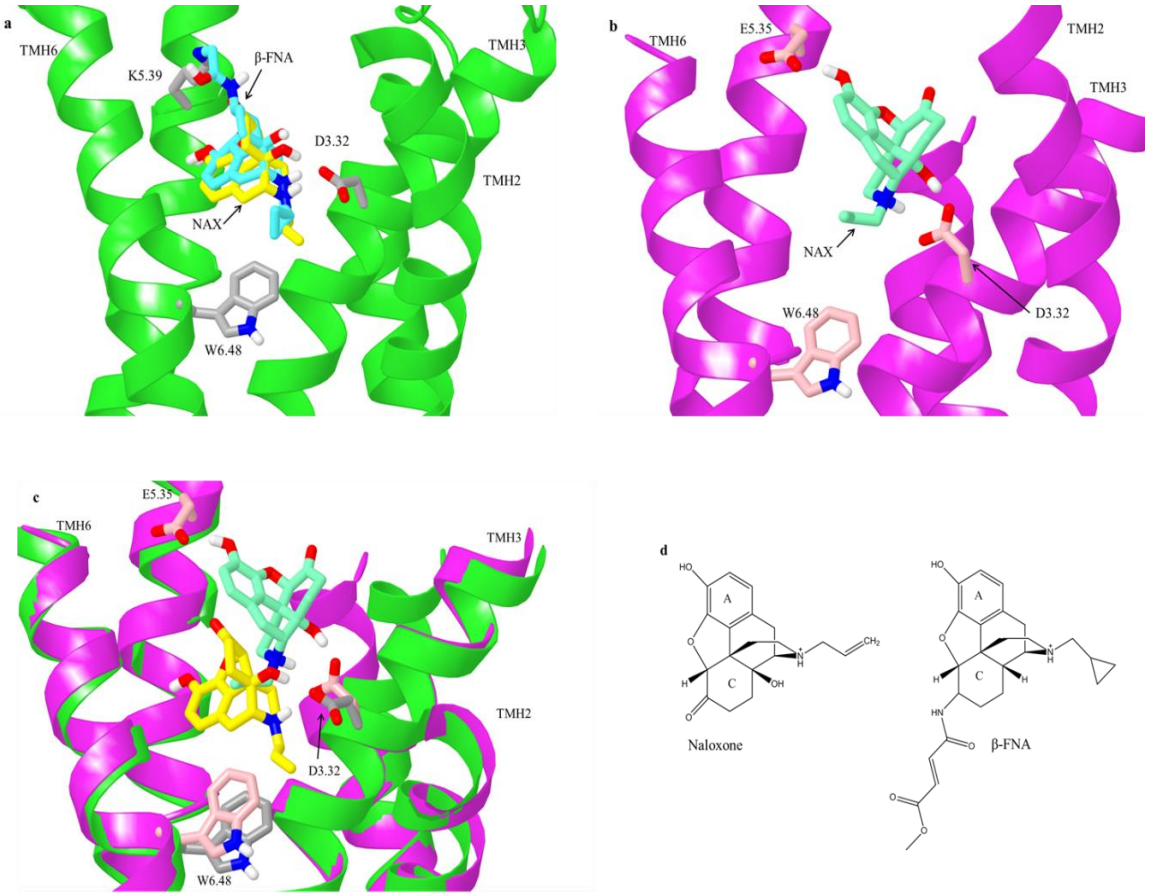

Figure 3.4. Naloxone docked in the WT MOR (4a), S4.54A MT MOR (4b) and ligand structures (4d). 4a. The WT MOR (lime backbone) with the crystallized covalently bound antagonist β-FNA (cyan) at K5.39 and the Glide docked naloxone (yellow). 4b. The S4.54A MT MOR (magenta backbone) with naloxone (sea green) docked using Glide. The D3.32 interaction was maintained and an interaction with E5.35 was added in the MT MOR. 4c. A comparison of the WT MOR with naloxone (yellow) and the S4.54A MT MOR with naloxone (sea green) models. In the MT MOR naloxone has rotated and sits higher and more extracellularly in the binding pocket compared to the WT MOR. 4d. Structures of naloxone and β-FNA

Potassium Current and cAMP Results of various S4.54 Mutants

Potassium current was tested in various S4.54 MOR mutants to determine if any additional mutations gave rise to the phenotype of naloxone acting as a partial or full agonist at the MOR as seen in the S4.54A mutant MOR (Figure 3.6a). Surprisingly, upon mutation to leucine and phenylalanine, naloxone induced approximately 15% of the

maximal current induced by DAMGO, a full peptide agonist at the MOR. The S4.54 mutations to glutamine, threonine, isoleucine and valine showed naloxone acting as an antagonist, as seen the in WT MOR.

Subsequently, intracellular cAMP levels were tested for S4.54 mutations to glycine (Figure 3.6b), isoleucine (Figure 3.6c) and phenyalanine (Figure 3.6d) mutants. Both the glycine and phenylalanine mutants showed that naloxone and naltrexone were able to decrease cAMP level, indicative of agonist behavior as seen in with DAMGO. In the isoleucine mutant, neither naloxone nor naltrexone inhibited cAMP level and both ligands acted as antagonists, consistent with their WT MOR phenotype. CTOP, a MOR peptide antagonist did not have an altered phenotype in any of the mutations, including the S4.54G and S4.54F mutants at which the alkaloid ligands had an altered phenotype

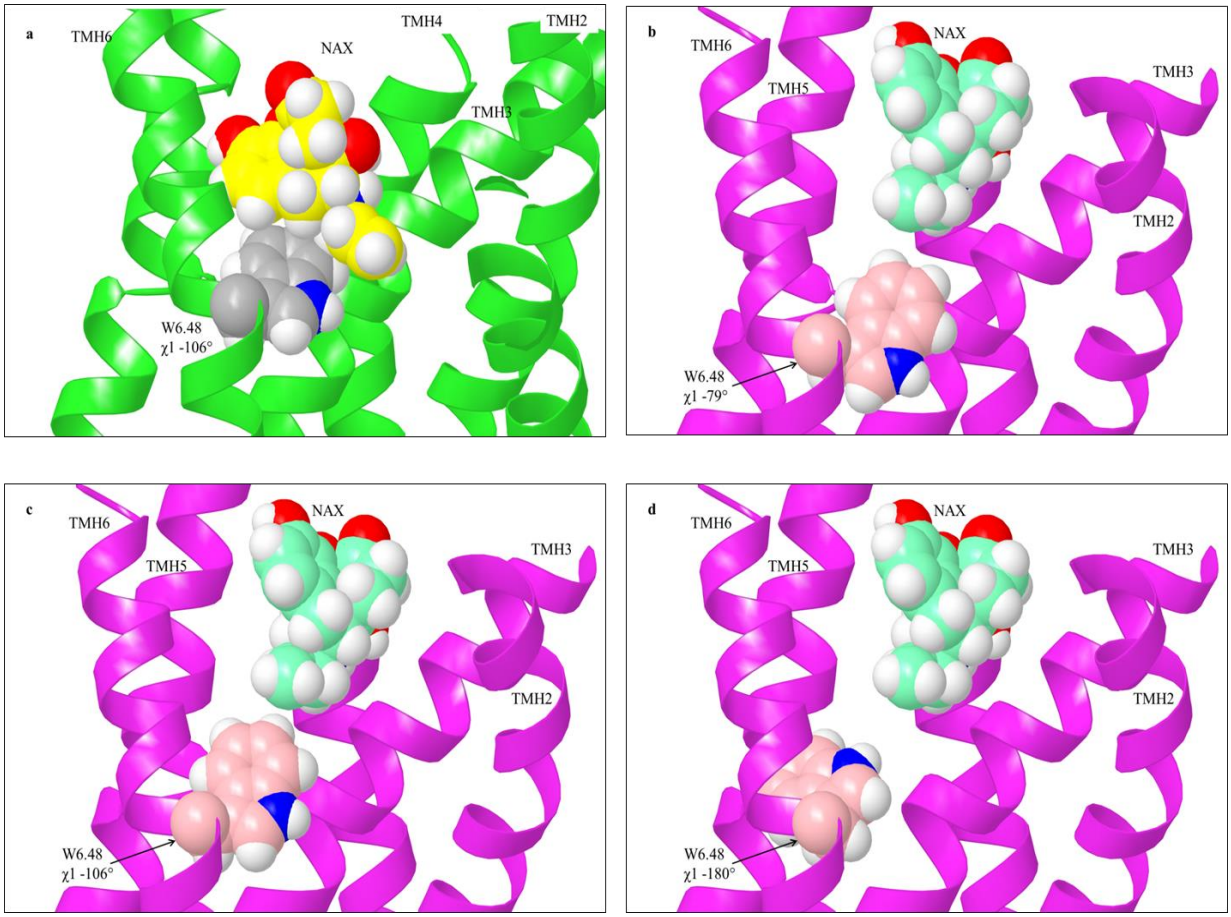

Figure 3.5. Space filling representation of naloxone and W6.48 in the WT MOR (5a) and S4.54A MT MOR (5b-d). 5a. Naloxone (yellow) prohibits a change in conformation of W6.48 (gray) between the inactive and active conformations in the WT MOR. A 30° change to a value of -106° in the conformation of W6.48 causes steric interactions with naloxone in the WT MOR and thus W6.48 cannot undergo the rotameric changes needed as part of receptor activation. 5b-d. In the S4.54A MT MOR, naloxone (sea green) does not prevent the rotameric changes of W6.48 (lt. pink) during activation. In the inactive state, W6.48 is in *g+* with a χ1 dihedral value of -79° (5b). As W6.48 flips from *g+* to *trans*, naloxone does not prohibit this movement. 5c shows W6.48 with a χ1 value of -106, the same as shown in the WT MOR where naloxone blocks this movement (5a). 5d shows W6.48 in a fully trans conformation since naloxone sits too high to block its rotameric changes.

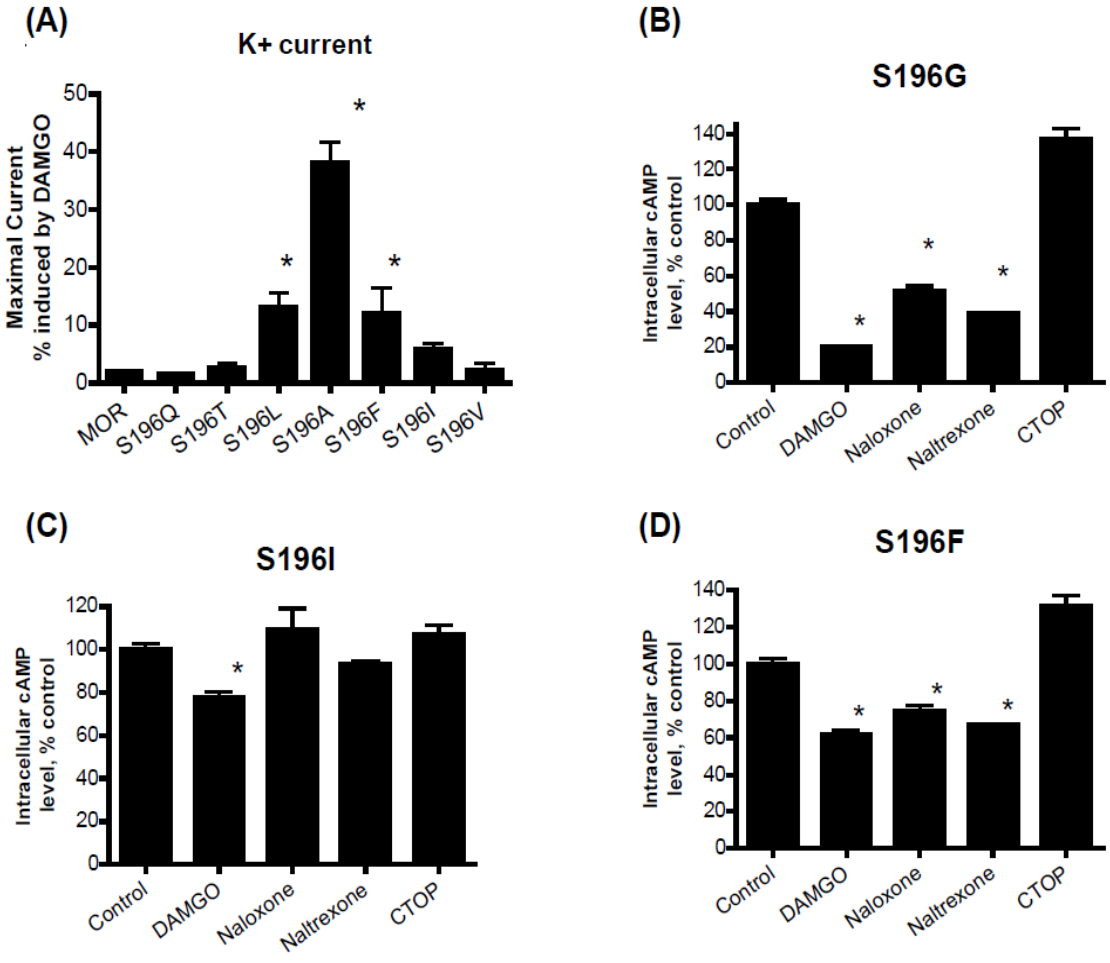

Figure 3.6. Various amino acid substitution at Ser4.54 (Ser^{196}) of rat MOR on receptor activities. In (A), *Xenopus* oocytes were injected with cRNAs of various Ser4.54 mutants of MOR and the maximal K^+ current induced by 1 μM naloxone was compared to those induced by 1 μM DAMGO as described in Methods. Each bar represents the average ± SEM of 4-10 oocytes. In (B), (C) and (D), the ability of 100 nM opioid ligand to inhibit 10 μM forskolin-stimulated intracellular [^{3}H]cAMP production in CHO cells stably expressing S196G (B), S196I (C) or S196F (D) mutant was determined as described in Method. Bars represent average±SEM from 4-6 wells. Statistical significance was determined by ANOVA and Fisher PLSD post-hoc analyses. In (A), statistical analyses were carried out by comparing the relative K^+ current induced by naloxone in oocytes injected with mutant cRNAs to those injected with wild type MOR cRNAs. In (B) to (D), statistical analyses were carried out by comparing the forskolin-stimulated [^{3}H]cAMP level in the presence of drug to that of control. * denotes $p < 0.05$.

Conformational Memories Results

A representative MT TMH4 was selected from the CM output for each of the mutants and superimposed onto the intracellular end of the WT MOR crystal structure TMH4, as shown in Figure 3.7a. This figure shows the MOR crystal structure TMH4 in yellow, with the S4.54I (light blue), S4.54V (maroon), S4.54L (sea green), S4.54A (magenta), S4.54F (royal blue) and S4.54G (red) output. The S4.54I and S4.54V mutant TMH4 helices match the TMH4 seen in the MOR crystal structure. However, the S4.54L/F/G helices are very similar to the S.454A mutant model shown earlier.

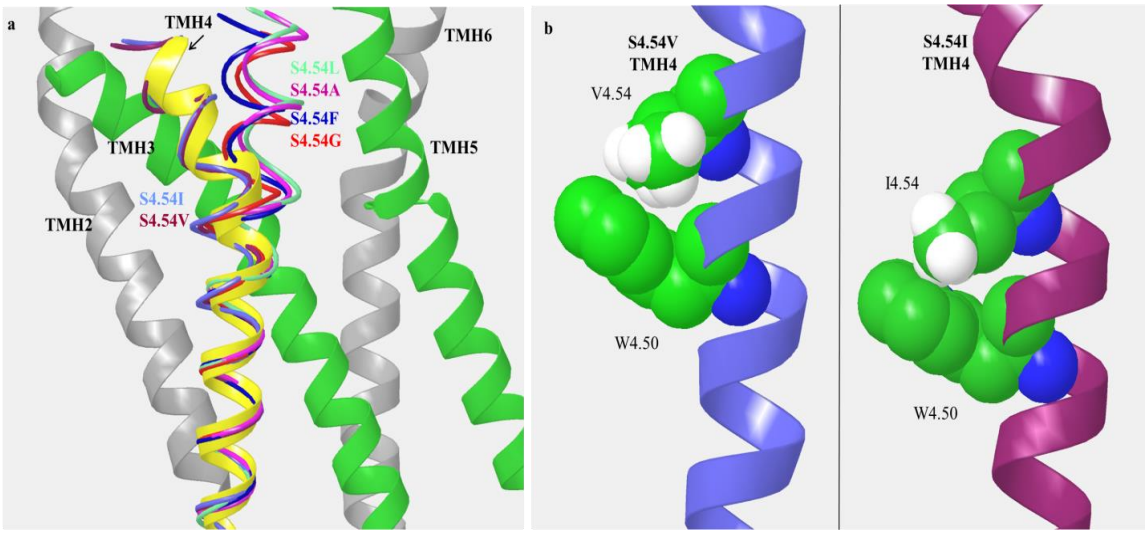

Figure 3.7. Figure 3.7a shows the WT MOR TMH4 in yellow, along with each of the mutant CM output selected superimposed on the intracellular end of the helix. As shown, the S4.54L (sea green), S4.54F (royal blue) and S4.54G (red) mutants all bend into the receptor, much like the S4.54A mutant helix as described in Figure 3.3. The S4.54I (maroon)/V (lt. blue) mutants have a similar shape to the WT TMH4. Figure 3.5b shows an up close picture of the methyl groups of the V4.54 (left) and I4.54(right) mutants and their Van-der-Waals packing with W4.50.

S4.54V Conformational Memories Results

In the run without constraints on the chi1 dihedral, V4.54 preferred a *g*+ orientation in a 2:1 ratio vs *g*- and a 3:1 ratio with *trans*. In the output, there were 66 *g*+, 34 *g*- and 20 *trans* χ1 dihedrals of V4.54. Upon examination, it was determined that V4.54 was able to orient itself in the g+ conformation to maximize hydrophobic interactions with the ring system of W4.50 as shown in Figure 3.7b (light blue, left). The interaction between W4.50 and V4.54 is -26kJ/mol. Despite the loss of the TMH3/TMH4 hydrogen bond network, a valine sidechain at position 4.54 is able to mimic the shape of the WT TMH4 due to this specific interaction.

S4.54I Conformational Memories Results

In the run without constraints on the χ1 dihedral, I4.54 preferred to be *g*+. Of the 120 output, there were 94 in *g*+, 4 in *g*- and 7 in *trans*. Upon inspection, it was determined that the I4.54 was able to point its methyl groups at the ring system of W4.50 and increase hydrophobic interactions as shown in Figure 3.7b (right, magenta). This interaction is very similar to the one seen by the S4.54V TMH4, also shown in Figure 3.7b (left, lt. blue). The interaction between W4.50 and I4.54 was measured to be -22kJ/mol. Due to this interaction, the I4.54 mutant TMH4 maintains a wild type shape even though there is a loss of the TMH3/TMH4 hydrogen bonding network seen in the crystal structure.

S4.54L Conformational Memories Results

In the run without constraints on the chi1 dihedral, L4.54 preferred to be trans vs g+ in approximately a 2:1 ratio (77 vs 43). There were no output with the chi1 in *g*-, as putting a leucine in *g*- would cause steric clashes with the backbone. It was evident that the S.454L output was strikingly different from the S4.54I/V output in that the shape of the helix did not match the wild type TMH4 from the crystal structure. Upon examination, it was determined that the leucine was unable to point its methyl groups at W4.50, as seen in both the valine and isoleucine output. The interaction energy between W4.50 and L4.54 was a marginal -12kJ/mol, much less than the isoleucine and valine mutants. With the S4.54L MT TMH4 not able to maintain the hydrogen bonding network seen between TMH3/TMH4 in the WT MOR, nor being able to increase hydrophobic interactions with W4.50 to maintain the WT TMH4 helical shape, the S4.54L MT TMH4 is free to straighten and give rise to naloxone's ability to act as a partial agonist.

S4.54G Conformational Memories Results

Unlike the other S4.54 mutants reported herein, the S4.54G gives rise to additional flexibility of TMH4. In the CM output, all 120 output structures had an unwound region in the helix near G4.54 that allowed for a higher turn ratio with 5 residues per turn instead of the traditional 4 residues per turn. This mutation prevents the TMH3/TMH4 hydrogen bonding network from forming and combined with the higher turn ratio, shifts the extracellular end of TMH4 towards TMH5, giving rise to

naloxone's ability to act as a partial agonist, much like the S4.54A MT TMH4 described herein.

S4.54F Conformational Memories Results

In the χ1 unconstrained run with S4.54F, the phenylalanine preferred to be in *trans* by a 3:1 ratio over *g*+ (93 vs. 27) and there were no output in *g*-. While this mutant gives rise to naloxone acting as a partial agonist like the alanine, glycine and leucine mutants, the F4.54 was able to maximize hydrophobic stacking interactions with W4.50, as seen in the isoleucine and valine mutants. The interaction energy between W4.50 and F4.54 was calculated to be -20kJ/mol, similar to that of the isoleucine and valine mutants. Upon examination, it became clear that because of size, a phenylalanine at 4.54 prevents TMH4 from taking the wild type conformation. In the WT MOR, Y3.34 is pointed directly at S4.54. Upon mutation of the S4.54 to phenylalanine, there are major steric overlaps with the Y3.34. The F4.54MT TMH4 has to undertake a straighter conformation, like those seen in the S4.54A and S4.54L mutants to be able to fit in the receptor.

Discussion

Geometry of TMH4

Proline residues are the most common helix deforming residues. In addition to leaving the *i-4* backbone carbonyl without its normal hydrogen bond donor, the proline also

sterically prevents the *(i-3)*-carbonyl-(*i* + *l*)-amide backbone hydrogen bond from forming.[39] However, other residues such as serines and threonines can induce structural deformations in helices as well.[40] The hydrogen bonding capacity of serine or threonine residues in α-helices can be satisfied by an intrahelical hydrogen bond interaction, in either the *g-* or *g+* conformation, between the O-γ atom and the *i-3* or *i-4* carbonyl oxygen. Serine and threonine residues in the *g-* conformation can induce a bend in an α-helix, and we have found that changes in wobble angle and face shift can also occur.

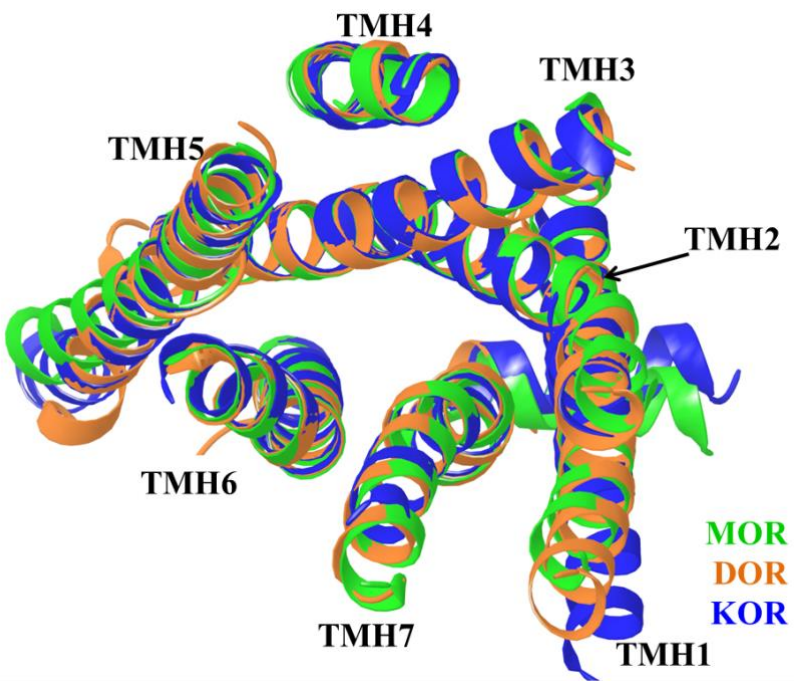

Figure 3.8. An extracellular view of the MOR (lime), DOR (orange) and KOR (blue) crystal structures. The structures were superimposed using the most conserved residue in each helix and are very similar. The MOR and DOR have a P4.59 but the KOR has a S4.59. The Ser in the KOR is mimicking the behavior of a P4.59 by forming a hydrogen bond with the *i-3* backbone carbonyl.

In many class A GPCR's there is a proline in TMH4 at either residue position 4.59 or 4.60. In the cannabinoids, beta-adrenergic, sphingosine -1-phosphate 1, and adenosine receptors, the proline is found at position 4.60, but in the orexin, dopamine, mu opioid, delta opioid and chemokine 4 receptors, the proline is found at position 4.59. The Pro at 4.59 contributes to a kink at the extreme extracellular end of TMH4 in the MOR and DOR structures. The kappa opioid receptor lacks the Pro at 4.59, but has a Ser at this position. Figure 3.8 illustrates that the geometry of TMH4 in the MOR (lime), DOR (orange), and KOR (blue) are very similar. The KOR TMH4 is able to mimic the proline kink in MOR and DOR because S4.59 can from a hydrogen bond with the backbone carbonyl of V4.56, the *i-3* residue, and bend the helix.

A hydrogen bonding network on TMH3 and TMH4 also contributes to the relative positions of these two helices in the opioid receptor bundles. In each of the three opioid receptors, there are three lipid facing residues that need to satisfy their hydrogen bonding capabilities: S4.54, S3.30 and Y3.34. These three residues along with the backbone carbonyls of W4.50 and G4.57 form a series of interactions that appear to pull TMH4 to keep it packed close to TMH3, while contributing to the kinking of the extracellular end of TMH4, as seen in Figure 3.1. Y3.34 forms a hydrogen bond with S4.54, which pulls TMH4 close to TMH3. S3.30 also forms a hydrogen bond with the backbone carbonyl of G4.57 which aids in pulling TMH4 towards TMH3. Additionally, P4.59 provides further kinking of the extreme extracellular end of TMH4 away from TMH5.

When the S4.54 is mutated to an alanine in the MOR, the hydrogen bond with Y3.34 is eliminated. Because this interaction is lost, TMH4 is not held close enough to

TMH3 for the S3.30/G4.57 interaction to take place. Consequently, the overall shape of TMH4 in the S4.54A mutant receptor is altered such that TMH4 is less kinked and moves its extracellular end away from TMH3 towards TMH5 (see Figure 3.3).

Ligand Binding Pocket Changes During R to R* Transition

The striking phenotype of the S4.54A mutant is that naloxone changes from an antagonist to a partial agonist. This change is likely due to a structural change in the alkaloid binding pocket. The structural characteristics that define the GPCR inactive (R) and active (R*) states have been deduced primarily from biophysical studies of rhodopsin and the β2-AR receptor. In the inactive or off state (R), the intracellular (IC) end of TMH6 is bent towards TMH3 and a salt bridge between R3.50 and E/D6.30 on the intracellular side of the TMH bundle forms an "ionic lock". In the activated state, TMH6 undergoes a conformational change, straightening in the highly conserved CWXP hinge region.[41, 42, 43, 44, 45, 46] This results in the intracellular ionic lock breaking as TMH3 and TMH6 move away from each other.[47] Previous studies have shown that while the MOR does not form an "ionic lock" at the exact same location as rhodopsin, it does form a strong hydrogen bond between R3.50 and T6.34[36] that serves the same purpose for MOR. The R3.50 and T6.34 interaction is indeed present in the μ-opioid crystal structure with antagonist β-FNA present.[21]

The change from the inactive to active states also results in changes within the ligand binding pocket. In the R state, a tryptophan residue in the CWXP motif on TMH6, W6.48, adopts a $g+$ χ^1 dihedral angle. This conformation in rhodopsin is due to the close

proximity of the beta-ionone ring of rhodopsin's covalently bound ligand, 11-cis-retinal to W6.48, such that the tryptophan is locked in place.[6,5,4] W6.48 is part of the highly conserved TMH6 CWXP motif and has been identified as important for GPCR activation through early mutagenesis studies. A recent x-ray crystal structure of a constitutively active rhodopsin mutant suggests that when rhodopsin is activated and undergoes the isomerization of 11-cis retinal to all-trans-retinal, the beta-ionone ring is shifted 4.3Å towards the cleft between TMH5 and TMH6 and W6.48 is released from its locked position. The indole group of W6.48 moves 3.6Å away from its ground-state position as a consequence of rhodopsin activation[48] and W6.48 undergoes a change in its $\chi 1$ angle from *g+* → *trans*.[49] Although this change is not seen in recent activated GPCR crystal structures, it is possible that such a change is transient and therefore not captured in the crystalline state. In fact, in molecular dynamics simulations of cannabinoid CB2 receptor activation by its endogenous ligand, we observed such a transient change in W6.48.[50] Likewise, a rotameric change of W6.48 has been documented to occur in microsecond long molecular dynamics simulations[20] of the β-2 adrenergic receptor in complex with the Gs protein.

In the MOR crystal structure, the antagonist, β-FNA is covalently bound to K5.39 via an alkyl chain on the C ring of the fused ring structure (see Figure 3.4d). The N-substituent, a methylcyclopropyl is wedged between W6.48 and Y7.43. The A ring of the backbone structure of β-FNA sits above W6.48 and restricts its movement. To determine the location of naloxone in the MOR, we removed β-FNA and used Glide, a ligand docking program, to dock naloxone in the WT MOR. As illustrated in Figure 3.4a, the

Glide dock of naloxone in the MOR crystal structure[21] mimics the placement of β-FNA. Here, the naloxone C-ring (see Figure 3.4d) restricts the movement of W6.48. Figure 3.5a illustrates that even a 30° change in conformation of W6.48 is not possible due to steric clashes with naloxone. Further movement of W6.48 towards an active conformation would increase these steric clashes between W6.48 and naloxone in the WT MOR model.

Figure 3.9 presents a comparison of the recently released DOR crystal structure[22] complexed with naltrindole, the MOR crystal structure with β-FNA and our dock of naloxone in WT MOR.

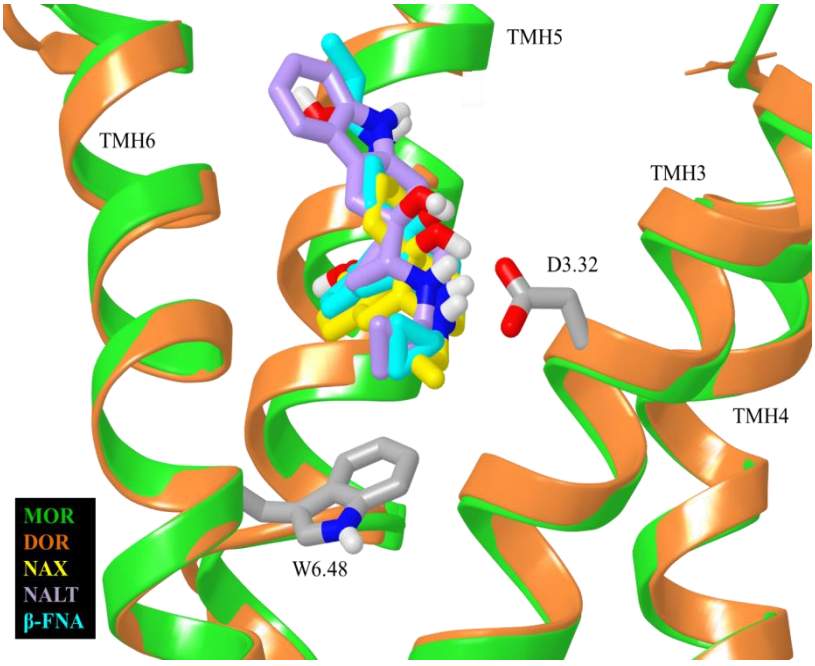

Figure 3.9. A comparison of the MOR crystal structure with β-FNA (cyan) and DOR crystal structure with naltrindole (purple), and the Glide docked naloxone (yellow) in MOR. All three ligands occupy the same general binding area of the receptors and interact with D3.32. Naloxone sits slightly lower and closer to D3.32 and is likely able to do so since there is no large side chain or indole ring off of its C-ring

This figure illustrates that all three ligands occupy the same general receptor region. Of the three ligands, naloxone (yellow) is shifted closest to the primary interaction site, D3.32 (gray). Naltrindole (purple) has a large indole ring attached to the C-ring of the opioid backbone structure which prevents naltrindole from binding deeper in the binding pocket, very similar to the covalent attachment of β-FNA (cyan) in the MOR crystal structure. Naloxone, which does not have a large sidechain or ring system off of the C-ring, is free to shift towards D3.32.

Our Glide docking studies suggest that the conformational changes produced by the S4.54A mutation on TMH packing (see Figure 3.3) results in naloxone sitting higher in the binding pocket (see Figure 3.4c). One important consequence of this new position is that naloxone has rotated to include an interaction with E5.35, therefore moving away from W6.48 such that W6.48 movement is no longer blocked by naloxone. This change is likely the reason why naloxone can act as a partial agonist in the S4.54A MOR mutant.

S4.54X MOR Mutations

Using a potassium current assay, we were able to identify two additional S4.54 mutations (S4.54L, S4.54F) that give rise to the unusual phenotype of naloxone acting as a partial agonist at the MOR. Subsequent cAMP assays identified an additional mutant, S4.54G, upon which naloxone also acted as a partial agonist. Surprisingly, upon mutation of S4.54 to an isoleucine or valine, naloxone remained acting as an antagonist, as seen in the wild type receptor. Each of these mutations results in the loss of the TMH3/TMH4 hydrogen bonding network seen in the wild type MOR. Along with

naloxone, naltrexone, DAMGO and CTOP were tested in the cAMP assays of the S4.54G, S4.54I and S4.54F mutants (see Figure 3.6b-d). Naltrexone is structurally very similar to naloxone, and would be expected to behave similarly. Both DAMGO and CTOP are peptide ligands and do not share a binding pocket with the alkaloid ligands such as naloxone and naltrexone. Therefore, their behavior may or may not be affected by various mutations on TMH4 and would not be expected to behave the same as the alkaloid ligands.

Upon examination of the S4.54I and S4.54V Conformational Memories output, we have determined that the isoleucine and valine mutant MORs are able to point their methyl groups directly at the ring system of W4.50, as seen in Figure 3.7b. In doing so, the hydrophobic interactions between W4.50 and I/V4.54 are maximized and the mutant TMH4 helix is able to maintain the wild type conformation even though the hydrogen bonding network seen in the crystal structure is disrupted.

Although the S4.54I and S4.54V mutant TMH4s are able to point their methyl groups at the ring system of W4.50, the S4.54L mutant is unable to do so without undertaking a *g*- conformation. Undertaking a *g*- conformation would cause a steric clash with the backbone, and thus a leucine at position 4.54 would have to remain in *g*+ or *trans*. The interaction energy between W4.50 and L4.54 is -12kJ/mol, compared to -22kJ/mol for the S4.54I and -26kJ/mol for the S4.54V mutants. As shown in Figure 3.7a, the S4.54L mutant TMH4 adopts the same conformation seen in the S4.54A MT MOR due to its inability to maximize interactions with W4.50 and disruption of the TMH3/TMH4 hydrogen bonding network seen in the wild type MOR.

Unlike the S4.54L mutant MOR, the S4.54F mutant is able to maximize interactions with W4.50 and yet, the phenylalanine mutant also gives rise to naloxone acting as a partial agonist. The offset parallel stack between F4.54 and W4.50 gives rise to an interaction energy of -20kJ/mol between the two residues, similar to that of the valine and isoleucine mutants. The TMH3/TMH4 hydrogen bonding network residue, Y3.34 points directly at S4.54 in the WT MOR, as shown in Figure 3.1b. Thus, a S4.54F mutation involves a large steric clash between the two residues if the receptor cannot adjust to the mutation. Therefore, we find that a S4.54F mutation and the loss of the hydrogen bonding network causes TMH4 to undertake a straighter conformation such that the helix is closer to TMH5, much like the S4.54A MT MOR model.

Upon mutation of S4.54 to glycine, naloxone displayed a partial agonist phenotype (Figure 3.6b). We find that although this mutation disrupts the TMH3/TMH4 hydrogen bonding network, it also allows for extra flexibility in the helix. The output structures for the S4.54G mutant MOR had an unwound region near G4.54. This region of the helix had a higher turn ratio of 5 residues per turn as opposed to the traditional 4 residues per turn seen in an alpha helix. The unwound region with a higher turn ratio shifts the extracellular end of S4.54G TMH4 towards TMH5, thus giving rise to naloxone's ability to act as a partial agonist.

Conclusions

The work presented here suggests that the origin of the unusual phenotype of the S4.54A mutant lies in the loss of a single key hydrogen bond between S4.54 and Y3.34 and the ensuing geometrical changes in the binding pocket which prevent naloxone from restricting the motion of W6.48 in the mutant MOR. We also propose that the S4.54I and S4.54V mutant MORs are able to maintain a wild type TMH4 conformation due to increased hydrophobic interactions with W4.50; accordingly naloxone maintains wild type activity. Upon mutation of S4.54L, S4.54G or S4.54F, the TMH3/TMH4 hydrogen bonding network is broken and each of the mutants are unable to maintain a wild type conformation. Consequently, naloxone displays partial agonist activity at these MORs much like the S4.54A mutant MOR described previously and herein.

References

1. Chen, S. L.; Ma, H. I.; Han, J. M.; Tao, P. L.; Law, P. Y.; Loh, H. H., dsAAV type 2-mediated gene transfer of MORS196A-EGFP into spinal cord as a pain management paradigm. *Proceedings of the National Academy of Sciences of the United States of America* **2007,** *104* (50), 20096-101.

2. Kao, J.; Chen, S.; MA, H.; Law, P. Y.; Tao, P. L.; Loh, H. H., Intrathecal delivery of a mutant Mu-opioid receptor activated by naloxone as a possible antinociceptive paradigm. *The Journal of Pharmacology and Experimental Therapeutics* **2010,** *334* (3), 739-45.

3. Portoghese PS, L. P. a. L. H., Effect of Opioid Receptor Ligands on the Mu S196A Knock-In and Mu Knockout Mouse Vas Deferens. *European Journal of Pharmacology* **2003,** *478*, 207-210.

4. Palczewski, K.; Kumasaka, T.; Hori, T.; Behnke, C. A.; Motoshima, H.; Fox, B. A.; Le Trong, I.; Teller, D. C.; Okada, T.; Stenkamp, R. E.; Yamamoto, M.; Miyano, M., Crystal structure of rhodopsin: A G protein-coupled receptor. *Science* **2000,** *289* (5480), 739-45.

5. Okada, T.; Fujiyoshi, Y.; Silow, M.; Navarro, J.; Landau, E. M.; Shichida, Y., Functional role of internal water molecules in rhodopsin revealed by X-ray crystallography. *Proceedings of the National Academy of Sciences of the United States of America* **2002,** *99* (9), 5982-7.

6. Li J, E. P., Burghammer M, Villa C and Schertler GF, Structure of Bovine Rhodopsin in a Trigonal Crystal Form. *J Mol Biol* **2004,** *3443* (5), 1429-38.

7. Choe, H. W.; Kim, Y. J.; Park, J. H.; Morizumi, T.; Pai, E. F.; Krauss, N.; Hofmann, K. P.; Scheerer, P.; Ernst, O. P., Crystal structure of metarhodopsin II. *Nature* **2011,** *471* (7340), 651-5.

8. Cherezov, V.; Rosenbaum, D. M.; Hanson, M. A.; Rasmussen, S. G.; Thian, F. S.; Kobilka, T. S.; Choi, H. J.; Kuhn, P.; Weis, W. I.; Kobilka, B. K.; Stevens, R. C., High-resolution crystal structure of an engineered human beta2-adrenergic G protein-coupled receptor. *Science* **2007,** *318* (5854), 1258-65

9. Rasmussen, S. G.; Choi, H. J.; Fung, J. J.; Pardon, E.; Casarosa, P.; Chae, P. S.; Devree, B. T.; Rosenbaum, D. M.; Thian, F. S.; Kobilka, T. S.; Schnapp, A.; Konetzki, I.; Sunahara, R. K.; Gellman, S. H.; Pautsch, A.; Steyaert, J.; Weis, W. I.; Kobilka, B. K., Structure of a nanobody-stabilized active state of the beta(2) adrenoceptor. *Nature* **2011,** *469* (7329), 175-80.

10. Rasmussen, S. G.; Choi, H. J.; Rosenbaum, D. M.; Kobilka, T. S.; Thian, F. S.; Edwards, P. C.; Burghammer, M.; Ratnala, V. R.; Sanishvili, R.; Fischetti, R. F.; Schertler, G. F.; Weis, W. I.; Kobilka, B. K., Crystal structure of the human beta2 adrenergic G-protein-coupled receptor. *Nature* **2007,** *450* (7168), 383-7.

11. Rosenbaum, D. M.; Cherezov, V.; Hanson, M. A.; Rasmussen, S. G.; Thian, F. S.; Kobilka, T. S.; Choi, H. J.; Yao, X. J.; Weis, W. I.; Stevens, R. C.; Kobilka, B. K., GPCR engineering yields high-resolution structural insights into beta2-adrenergic receptor function. *Science* **2007,** *318* (5854), 1266-73.

12. Rasmussen, S. G.; DeVree, B. T.; Zou, Y.; Kruse, A. C.; Chung, K. Y.; Kobilka, T. S.; Thian, F. S.; Chae, P. S.; Pardon, E.; Calinski, D.; Mathiesen, J. M.; Shah, S. T.; Lyons, J. A.; Caffrey, M.; Gellman, S. H.; Steyaert, J.; Skiniotis, G.; Weis, W. I.; Sunahara, R. K.; Kobilka, B. K., Crystal structure of the beta2 adrenergic receptor-Gs protein complex. *Nature* **2011,** *477* (7366), 549-55.

13. Warne, T.; Serrano-Vega, M. J.; Baker, J. G.; Moukhametzianov, R.; Edwards, P. C.; Henderson, R.; Leslie, A. G.; Tate, C. G.; Schertler, G. F., Structure of a beta1-adrenergic G-protein-coupled receptor. *Nature* **2008,** *454* (7203), 486-91.

14. Moukhametzianov, R.; Warne, T.; Edwards, P. C.; Serrano-Vega, M. J.; Leslie, A. G.; Tate, C. G.; Schertler, G. F., Two distinct conformations of helix 6 observed in antagonist-bound structures of a beta1-adrenergic receptor. *Proceedings of the National Academy of Sciences of the United States of America* **2011,** *108* (20), 8228-32.

15. Jaakola, V. P.; Griffith, M. T.; Hanson, M. A.; Cherezov, V.; Chien, E. Y.; Lane, J. R.; Ijzerman, A. P.; Stevens, R. C., The 2.6 angstrom crystal structure of a human A2A adenosine receptor bound to an antagonist. *Science* **2008,** *322* (5905), 1211-7.

16. Carroll, I.; Thomas, J. B.; Dykstra, L. A.; Granger, A. L.; Allen, R. M.; Howard, J. L.; Pollard, G. T.; Aceto, M. D.; Harris, L. S., Pharmacological properties of JDTic: a novel kappa-opioid receptor antagonist. *Eur J Pharmacol* **2004,** *501* (1-3), 111-9.

17. Wu, B.; Chien, E. Y.; Mol, C. D.; Fenalti, G.; Liu, W.; Katritch, V.; Abagyan, R.; Brooun, A.; Wells, P.; Bi, F. C.; Hamel, D. J.; Kuhn, P.; Handel, T. M.; Cherezov, V.; Stevens, R. C., Structures of the CXCR4 Chemokine GPCR with Small-Molecule and Cyclic Peptide Antagonists. *Science* **2010,** *330* (6007), 1066-71.

18. Chien, E. Y.; Liu, W.; Zhao, Q.; Katritch, V.; Han, G. W.; Hanson, M. A.; Shi, L.; Newman, A. H.; Javitch, J. A.; Cherezov, V.; Stevens, R. C., Structure of the human dopamine d3 receptor in complex with a d2/d3 selective antagonist. *Science* **2010,** *330* (6007), 1091-5.

19. T., S., Structure of the human histamine H1 receptor complex with doxepin. *Nature* **2011,** *475*, 65-70.

20. Lynch, D.; Hurst, D.; Romo, T.; Grossfield, A.; Reggio, P.; Pitman, M., Characterizing the Motion of W6.48 in the Active State of a GPCR. *2012 Biophysical Society Meeting Abstracts. Biophysical Journal* **2012,** *Supplement* (Abstract).

21. Manglik, A.; Kruse, A.; Kobilka, T.; Thian, F. S.; Mathiesen, J.; Sunahara, R.; Pardo, L.; Weis, W. I.; Kobilka, B. K.; Granier, S., Crystal Structure of the Mu-Opioid receptor bound to a morphinan antagonist. *Nature* **2012**.

22. Granier, S.; Manglik, A.; Kruse, A. C.; Kobilka, T. S.; Thian, F. S.; Weis, W. I.; Kobilka, B. K., Structure of the delta-opioid receptor bound to naltrindole. *Nature* **2012,** *485* (7398), 400-4.

23. Wu, H.; Wacker, D.; Mileni, M.; Katritch, V.; Won Han, G., Structure of the human kappa opioid receptor in complex with JDTic. *Nature* **2012**.

24. Yang, W.; Law, P. Y.; Guo, X.; Loh, H. H., In vivo activation of a mutant mu-opioid receptor by antagonist: future direction for opiate pain treatment paradigm that lacks undesirable side effects. *Proc Natl Acad Sci U S A* **2003,** *100* (4), 2117-21.

25. Claude-Geppert, P. A.; Liu, J.; Solberg, J.; Erickson-Herbrandson, L. J.; Loh, H. H.; Law, P. Y., Antagonist efficacy in MORS196L mutant is affected by the interaction between transmembrane domains of the opioid receptor. *J Pharmacol Exp Ther* **2005,** *313* (1), 216-26.

26. Dascal, N.; Lim, N. F.; Schreibmayer, W.; Wang, W.; Davidson, N.; Lester, H. A., Expression of an atrial G-protein-activated potassium channel in Xenopus oocytes. *Proceedings of the National Academy of Sciences of the United States of America* **1993,** *90* (14), 6596-600.

27. Coleman, A., Translation of eukaryotic messenger RNA in Xenopus oocytes. In *Transcription and Translation*, Higgins, B. H. a. S., Ed. IRL Press: 1984.

28. Stuhmer, W., Electrophysiological recording from Xenopus oocytes. *Methods Enzymol* **1992,** *207*, 319-39.

29. Law, P. Y.; Hom, D. S.; Loh, H. H., Opiate receptor down-regulation and desensitization in neuroblastoma X glioma NG108-15 hybrid cells are two separate cellular adaptation processes. *Mol Pharmacol* **1983,** *24* (3), 413-24.

30. White, A. A.; Karr, D. B., Improved two-step method for the assay of adenylate and guanylate cyclase. *Anal Biochem* **1978,** *85* (2), 451-60.

31. Konvicka, K.; Guarnieri, F.; Ballesteros, J. A.; Weinstein, H., A proposed structure for transmembrane segment 7 of G protein-coupled receptors incorporating an asn-Pro/Asp-Pro motif. *Biophys J* **1998,** *75* (2), 601-11.

32. Whitnell, R. M.; Hurst, D. P.; Reggio, P. H.; Guarnieri, F., Conformational memories with variable bond angles. *J Comput Chem* **2008,** *29*, 741-752.

33. Marti-Renom, M. A.; Stuart, A. C.; Fiser, A.; Sanchez, R.; Melo, F.; Sali, A., Comparative protein structure modeling of genes and genomes. *Annu Rev Biophys Biomol Struct* **2000,** *29*, 291-325.

34. Fiser, A.; Do, R. K.; Sali, A., Modeling of loops in protein structures. *Protein Sci* **2000,** *9* (9), 1753-73.

35. Sali, A.; Blundell, T. L., Comparative protein modelling by satisfaction of spatial restraints. *J Mol Biol* **1993,** *234* (3), 779-815.

36. Huang, P.; Visiers, I.; Weinstein, H.; Liu-Chen, L. Y., The local environment at the cytoplasmic end of TM6 of the mu opioid receptor differs from those of rhodopsin and monoamine receptors: introduction of an ionic lock between the cytoplasmic ends of helices 3 and 6 by a L6.30(275)E mutation inactivates the mu opioid receptor and reduces the constitutive activity of its T6.34(279)K mutant. *Biochemistry* **2002,** *41* (40), 11972-80.

37. Visiers, I.; Braunheim, B. B.; Weinstein, H., Prokink: a protocol for numerical evaluation of helix distortions by proline. *Protein Eng* **2000,** *13* (9), 603-6.

38. Surratt, C.; PS, J.; A, M.; BK, S.; CJ, B.; JB, W.; GR, U., Mu opiate receptor. Charged transmembrane domain amino acids are critical for agonist recognition and intrinsic activity. *J Biol Chem* **1994,** *269* (32), 20548-553.

39. von Heijne, G., Proline kinks in transmembrane alpha-helices. *J Mol Biol* **1991,** *218* (3), 499-503.

40. Ballesteros JA, D. X., Olivella M, Haaksma EE and Pardo L, Serine and Threonine Residues Bend Alpha-Helices in the chi(1) = g- conformation. *Biophys J* **2000,** *79* (5), 2754-60.

41. Farrens, D. L.; Altenbach, C.; Yang, K.; Hubbell, W. L.; Khorana, H. G., Requirement of Rigid-Body Motion of Transmembrane Helicies for Light-Activation of Rhodopsin. *Science* **1996,** *274*, 768-770.

42. Ghanouni, P., Steenhuis, JJ., Farrens D and Kobilka, B., Agonist Induced conformational Changes in the G-Protein Coupling Domain of the Beta-2-Adrenergic Receptor. *Proc Natl Acad Sci* **2001,** *98* (11), 5997-6002.

43. Javitch, J. A.; Fu, D.; Liapakis, G.; Chen, J., Constitutive activation of the beta2 adrenergic receptor alters the orientation of its sixth membrane-spanning segment. *J Biol Chem* **1997,** *272* (30), 18546-9.

44. Jensen, A. D.; Guarnieri, F.; Rasmussen, S. G.; Asmar, F.; Ballesteros, J. A.; Gether, U., Agonist-induced conformational changes at the cytoplasmic side of transmembrane segment 6 in the beta 2 adrenergic receptor mapped by site-selective fluorescent labeling. *J Biol Chem* **2001,** *276* (12), 9279-90.

45. Lin, S. W.; Sakmar, T. P., Specific tryptophan UV-absorbance changes are probes of the transition of rhodopsin to its active state. *Biochemistry* **1996,** *35* (34), 11149-59.

46. Nakanishi, J.; Takarada, T.; Yunoki, S.; Kikuchi, Y.; Maeda, M., FRET-based monitoring of conformational change of the beta2 adrenergic receptor in living cells. *Biochem Biophys Res Commun* **2006,** *343* (4), 1191-6.

47. Ballesteros, J. A.; Jensen, A. D.; Liapakis, G.; Rasmussen, S. G.; Shi, L.; Gether, U.; Javitch, J. A., Activation of the beta 2-adrenergic receptor involves disruption of an ionic lock between the cytoplasmic ends of transmembrane segments 3 and 6. *J Biol Chem* **2001,** *276* (31), 29171-7.

48. Standfuss, J.; Edwards, P. C.; D'Antona, A.; Fransen, M.; Xie, G.; Oprian, D. D.; Schertler, G. F., The structural basis of agonist-induced activation in constitutively active rhodopsin. *Nature* **2011,** *471* (7340), 656-60.

49. Shi, L.; Liapakis, G.; Xu, R.; Guarnieri, F.; Ballesteros, J. A.; Javitch, J. A., Beta2 adrenergic receptor activation. Modulation of the proline kink in transmembrane 6 by a rotamer toggle switch. *J Biol Chem* **2002,** *277* (43), 40989-96.

50. Hurst, D. P.; Grossfield, A.; Lynch, D. L.; Feller, S.; Romo, T. D.; Gawrisch, K.; Pitman, M. C.; Reggio, P. H., A lipid pathway for ligand binding is necessary for a cannabinoid G protein-coupled receptor. *J Biol Chem* **2010,** *285* (23), 17954-64.

CHAPTER IV

MOLECULAR STUDIES OF A S4.54L/T7.44A/C7.47S TRIPLE MUTANT MOR AT WHICH NALOXONE ACTS AS A FULL AGONIST

Introduction

For centuries the most consistent treatment for chronic and acute pain has been agonists of the opioid receptors.[1] Although there are three known opioid receptors, mu, delta and kappa, only mu receptor agonists, such as morphine and hydrocodone, consistently produce analgesic effects.[1,2] According to the IMS Health study of prescriptions in 2010, the number one prescribed medication was Vicodin® (hydrocodone and Tylenol) with 131 billion prescriptions filled. While these medications are effective at treating pain, they are also widely abused and can be addictive. Thus, the need for effective pain management without addiction and lessened side effects is essential.

Targeted gene therapy of opioids can be used to attenuate pain, as mentioned in the previous chapter using a single mutant of the mu-opioid receptor along with the traditional antagonist, naloxone.[3,4,5] However, the single mutant MOR described previously only provides naloxone with the ability to act as a partial agonist. Law and coworkers have published additional studies using a S4.54L/T7.44A/C7.47S triple mutant MOR that gives rise to naloxone acting as a full agonist.[6] While this gene therapy has been shown in cells and in spinal cord, the underlying mechanism is unknown and thus

the goal of this paper is to determine the molecular mechanism by which naloxone can act as a full agonist at the triple mutant MOR.

The binding pocket for mu opioid ligands is formed by TMHs 3, 5 and 6 in the wild type receptor, as seen in the crystal structure with β-FNA[7] and in our glide dock of naloxone (See Chapter 3). As discussed previously, S4.54 does not face into the receptor or the binding pocket; rather it is on the outer lipid interface of TMH4. Interestingly, both of the mutated residues on TMH7 (T7.44 and C7.47) in the triple mutant MOR also face lipid. We report here that the combination of the S4.54L mutation on TMH4 along with TMH7 face shift changes occur upon mutation of T7.44 and C7.47 produce overall packing changes that give rise to a different binding pocket than seen in the wild type or single mutant MORs. These changes result in naloxone's ability to fully activate the S4.54L/T7.44A/C7.47S MOR.

Methods

Conformational Memories Technique

We explored the wild type TMH7 sequence of the MOR as well as the T7.44A/C7.47S mutant TMH7 using Conformational Memories[8], as described previously. Briefly, an alpha helical TMH with the WT hMOR sequence was used as a starting point for this calculation. The region of A7.40 to P7.50 was considered the flexible region in both the WT calculations and the T7.44A/C7.47S mutant calculations. Backbone φ and ψ torsions in regions of interest were allowed to vary ±50°, while all

other backbone torsion angles were allowed to vary ±10°. Side chain torsions were allowed to vary ±180°. The exploratory phase starts at 3000K with 50,000 Monte Carlo steps applied to each torsion or bond angle variation, with cooling to 310K over 18 steps. The biased annealing phase starts at 749K and cools to 310K in 7 steps. There were 120 output TMH7 conformers generated in a distance-dependent dielectric at 310 K. The CM output helices were subsequently evaluated in the context of the MOR TMH bundle and an appropriate helix was chosen for substitution into the MOR model (see next section).

Construction of the TMH Region of the S4.54L/T7.44A/C7.47S MT MOR and Ligand Docking

The recently published MOT WT x-ray crystal structure[7] was used to create a homology model for the S4.54L/T7.44A/C7.47S triple mutant MOR model. As reported for the S4.54A single mutant MOR, the MOR crystal structure was pulled apart 2Å in each direction from the center of the bundle. The S4.54A TMH4 from the single mutant model was substituted in place of the WT TMH4. The selected T7.44A/C7.47S CM output helix was superimposed onto TMH7 of the crystal structure using the Cα atoms from L7.48 to F7.55. The transmembrane regions of the resultant S4.54L/T7.44A/C7.47S MOR model were energy minimized to allow the TMHs to pack such that there were no large gaps. The minimization protocol used included a 500 step energy minimization using the OPLS2005 all atom force field in Macromodel 9.1 (Schrodinger, 2006) and a distance-dependent dielectric with extended cutoffs. The backbone phi/psi dihedrals of the TMHs were constrained with a force of 500kJ/mol to

preserve their geometries. The minimization was set to converge to 0.05kJ/mol·Å^2. The converged output structure was selected as the model for the S4.54L/T7.44A/C7.47S MT MOR by comparing the TMH regions of the mutant and wild type receptors to ensure that the TMH region of the mutant receptor was not over-packed. Naloxone was docked in the resultant triple mutant model using Glide (Schrodinger 2006) with D3.32 as the primary interaction site for the ligand. The dock with the best Glide score was used for further study.

Due to the differences in the extracellular region, and overall changes in the receptor packing, all loops were calculated in MODELLER v9.1.[9,10,11] Restraints were added to the MODELLER run such that the disulfide bond with C3.25 and the beta sheet regions of the EC2 loop were preserved. The helical portion of the IC2 loop was also preserved. The IC3 loop was not resolved in the crystal structure therefore MODELLER was used to determine a likely loop conformation. Once the loops were added, naloxone was re-docked in the full model using Glide. The dock with the best Glide score was used for the final S4.54L/T7.44A/C7.47S MT MOR/naloxone complex model. The resultant WT MOR/naloxone and S4.54L/T7.44A/C7.47S MOR/naloxone complexes were compared in order to investigate the possible origins of naloxone's full agonist behavior in the S4.54L/T7.44A/C7.47S MT MOR at the molecular level.

Results

WT MOR Conformational Memories Results

CM calculations were used to determine the flexibility of WT TMH7, as well as that of the T7.44A/C7.47S MT TMH7. After superimposing on the intracellular end, the CM output from the WT and T7.44A/C7.47S were compared. As shown in Figure 4.1, the WT CM output (magenta) are clustered together tightly, while the T7.44A/C7.47S MT TMH7 CM output (blue) have a larger spread.

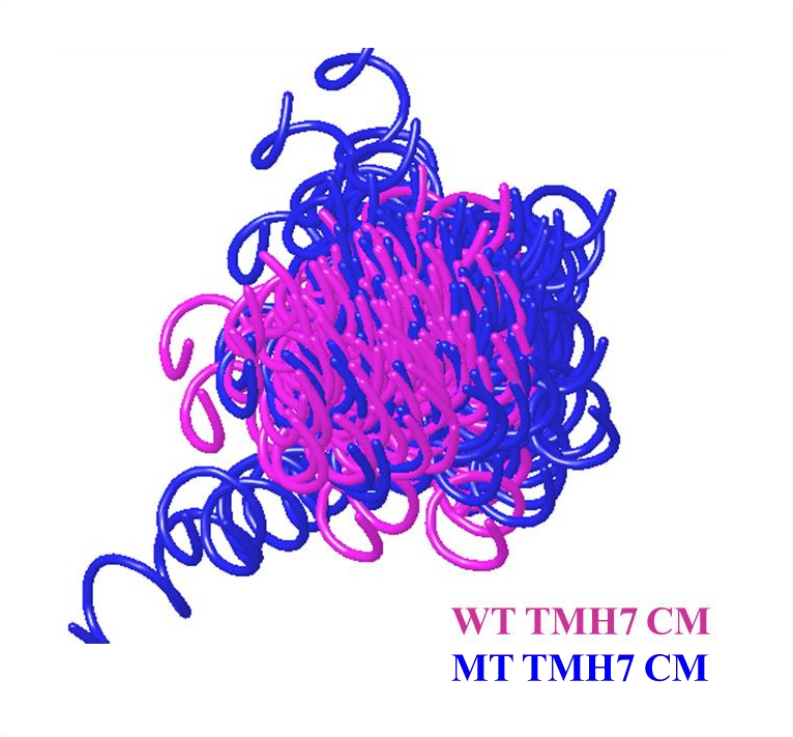

Figure 4.1. An extracellular view of Conformational Memories (CM) output of WT TMH7 (magenta) and T7.44A/C7.47S MT TMH7 (blue).

T7.44A/C7.47S Conformational Memories Results

The biased Monte Carlo/simulated annealing technique, Conformational Memories was used here to explore the conformational consequences of the T7.44A/C7.47S mutations in the MOR. Figure 4.2 shows the CM output for the T7.44A/C7.47S TMH7 superimposed using the Cα atoms of residues L7.48-F7.55 on TMH7 of the WT MOR. The most striking difference between the CM output and WT MOR TMH7 was that the extracellular end of the CM output bends towards the center of the receptor. Additionally, none of the output looks like the WT TMH7 seen in the crystal structure with many of the CM output kinking towards TMH1 or TMH6. The TMH7 chosen for use in the S4.54L/T7.44A/C7.47S mutant receptor is colored in red with the WT TMH7 colored yellow. The S4.54A MT TMH4 used is shown in magenta as well. Prokink[12] was used to determine the bend, wobble and face shift angles of the WT TMH7 (B=45.3°, W=46.3°, FS=-106.2°) and the MT TMH7 (B=37.1°, W=-60°, FS=116.6°). As shown in Figure 4.2, the extracellular end of the MT TMH7 moves inward slightly and toward TMH6.

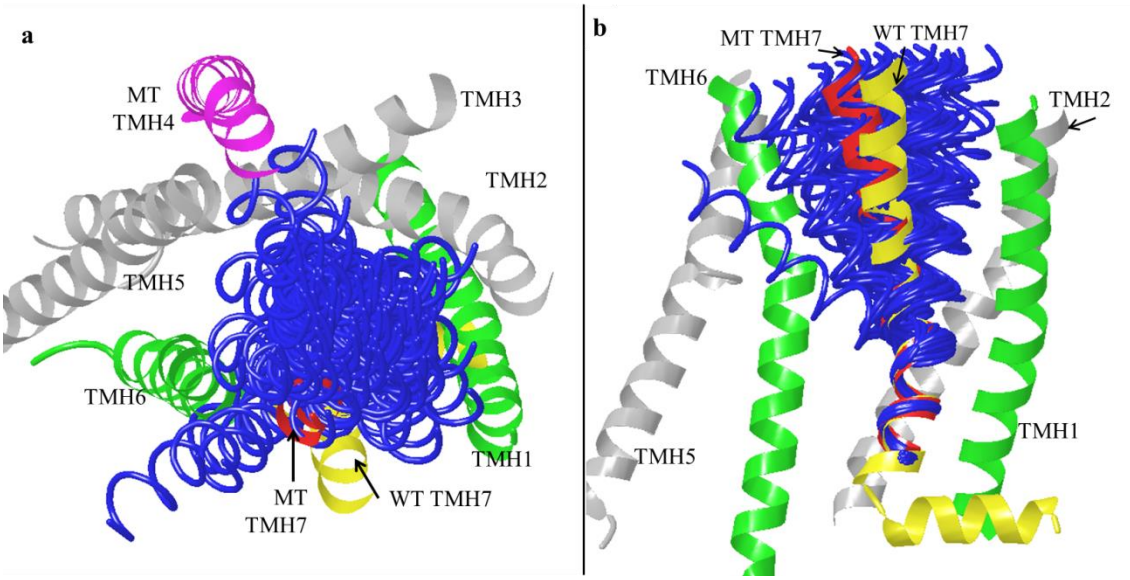

Figure 4.2. Conformational Memories (CM) output of T7.44A/C7.47S MT TMH7. An extracellular view (a) and a view from lipid (b) showing the WT MOR in gray (TMH2, 3, 5) and lime (TMH 1 and 6), the S4.54A MT TMH4 in magenta and WT TMH7 in yellow. The CM output is shown in blue tube displays with the T7.44A/C7.47S TMH7 selected in red.

Creation of S4.54L/T7.44A/C7.47S Triple Mutant MOR Model

A homology model of the S4.54L/T7.44A/C7.47S triple mutant MOR was developed using the published mu-opioid crystal structure (PDB Code: 4DKL)[7] and the results of the Conformational Memories studies of TMH4, as well as TMH7. Once the triple mutant MOR model was completed, the transmembrane regions were superimposed onto the MOR crystal structure template using the most conserved residue in each respective helix.

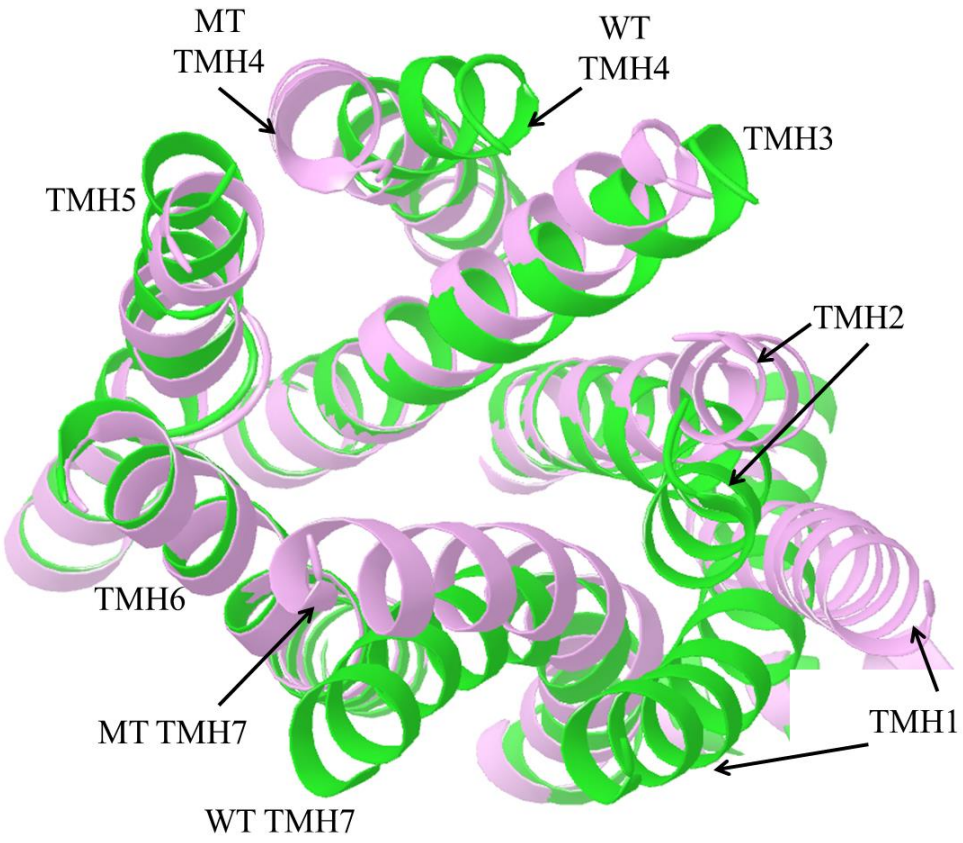

Figure 4.3. An extracellular view of the WT MOR (lime) and the S4.54L/T7.44A/C7.47 triple mutant, TMT, (lavender) MOR models. There were significant changes in TMHs 1, 2, 4, and 7 and minor changes in TMHs 3 and 5.

The superimposed receptors are shown in Figure 4.3, with the WT MOR in lime and the triple mutant (TMT) MOR shown in lavender. As shown, there are significant changes in the backbone structure of TMHs 1, 2, 4 and 7, with a minor shift in TMHs 3 and 5 and no changes in TMH6 between the WT MOR and the TMT MOR. The extracellular movement of TMH3 was found to not be significant. The changes in TMH4 and TMH5 are the same in the TMT as in the S4.54A SMT MOR model and thus the

hydrogen bond network between TMH3 and TMH4 in the S4.54L/T7.44A/C7.47S TMT MOR is disrupted.

The movement of TMHs 1, 2 and 7 can be seen Figures 4.4(a) (TMH2 and 7) and 4.4(b) (TMH1). As shown, TMH7 moves into the bundle and towards TMH6, TMH2 moves away from TMH1 and towards TMH3 and pulls back away from the center of the receptor. In the triple mutant model, TMH1 pulls back significantly when compared to the WT MOR (Figure 4.4(b)). The Cα of A1.32 at the extracellular end of TMH1 moves 10.89Å, Cα Y2.64 moves 5.35Å, and Cα W7.35 moves 6.59Å between the two models.

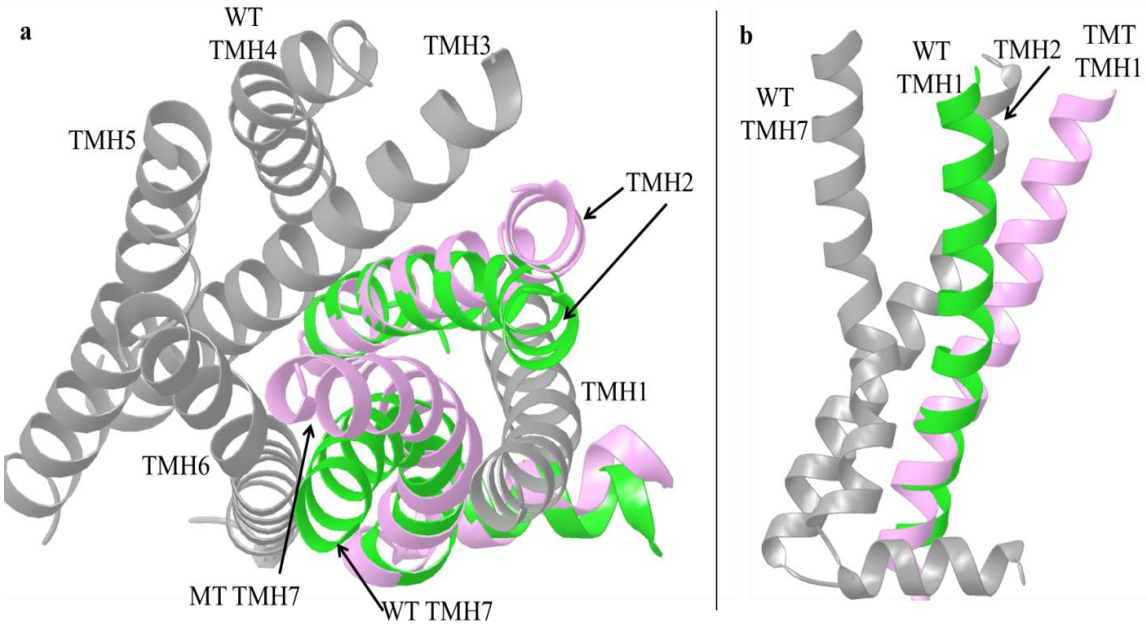

Figure 4.4. A zoomed in extracellular view of the WT MOR (lime /gray) and the TMT MOR model in lavender. (a) TMH2 and TMH7 are compared on the left. (b) The TMH1 difference is shown on the right.

Upon visual inspection it can be seen that in the triple mutant MOR, TMH1 and TMH7 are further apart than in the WT MOR (see Figures 4.3 and 4.4). A measurement of the distance between the Cα's atoms of A1.32 and W7.35 indicates that these two extracellular residues move apart by almost 6Å. In the WT MOR, the Cα's are 12.4Å apart, but in the TMT MOR they are 18.3Å apart. Interestingly, there is no gap between TMH1 and TMH7 as shown in Figure 4.5.

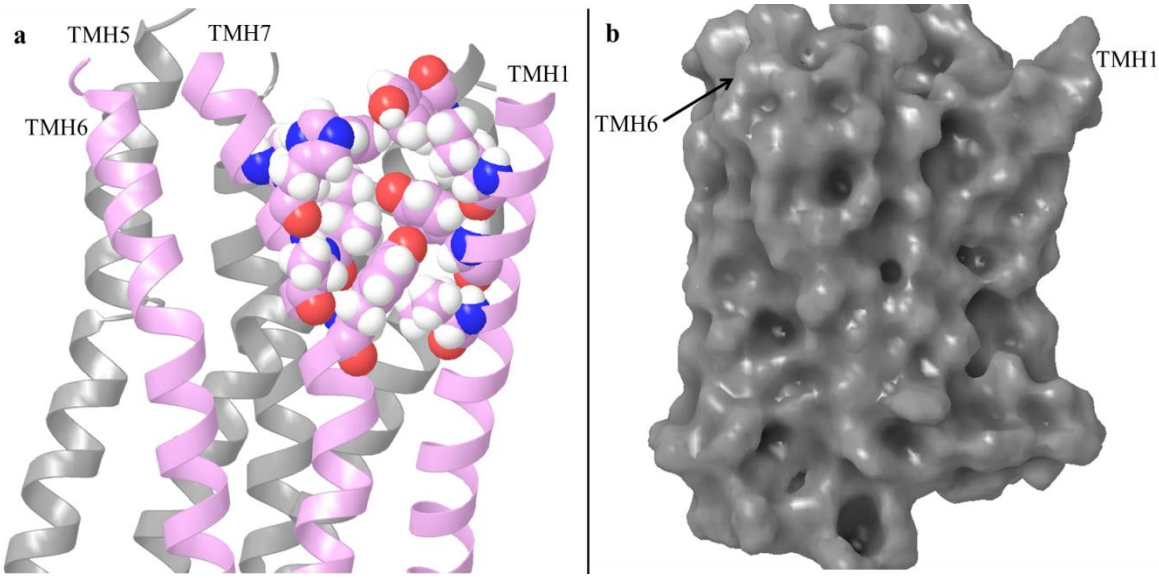

Figure 4.5. A view from lipid of the packing of TMH1 and TMH7 in the triple mutant MOR model. (a) shows residues involved in the packing of TMH1/7 in VdW representation and include I1.35, Y1.39, V1.42, Y2.64, W7.35, H7.36, I7.39 and Y7.43. (b) shows a surface representation of the triple mutant MOR model. It can be seen that there are no holes where a lipid could penetrate the receptor in the TMH2-7 region.

In Figure 4.5 (a), TMH1, 6 and 7 are shown in lavender with other helices in gray in the TMT MOR model. As shown, there are a significant number of bulky residues on the TMH1/2/7 interface that prevent a hole from opening between the two helices. These

residues include I1.35, Y1.39, V1.42, Y2.64, W7.35, H7.36, I7.39 and Y7.43 in the triple mutant MOR. Shown in surface representation in Figure 4.4 (b), it can be seen that although these helices are far apart, there are no holes where a lipid could possibly penetrate and disrupt the receptor.

In all three (mu, delta and kappa) opioid crystal structures there is a hydrogen bond interaction between Y7.43 and D3.32, as shown in Figure 4.6 for the WT MOR crystal structure (lime backbone, yellow residues). In our triple mutant model, this interaction has been broken due to the rotation and movement of TMH7. As shown, while there is slight movement of TMH3, the Cα atom of D3.32 remains in the same area with only minimal movement (1.01Å) in the TMT model compared to the MOR crystal structure.

As depicted in the WT MOR (lime backbone, yellow residues) D3.32 and Y7.43 are pointed towards each other and form a hydrogen bond. However, in the TMT MOR (lavender backbone, pink residues), TMH7 has moved and rotated such that Y7.43 does not point into the receptor; rather it is on the TMH1/7 lipid interface. Interestingly, TMH6 does not change shape between the WT MOR and TMT MOR models shown in Figure 4.3. Seen in Figure 4.6, W6.48 has minimal movement in the TMT MOR model (Cα moves by less than 1Å) and is in the same conformation in the WT MOR and the TMT MOR. Since both W6.48 and D3.32 move only a minimal amount, these two residues were used in measurements with Y7.43 to quantitate the movement of the central area of TMH7. The Cα distance between D3.32 and Y7.43 in the WT MOR was 9.8Å

and increased to 12.1Å in the TMT MOR. The Cα distance between W6.48 and Y7.43 in the WT MOR was 8.7Å and increased to 12.6Å in the TMT MOR.

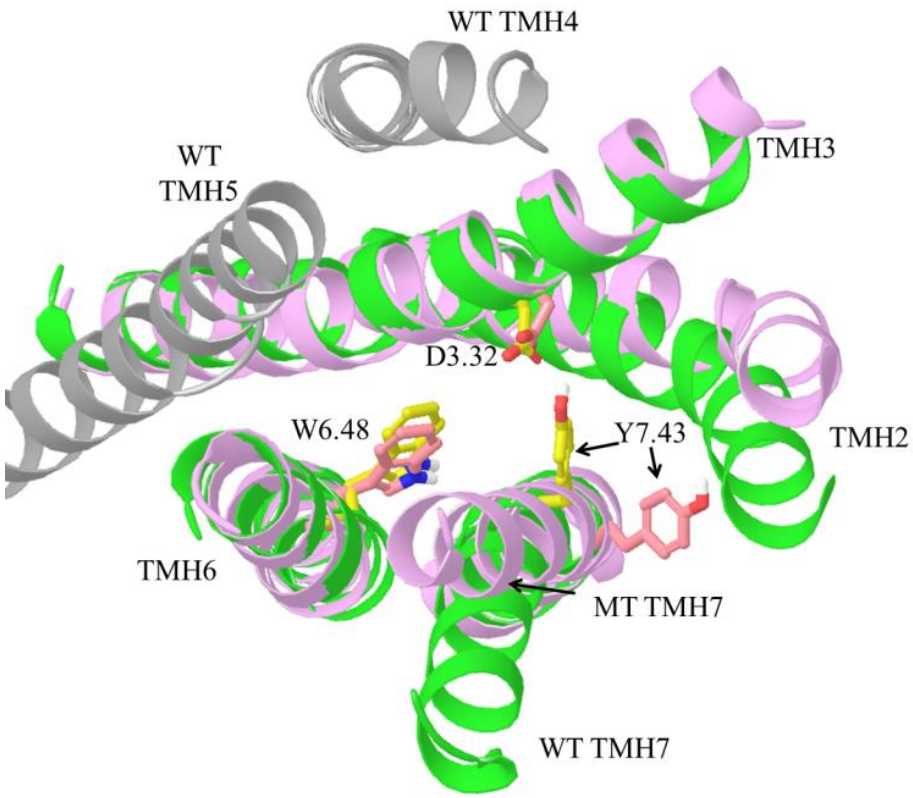

Figure 4.6. An extracellular view of the WT MOR (lime) and TMT MOR (lavender) models superimposed with D3.32, W6.48 and Y7.43 highlighted in yellow (WT) and pink (TMT). TMH7 rotates in the TMT and the D3.32/Y7.43 hydrogen bond interaction is broken as Y7.43 rotates away from the center of the receptor. TMH1 is omitted here for clarity.

Naloxone Docking Studies

S4.54L/T7.44A/C7.47S Triple Mutant MOR. Glide was used to identify a binding site for naloxone in the triple mutant MOR model (Figure 4.7) and the dock with the best score (-5.673) was chosen for naloxone docking studies. In this docked position, naloxone (pink) maintains the hydrogen bond interaction with D3.32 that has been shown experimentally and in the naloxone dock in the WT MOR (see Chapter 2 and Figure 4.7). Naloxone maintains VdW interactions with Y3.34 and M3.36 in the TMT MOR, but loses the W6.48 interaction. Also, in the TMT MOR model, naloxone picks up significant interactions with I3.29, W7.35 and C7.38. In addition to these interactions, naloxone also interacts with L155 in the E2 loop. In Figure 4.7 (a), naloxone can be seen in a space filling representation looking from lipid through TMH1 along with some of the residues it interacts with in gray. In Figure 4.7 (b), naloxone is seen with a view from TMH6 so that the residues on TMH3 can be visualized.

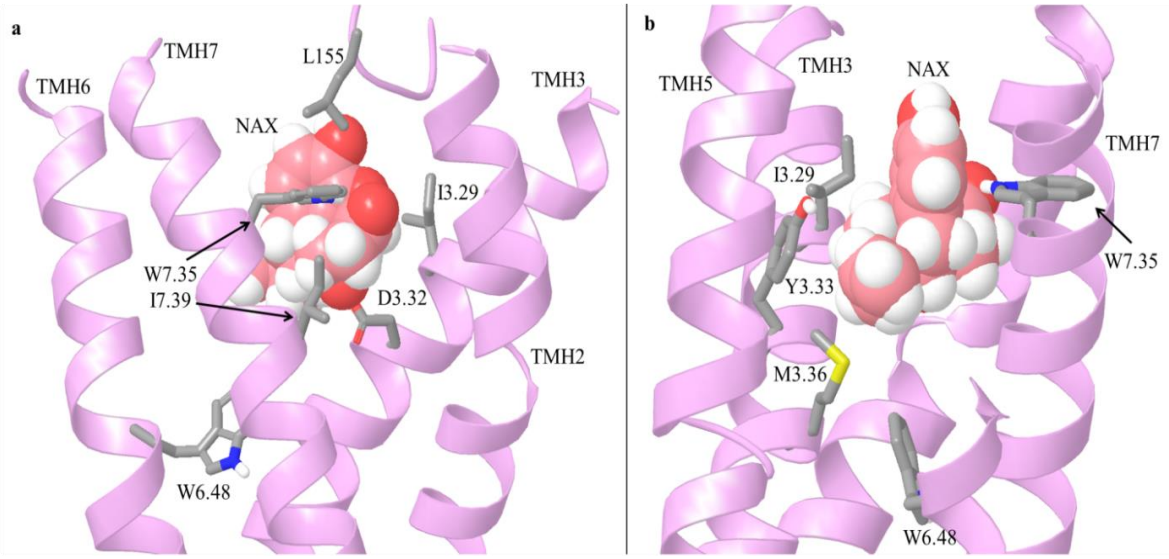

Figure 4.7. The docked position of naloxone in the S4.54L/T7.44A/C7.47S MT MOR model. (a). A view of naloxone's (pink, space filling) binding pocket looking through TMH1 in the TMT MOR model. Naloxone maintains a hydrogen bond interaction with D3.32 and picks up interactions with L155, I7.39 and W7.35. (b) A cut away view from TMH6 showing naloxone's interactions with I3.29, Y3.33 and M3.36 in gray.

Naloxone binds higher and in a different location in the triple mutant MOR than it does in the WT MOR crystal structure as shown in Figure 4.8. In the WT MOR crystal structure dock of naloxone, the alkaloid backbone of naloxone is located between TMH 3, 5, and 6 (as discussed previously) but in the TMT MOR, naloxone has re-oriented in the binding pocket and docks with the alkaloid backbone between TMH 2, 3, 6 and 7. In a view from between TMH1 and TMH7 (cut away for clarity), it can be seen that the alkaloid backbone of naloxone in the TMT model (pink) has rotated towards TMH2 and is higher in the binding pocket than in the WT MOR dock (yellow naloxone).

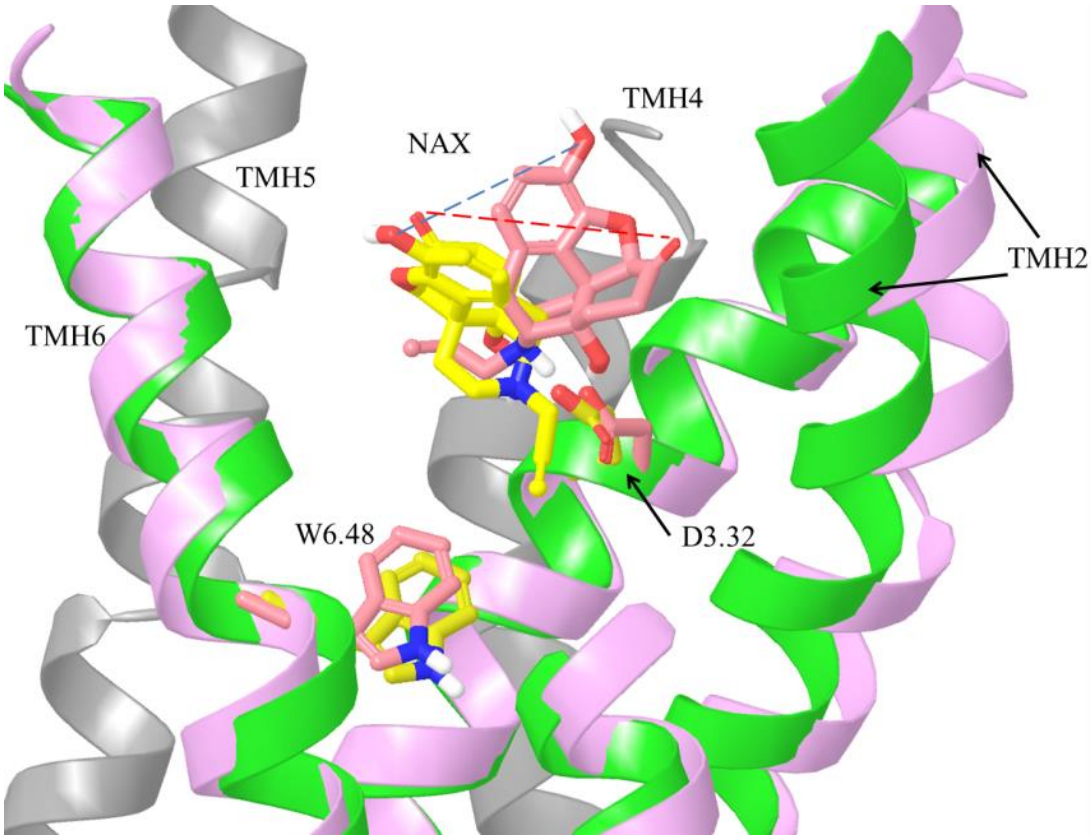

Figure 4.8. A lipid view from TMH7 of the WT MOR (lime, yellow residues) and TMT MOR (gray, pink residues) models superimposed with naloxone docked. The A-ring hydroxyl of the alkaloid backbone of naloxone moves extracellularly 6.7Å (blue line) and the C-ring carbonyl moves 7.3Å in the TMT MOR backbone, as indicated by the red dashed line.

As shown in Figure 4.8, the A-ring hydroxyl of the alkaloid backbone of naloxone moves 6.7Å extracellularly, away from TMH6 towards TMH3 in the TMT MOR dock (pink naloxone—see blue dashed line which references the position of naloxone (yellow) in the WT MOR). Additionally, the C-ring carbonyl oxygen flips 180° away (7.3Å) from TMH5 and towards TMH2 in the TMT dock of naloxone, as shown by the red dashed line in Figure 4.8. The alkaloid fused ring system of naloxone restricts movement of W6.48 in the WT MOR, but does not restrict movement of W6.48 in the TMT MOR.

The charged nitrogen of naloxone is 11Å away from the Cα carbon of W6.48 in the TMT MOR but only 9Å away in the WT MOR.

Discussion

Geometry of TMH7

As previously discussed, while proline residues are the most common helix deforming residues, glycines, serines and threonines can also deform helices.[13] In addition to leaving the *i-4* backbone carbonyl without its normal hydrogen bond donor, the proline also sterically prevents the *(i-3)*-carbonyl-(*i* + *l*)-amide backbone hydrogen bond from forming.[13] The hydrogen bonding capacity of serine or threonine residues in α-helices can be satisfied by an intrahelical hydrogen bond interaction, in either the *g-* or *g+* conformation, between the O-γ atom and the *i-3* or *i-4* carbonyl oxygen. Serine and threonine residues in the *g-* conformation can induce a bend in an α-helix, and we have found that changes in wobble angle and face shift can also occur.[14] For example, in the kappa opioid receptor (KOR) crystal structure, there is no proline at position 4.59 as seen in both the mu and delta opioid receptors. Interestingly, the shape of TMH4 in the KOR is the same as the shape in the MOR and DOR. The KOR TMH4 is able to mimic the proline kink seen in the MOR and DOR because it has a S4.59 which can form a hydrogen bond with the backbone carbonyl of V4.56, the *i-3* residue and bend the helix.

In the MOR crystal structure, C7.47 faces lipid on the TMH1/7 interface and is in a *g-* conformation with a χ1 dihedral value of 82°. Although a relatively weak

interaction, C7.47 forms a hydrogen bond with the backbone carbonyl of T7.44, the *i-3* residue. In both the delta and kappa opioid receptors, the residue at position 7.47 is a serine and undertakes the *g-* conformation in the crystal structure.

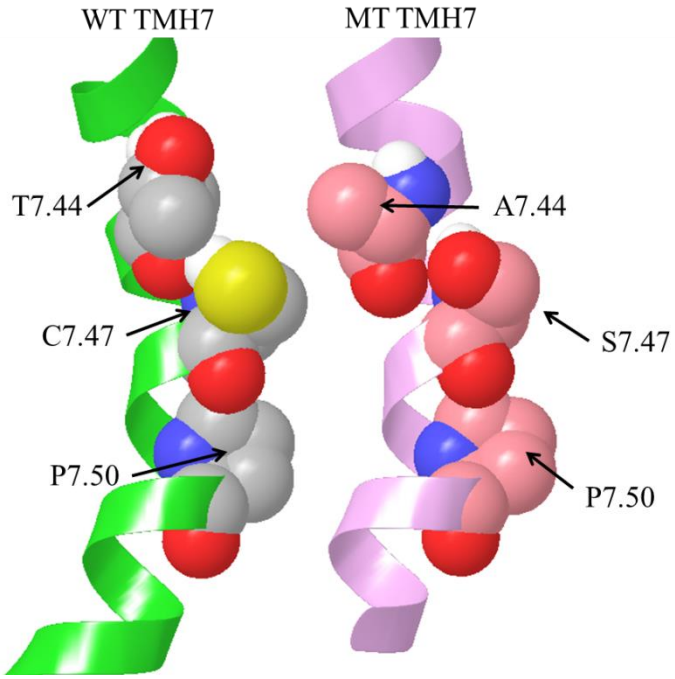

Figure 4.9. A close up picture of TMH7 in the WT MOR (left, lime) and the TMT MOR (right, lavender) in the region of the T7.44A/C7.47S mutations. As shown, both the alanine and serine are smaller than the threonine and cysteine and allow for extra flexibility of TMH7.

By mutating C7.47 in the MOR to a serine, the hydrogen bond is strengthened and thus the new residue may aid in deforming TMH7. Also, the cysteine to serine mutation allows for greater flexibility of TMH7 since the large sulfur atom has been replaced by a smaller oxygen atom in the serine as shown in Figure 4.9. Additionally, the T7.44A

mutation results in the loss of steric bulk of the threonine to just the methyl group of the alanine, also shown in Figure 4.9.

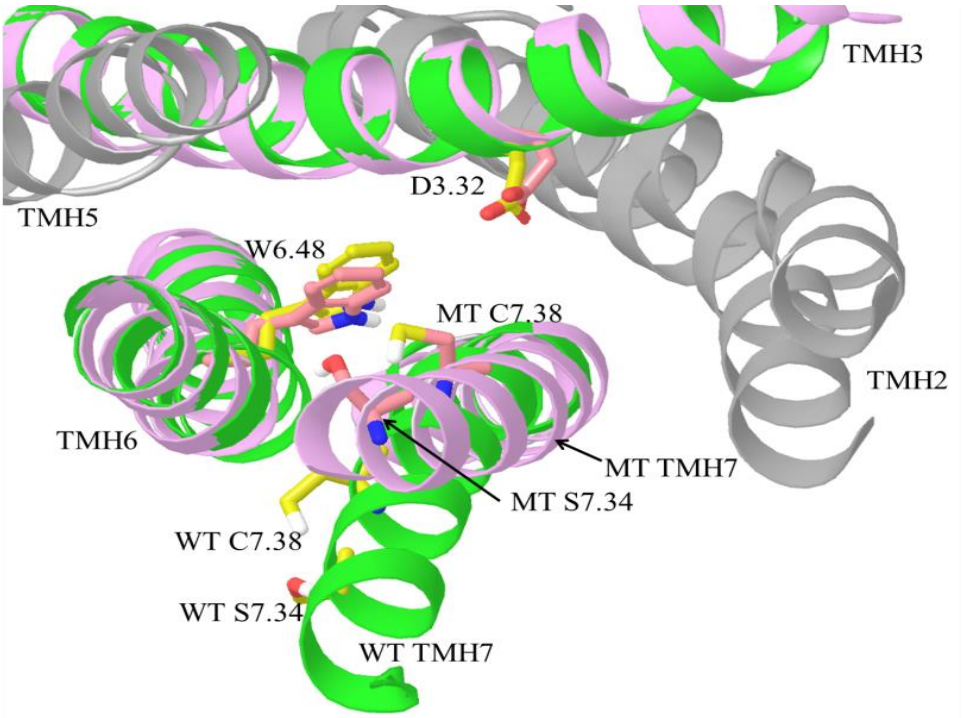

Figure 4.10. An extracellular view of the WT MOR (lime) and TMT MOR (lavender) displaying S7.34 and C7.37 in both receptors. In the TMT MOR model, these residues point into the binding pocket rather than staying on the lipid side of TMH7 as seen in the crystal structure.

Taken together, both the C7.47S and T7.44A mutations give TMH7 greater flexibility than seen in the WT, as shown in Figure 4.1. The WT TMH7 CM output helices are clustered together, while the T7.44A/C7.47S MT TMH7 CM output helices have a much larger spread.

In Class A GPCRs, residues 7.34 and 7.38 are located out of the TMH6/TMH7 interface, facing lipid. These residues are generally hydrophobic, however in the opioids

they are generally a S7.34 and C7.37. The exception to this is in the DOR, where 7.34 is an alanine. Given that these residues face lipid, they will form hydrogen bonds with the backbone of the TMH to satisfy their hydrogen bond capability. In the MOR crystal structure, S7.34 is in g- with a χ1 dihedral of 59° and can hydrogen bond to both the *i-3* and *i-4* carbonyl oxygen. As shown in Figure 4.10, both S7.34 and C7.38 are on the lipid interface of TMH6/TMH7 in the MOR crystal structure (lime). However, as a result of the additional flexibility and movement of the T7.44A/C7.47S TMH7 both S7.34 and C7.38 have rotated and are on the inside of the bundle in the triple mutant MOR model (Figure 4.10, lavender backbone). In the WT MOR, the Cα of W6.48 and S7.34 are 13.7Å apart, but come closer together in the TMT MOR, with a distance of 11.7 Å. Additionally, the Cα of D3.32 and S7.34 are 20Å apart in the WT MOR, but that distance decreases to 14.6 Å in the TMT MOR. As a result of the additional flexibility and movement of TMH7, there is a large face shift and bend difference in the T7.44A/C7.47S TMH7. The face shift in the WT TMH7 is -106.2°, compared with 116.6° in the MT TMH7. The wobble in the WT TMH7 is 46.3° and is -60° in the MT TMH7.

Binding pocket changes in the S4.54L/T7.44A/C7.47S triple mutant MOR

In the TMT MOR, naloxone maintains its strong salt bridge interaction with D3.32, while also forming strong interactions with W7.35, C7.38 and I3.29. These interactions are made possible by the changes in the receptor binding pocket due to the movement of TMH7 and subsequently the position change of naloxone. As a result of

sitting higher in the binding pocket on the opposite side of the receptor, naloxone also picks up interactions with L155 in the E2 loop, Q2.60 and Q7.31.

As discussed in the previous chapter, as a GPCR undergoes activation, W6.48 changes its χ1 dihedral from *g+* to *trans*. For W6.48 to be able to shift in the MOR naloxone cannot be preventing that movement by either the alkaloid backbone or the N-allyl tail. As indicated by our Glide dock of naloxone, the fused ring system of the alkaloid backbone prevents the movement of W6.48 in the WT MOR. However, in the S4.54L/T7.44A/C7.47S triple mutant MOR, the nitrogen that hydrogen bonds with D3.32 is slightly higher in the binding pocket and the fused alkaloid backbone rotates away from TMH6 and towards TMH2 and TMH7. This rotation moves the hydroxyl of the A-ring of the alkaloid backbone 6.7 Å higher in the binding pocket as shown in Figure 4.8. Shown in Figure 4.11, in the TMT MOR, naloxone does not prohibit movement of W6.48. In Figure 4.11 (a), the χ1 dihedral of W6.48 is in g+ at -88°. Figures 4.11(b-d) show the movement of W6.48χ1 dihedral as it rotates from *g+* to *trans*, -110° (11b), -140° (11c) and -180° (11d). As depicted, W6.48 is free to move without being blocked by naloxone in the TMT MOR. Distance measurements indicate that during the rotation of W6.48, no atom of W6.48 or naloxone come closer together than a distance of 3.5Å at any point in time, including hydrogen atoms.

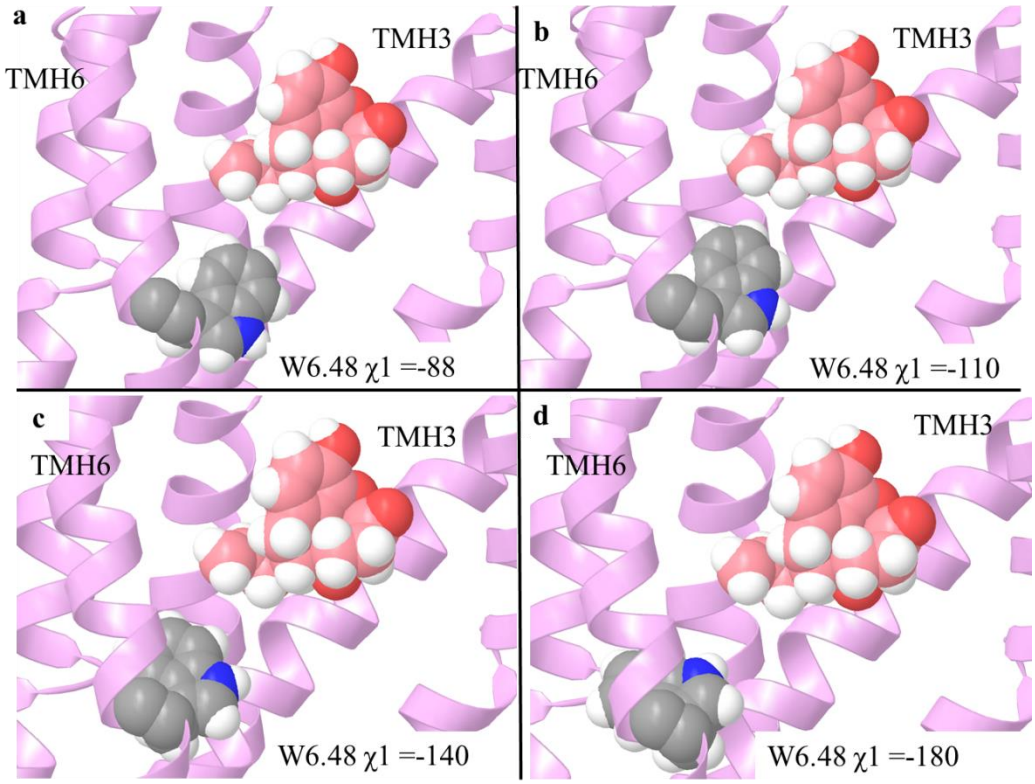

Figure 4.11. Movement of W6.48 in the TMT MOR Model. This figure shows the progression of W6.48 (gray, VdW) from a χ1 dihedral of *g+* (-80°) to *trans* (180°). This movement of W6.48 is unimpeded by naloxone which is shown in VdW display and pink.

Binding pocket changes in the S4.54A SMT MOR and S4.54L/T7.44A/C7.47S TMT MOR

In both the S4.54A SMT and S4.54L/T7.44A/C7.47S TMT MOR models, naloxone maintains interactions with D3.32 and M3.36 as seen in the dock of naloxone in the WT MOR crystal structure (see previous chapter). However, naloxone binds higher in both the SMT MOR and the TMT MOR as indicated by the difference in the distance between the Cα atoms of W6.48 and the N^+ on naloxone in each of the 3 models (9.0Å in the WT, 12Å in the SMT, and 12.5Å in the TMT). Additionally, as mentioned before,

naloxone rotates in the TMT model towards TMH2 such that the alkaloid backbone is shifted when compared to the WT MOR or the SMT MOR models. The difference of the Cα atom positions of D3.32 in the two mutant MOR models is very small (1.0Å), as is the difference in Cα atom positions of W6.48 (0.7Å). In the S4.54A SMT MOR model, naloxone is able to bind higher in part due to the face shift of TMH5 (see previous chapter) and a new hydrogen bond with E5.35.

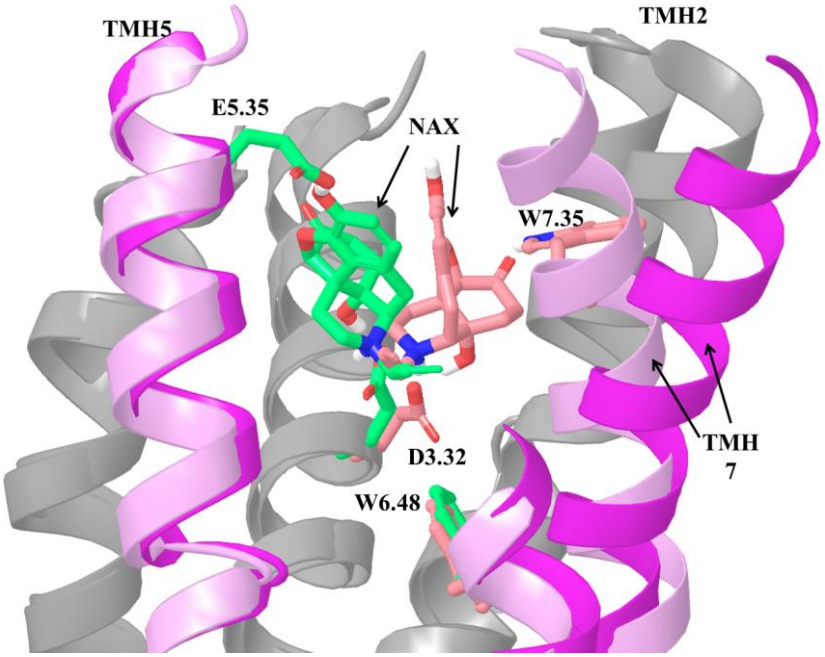

Figure 4.12. The S4.54A SMT MOR (magenta backbone, sea green residues) and the S4.54L/T7.44A/C7.47S TMT MOR (lavender backbone, pink residues) models with naloxone. Naloxone maintains the D3.32 interaction in both models but picks up an interaction with E5.35 in the SMT MOR and with S7.34 in the TMT models.

The protonated N atom of naloxone in the S4.54A SMT MOR is approximately 2Å from the protonated N atom of naloxone in the S4.54L/T7.44A/C7.47S TMT MOR

model. Also, in the TMT MOR, the C-ring carbonyl of naloxone moves 8.9Å when compared to the SMT MOR with naloxone. However, in the S4.54L/T7.44A/C7.47S TMT MOR, the shape of the receptor is altered such that naloxone is able to pick up interactions with W7.35 and C7.38, which is not seen in either the SMT MOR or the WT MOR. Due to the changes in the TMH7 region and naloxone's orientation, in the TMT MOR naloxone does not interact with E5.35, but instead interacts with W7.35. Figure 4.12 shows the S4.54A SMT MOR model (magenta helices, green residues) and the S4.54L /T7.44A/ C7.47S TMT MOR (lavender helices, pink residues) model with naloxone docked in both models. As shown, TMH7 in the TMT MOR (lavender) is pulled into the receptor towards TMH3 more than what is seen in the SMT (magenta) TMH7. Additionally, the A-ring hydroxyl of naloxone, which hydrogen bonds with E5.35 in the SMT, moves 7.0Å in the TMT model when compared with its location in the SMT model and the C-ring carbonyl oxygen moves 8.9Å in the TMT model.

Conclusions

In the S4.54A SMT MOR, the new position of naloxone allows it to bind higher and form a hydrogen bond with E5.35, therefore moving away from W6.48 such that W6.48 movement is no longer blocked by naloxone. This change is likely the reason why naloxone can act as a partial agonist in the S4.54A MOR mutant. Naloxone binds higher and in a different location in the S4.54L/T7.44A/C7.47S TMT MOR. In this new binding pocket where the alkaloid backbone is in the pocket formed by TMH2, 3 and 7 in

the TMT MOR, naloxone does not come close to W6.48. Upon activation in the TMT MOR, the χ1 dihedral of W6.48 can rotate from *g+* to *trans*, and the carbon atoms of the indole ring come no closer to any carbon of naloxone than 6Å at any point during the rotation. Additionally, in the TMT MOR, TMH7 rotates such that Y7.43 is on the TMH1/7 interface and its interaction with D3.32 is broken. The breakings of this interaction, as well as the changes in the overall packing of the receptor, together with naloxone's altered binding position are likely the underlying reasons for naloxone's full agonism in the triple mutant MOR.

References

1. Pasternak, G. W., *The Opiate Receptors*. 2nd ed.; Humana Press; 2nd ed. 2011: 2011; p 528.

2. Moal, K. L., *Neurobiology of Addiction*. Elsevier: 2005.

3. Chen, S. L.; Ma, H. I.; Han, J. M.; Tao, P. L.; Law, P. Y.; Loh, H. H., dsAAV type 2-mediated gene transfer of MORS196A-EGFP into spinal cord as a pain management paradigm. *Proc Natl Acad Sci U S A* **2007,** *104* (50), 20096-101.

4. Kao, J.; Chen, S.; MA, H.; Law, P. Y.; Tao, P. L.; Loh, H. H., Intrathecal delivery of a mutant Mu-opioid receptor activated by naloxone as a possible antinociceptive paradigm. *The Journal of Pharmacology and Experimental Therapeutics* **2010,** *334* (3), 739-45.

5. Portoghese PS, L. P. a. L. H., Effect of Opioid Receptor Ligands on the Mu S196A Knock-In and Mu Knockout Mouse Vas Deferens. *European Journal of Pharmacology* **2003,** *478*, 207-210.

6. Claude-Geppert, P. A.; Liu, J.; Solberg, J.; Erickson-Herbrandson, L. J.; Loh, H. H.; Law, P. Y., Antagonist efficacy in MORS196L mutant is affected by the interaction between transmembrane domains of the opioid receptor. *J Pharmacol Exp Ther* **2005,** *313* (1), 216-26.

7. Manglik, A.; Kruse, A.; Kobilka, T.; Thian, F. S.; Mathiesen, J.; Sunahara, R.; Pardo, L.; Weis, W. I.; Kobilka, B. K.; Granier, S., Crystal Structure of the Mu-Opioid receptor bound to a morphinan antagonist. *Nature* **2012**.

8. Whitnell, R. M.; Hurst, D. P.; Reggio, P. H.; Guarnieri, F., Conformational memories with variable bond angles. *J Comput Chem* **2008,** *29*, 741-752.

9. Fiser, A.; Do, R. K.; Sali, A., Modeling of loops in protein structures. *Protein Sci* **2000,** *9* (9), 1753-73.

10. Marti-Renom, M. A.; Stuart, A. C.; Fiser, A.; Sanchez, R.; Melo, F.; Sali, A., Comparative protein structure modeling of genes and genomes. *Annu Rev Biophys Biomol Struct* **2000,** *29*, 291-325.

11. Sali, A.; Blundell, T. L., Comparative protein modelling by satisfaction of spatial restraints. *J Mol Biol* **1993,** *234* (3), 779-815.

12. Visiers, I.; Braunheim, B. B.; Weinstein, H., Prokink: a protocol for numerical evaluation of helix distortions by proline. *Protein Eng* **2000,** *13* (9), 603-6.

13. von Heijne, G., Proline kinks in transmembrane alpha-helices. *J Mol Biol* **1991,** *218* (3), 499-503.

14. Ballesteros JA, D. X., Olivella M, Haaksma EE and Pardo L, Serine and Threonine Residues Bend Alpha-Helices in the chi(1) = g- conformation. *Biophys J* **2000,** *79* (5), 2754-60.

CHAPTER V

PARAMETERIZATION DEVELOPMENT OF THE N-ALLYL TAIL OF NALOXONE

Introduction

The mu opioid receptor is a Class A G-protein coupled receptor (GPCR) that is widely expressed throughout the peripheral and central nervous systems. Traditionally, drugs used for pain management activate the mu-opioid receptor (MOR) and include medications such as morphine and oxycodone. Antagonists of the mu-opioid receptor, such as naloxone and naltrexone are used in cases of opioid overdose to reverse the actions of MOR agonists. While it has been known for many years that these drugs work in the body, their exact mechanism and interactions have not been discovered. Computational studies and simulations can be used to determine exactly how opioid ligands behave in the receptor. Although there have been previous molecular dynamics simulations of the opioid receptors and their ligands,[1,2] parameters for these ligands have not been published.

In the work described here, we developed parameters for naloxone for use in molecular dynamics simulations employing a CHARMM force field.[3,4] These parameters were developed using an established parameterization method which compares molecular mechanical and quantum mechanical data, as previously published.[3,4,5]

The published CHARMM General Force Field (CGenFF) database[6] was used as a starting point due to its extensive list of atom types and parameters for organic compounds. Subsequently, a model compound was used to develop novel parameters for the N-allyl region of naloxone and is described herein.

Methods

The potential energy function applied by CHARMM is given in equation (1) below.

$$E = \sum_{\text{bonds}} K_b\left(b - b_0\right)^2 + \sum_{\text{angles}} K_\theta\left(\theta - \theta_0\right)^2 + \sum_{\text{U-B}} K_{UB}\left(s - s_0\right)^2 + \sum_{\text{dihedrals}} K_\phi\left[1 + \cos\left(n\phi - \delta\right)\right] + \sum_{\text{improper}} K_\psi\left(\psi - \psi_0\right)^2 + \sum_{\text{nonbonded}} \left\{ \varepsilon_{ij} \left[\left(\frac{R_{\min,ij}}{r_{ij}} \right)^{12} - \left(\frac{R_{\min,ij}}{r_{ij}} \right)^{6} \right] + \frac{q_i q_j}{\varepsilon_1 r_{ij}} \right\} \quad (1)$$

where K_b, K_θ, K_{UB}, K_φ, K_ψ are respectively the bond, angle, Urey-Bradley, dihedral, and improper dihedral force constants; b, θ, s, φ, ψ are respectively the bond length, bond angle, Urey-Bradley distance, dihedral angle, and improper dihedral angle, where the subscript zero represents the equilibrium value of each. The dihedral value also incorporates n, the periodicity, and δ, the phase. In the CHARMM force field nonbonded interactions, including attractive Van der Waals dispersion as well as short range repulsion, are included via the Lennard Jones 6-12 potential. Electrostatic interactions are included using the Coulombic potential. In equation 1, $R_{\min}$ is the distance between atoms at the Lennard-Jones minimum and ε is the well depth. The partial atomic charges,

q, and the effective dielectric constant, ε_l, are both included in the Coulombic contribution. Lastly, r_{ij} is the distance between atoms i and j.[3]

Force field parameters for naloxone were calculated by comparison to quantum mechanical (QM) calculated data. The structure of naloxone is displayed in Figure 5.1 along with the atomic naming convention used in this work. Atom types in naloxone were assigned according to those used in the CGenFF database[6] and are listed in Table 5.1 for each atom number which is labeled in Figure 5.1. The CGenFF types,[6] that the current naloxone parameters were derived from, are listed in Table 5.2.

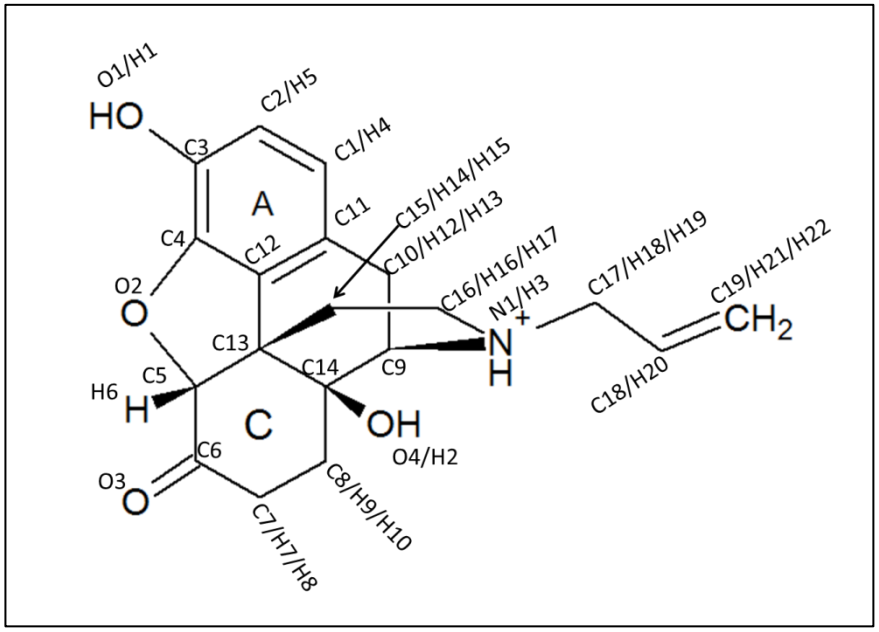

Figure 5.1. The structure of Naloxone is illustrated here along with the atomic numbering convention used in this work. Atom labels were assigned based upon atom types from the CGenFF library. Atom names were changed from six characters to three or four to be compatible with CHARMM27

Table 5.1. Listing of Atom Names, Types and Partial Charges for Naloxone
(See Figure 5.1 for atom numbering system)

Atom	Type	Partial Charge	Atom	Type	Partial Charge
O1	O11	-0.53	H1	HP1	0.42
O2	O351	-0.40	H2	HP1	0.42
O3	OD3	-0.48	H3	HP2	0.32
O4	O11	-0.64	H4	H61	0.12
N1	NP1	-0.40	H5	H61	0.12
C1	C61	-0.12	H6	HG1	0.09
C2	C61	-0.12	H7	HG2	0.09
C3	C61	0.11	H8	HG2	0.09
C4	CC0	0.13	H9	HG2	0.09
C5	C3C1	0.12	H10	HG2	0.09
C6	CO5	0.48	H11	HG1	0.09
C7	C21	-0.18	H12	HG2	0.09
C8	C21	-0.18	H13	HG2	0.09
C9	C14	0.21	H14	HG2	0.09
C10	C21	-0.18	H15	HG2	0.09
C11	CC0	0.00	H16	HG2	0.09
C12	CC0	0.00	H17	HG2	0.09
C13	C3C1	0.00	H18	HG2	0.09
C14	C01	0.22	H19	HG2	0.09
C15	C21	-0.18	H20	HG4	0.15
C16	C24	0.21	H21	HG5	0.21
C17	C24	0.21	H22	HG5	0.21
C18	CD1	-0.15			
C19	CD2	-0.42			

Model Compound

The major portion of naloxone for which there were no parameters is the N-allyl portion of the molecule. A model compound was used to represent this N-allyl portion during the parameterization of torsion angles. This model compound, PIPA, was chosen such that the atom types in it were as similar as possible to the atom types in the N-allyl

portion of naloxone. Figure 5.2 shows the model compound, PIPA (piperdine amine) with its atomic numbering convention.

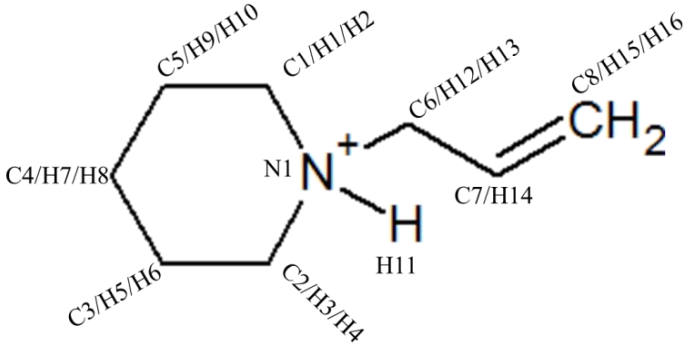

Figure 5.2. PIPA: Model compound for naloxone N-allyl torsion parameters. The model compound used for torsion parameters of the N-allyl portion of Naloxone, PIPA (piperdine amine) as well as its atomic numbering convention.

Non-bonded Parameters

Partial charges for naloxone atoms were taken from chemically similar atoms present in the CGenFF database.[6] The CGenFF database applies a charge of -0.115q to all aromatic carbons not bonded to heteroatoms and an equal and opposite charge to their hydrogen atoms. It also applies a charge of 0.09q to all aliphatic hydrogen atoms and an opposite charge that is the sum of all hydrogen atoms bonded to an aliphatic carbon if that carbon atom is not bonded to a heteroatom. In the model compound and naloxone, all atoms that fell under these guidelines were restricted to those charges. Charges not in these categories, such as O1, O2, C18 and C19 in naloxone were taken from various

compounds with known charges including propene, phenol, 2,3 epoxy or N-benzyl piperidine in the CGenFF database.

Internal Parameters

Many of the bond and angle parameters needed for naloxone were already present in the CGenFF database.[6] If a parameter for a bond or angle was missing, force constants, equilibrium bond lengths and bond angles listed for similar atom type interactions were used as a substitute. Torsion parameters for the rigid alkaloid backbone of naloxone were also substituted in this manner. However, because of the larger implication of the torsional force constants on the flexible N-allyl tail of naloxone, the remaining missing dihedral parameters were calculated according to the published CHARMM parameterization procedure.[7] This process compares the QM potential energy surface with the CHARMM calculated surface for each dihedral and using a Monte Carlo simulated annealing approach provides parameters that optimize the fit of the molecular mechanics dihedral surface to the quantum mechanical one.

The energy surfaces of each model compound were determined by rotating a subject torsion angle 360 degrees in increments of 10 degrees (or 180 degrees when the model compound was symmetric), thus creating 36 separate conformers (or 18) of the compound. Each of these conformers was optimized using HF/6-31G* in NWChem 5.1.1 with the rotated torsion held constant. A single-point energy calculation using MP2/6-31G* was then performed on each conformer. These energies were used to create a potential energy surface for each missing torsion angle. For model compounds with more

than one torsion angle missing, such as in PIPA, a separate potential energy surface was calculated for each dihedral.

In order to create an MM potential energy surface, each conformer was minimized using CHARMM with the missing torsion held constant. The potential energy surface created by CHARMM must reproduce the QM calculated surface for each torsion angle of interest. By using Guvench and MacKerell's Monte Carlo simulated annealing method [7] and their provided script (fit_dihedral.tar.gz and is available for downloading at http://mackerell.umaryland.edu/CHARMM_ff_params.html) the QM and MM potential energies were compared and the dihedral parameters were optimized. By testing different periodicity values, torsion parameters that generate a potential energy surface equivalent to the QM values were produced.

In the case of the N-allyl tail, multiple dihedrals that involved different rotatable bonds were missing in the model compound. Therefore, the torsion parameter closest to the least flexible part of the molecule was varied and determined first (e.g. the torsion closest to a piperdine ring), then the next closest dihedral was varied and determined. An iterative process was used to return to the first dihedral tested after determining values for the second dihedral until agreement of all missing dihedrals' potential energy surfaces were as accurate as possible.

Results & Discussion

In this section, we present the optimized CHARMM force field parameters for use with the CGenFF database. Table 5.2 lists all the atom names and types for naloxone. Table 5.3 provides a list of CGenFF atom types that were used as starting points for the development of the naloxone CHARMM parameters.

Table 5.2. CGenFF Atom Types Initially Assigned to Naloxone

naloxone Atom Type	CGENFF Atom Type
O351	OG3C51
OD3	OG2D3
O11	OG311
NP1	NG3P1
C21	CG321
C01	CG301
C14	CG314
C24	CG324
C61	CG2R61
CO5	CG2O5
CC0	CG2RC0
CD1	CG2D1
CD2	CG2D2
C3C1	CG3RC1
HP1	HGP1
HP2	HGP2
H61	HGR61
HG1	HGA1
HG2	HGA2
HG4	HGA4
HG5	HGA5

Charge Parameters

Charge calculations were not necessary for naloxone, or the model compound, PIPA. As mentioned in methods, the CGenFF database[6] applies a charge of -0.115q to all aromatic carbons not bonded to heteroatoms and an equal and opposite charge to their hydrogen atoms. It also applies a charge of 0.09q to all aliphatic hydrogen atoms and an opposite charge that is the sum of all hydrogen atoms bonded to an aliphatic carbon if that carbon atom is not bonded to a heteroatom. In the model compound and naloxone, all atoms that fell under these guidelines were restricted to those charges. Charges not in these categories, such as O1, O2, C18 and C19 in naloxone were adapted from various compounds with known charges including propene, phenol, 2,3 epoxy or N-benzyl piperidine in the CGenFF database. Charges for naloxone are shown in Table 5.1, and for PIPA, the model compound, in Table 5.3. Also in Table 5.3 are the atom names and types for PIPA.

Table 5.3. Atom Name, Type and Partial Charges for PIPA, the Model Compound for the N-allyl Portion of Naloxone.

Atom Name	Type	Partial Charge	Atom Name	Type	Partial Charge
N1	NP1	-0.4	H5	HG2	0.09
C1	C24	0.21	H6	HG2	0.09
C2	C24	0.21	H7	HG2	0.09
C3	C21	-0.18	H8	HG2	0.09
C4	C21	-0.18	H9	HG2	0.09
C5	C21	-0.18	H10	HG2	0.09
C6	C24	0.21	H11	HP2	0.32
C7	CD1	-0.15	H12	HG2	0.09
C8	CD2	-0.42	H13	HG2	0.09
H1	HG2	0.09	H14	HG4	0.15
H2	HG2	0.09	H15	HG5	0.21
H3	HG2	0.09	H16	HG5	0.21
H4	HG2	0.09			

Internal Parameters

The bond and angle and torsion parameters were initially assigned by substituting with already existing parameters from the CGennFF database.[6] Torsion parameters have a direct effect on the energy minima that the molecule will occupy. However, the fused ring system backbone of naloxone is rigid, so torsion parameters in this area were substituted with already existing parameters. A full listing of all bond angle and torsion parameters for naloxone is provided in Appendix A. The model compound used for parameter development of the N-allyl portion of naloxone, PIPA is shown in Figure 5.2.

The missing sections of torsion angles for the N-allyl substituent were C16-N1-C17-C18 and N1-C17-C18-C19 of naloxone. Using the model compound, PIPA, shown in Figure 5.2, the two torsions mentioned and seven other missing torsions involving the

same rotatable bonds were calculated. The protonated nitrogen ring of naloxone was mimicked by a piperidine ring and the allyl tail was reserved. By calculating these nine new torsion parameters, the molecular mechanics surfaces shown in Figures 5.3 and 5.4 resulted. As shown, initially the molecular mechanics surfaces were vastly different from the MP2/6-31G* NWChem surfaces in both the C-N-C-C (Figure 5.3) and N-C-C-C (Figure 5.4) primary dihedrals of PIPA. The initial CHARMM is shown in red, the final CHARMM in blue and the MP2/6-31G* NWChem is in black in both figures. The final molecular mechanics / CHARMM parameters and energy surfaces match the MP2/6-31G* NWChem surfaces are considerably improved.

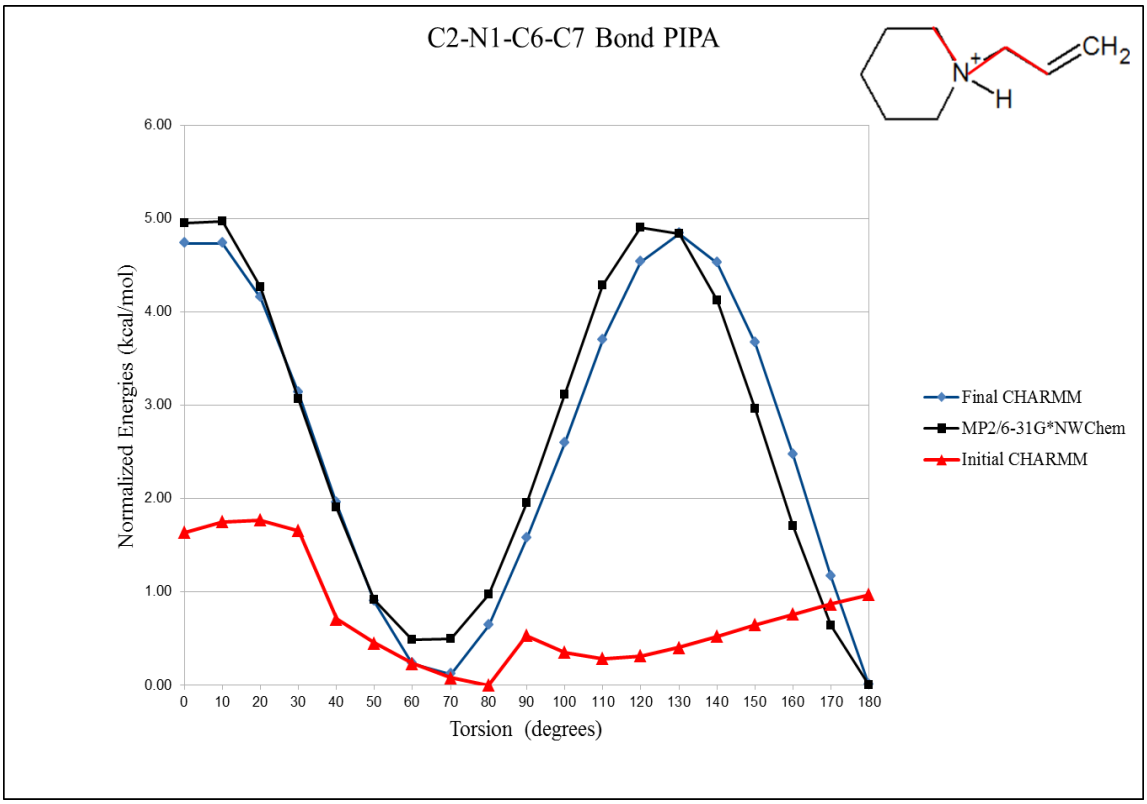

Figure 5.3. Potential energy surface of the first rotatable bond (N1-C6) of PIPA. This figure shows the initial MM surface (red), initial MP2/6-31G* NWChem surface (black) and final MM surface (blue) after development of parameters for both rotatable bonds in PIPA. Inset: Structure of PIPA is illustrated with the bond rotated in red.

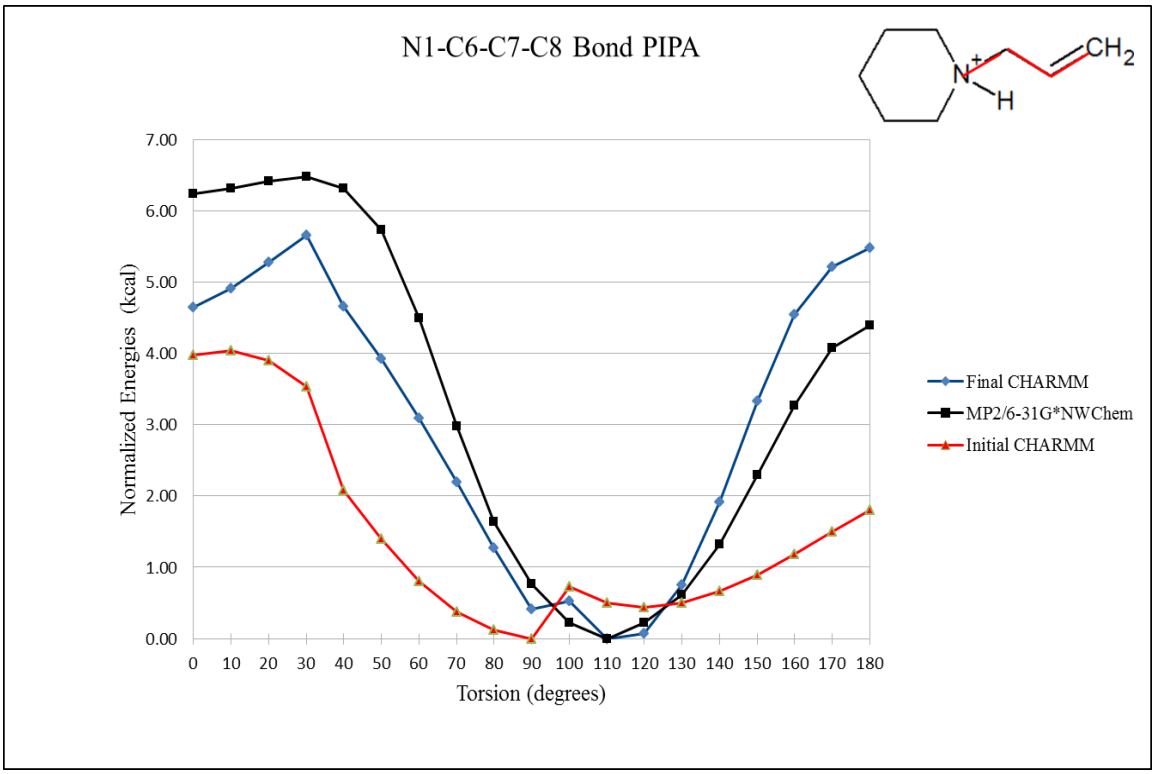

Figure 5.4. Potential energy surface of the second rotatable bond (C6-C7) of PIPA. This figure shows the initial MM surface (red), initial MP2/6-31G* NWChem surface (black) and final MM surface (blue) after development of parameters for both rotatable bonds in PIPA. Inset: Structure of PIPA is illustrated with the bond rotated in red.

Refinement

Previous studies in our lab[5] have shown that an experimental solid state IR spectrum can be compared with a calculated *in vacuo* molecular dynamics simulation of a ligand to further refine the calculated parameters. This type of study can also be utilized to refine bond and angle force constraints in CHARMM parameters. This type of study was originally planned, however various constraints prevented it from being undertaken in the work presented here.

Additionally, although the alkaloid backbone of naloxone is a rigid, fused ring system, the CHARMM parameters in this area should be optimized for the most accurate behavior of the molecule. Previous studies involving molecular dynamics simulations of opioid compounds have been elusive in parameters used for the ligands in the receptor-ligand complexes or have used a different simulation platform with different parameter needs.

Conclusions

The development of CHARMM parameters for Naloxone, including the N-allyl tail using previously published methods for parameter development was successful. The CGenFF library was used and was appropriate due to the large number of organic molecules and molecules with similar structure to naloxone. The use of a model compound, PIPA, allowed for calculation of missing dihedral parameters of the N-allyl portion of naloxone. The parameters for naloxone could be further refined and optimized using experimental and calculated IR spectrum to compare the developed parameters.

References

1. Kolinski, M.; Filipek, S., Study of a structurally similar kappa opioid receptor agonist and antagonist pair by molecular dynamics simulations. *Journal of molecular modeling* **2010,** *16* (10), 1567-76.

2. Zhang, Y.; Sham, Y. Y.; Rajamani, R.; Gao, J.; Portoghese, P. S., Homology modeling and molecular dynamics simulations of the mu opioid receptor in a membrane-aqueous system. *Chembiochem* **2005,** *6* (5), 853-9.

3. MacKerell, A. D., Jr.; Bashford, D.; Bellot, M.; Dunbrack, R. L. Jr.; Evanseck, J. D.; Field, M.J.; Fischer, S.; Gao, J.; Guo, H.; Ha, S.; Joseph-McCarthy, D.; Kuchnir, L.; Kuczera, K.; Lau, F. T. K.; Mattos, C.; Michnick, S.; Ngo, T.; Nguyen, D. T.; Prodhom, B.; Reiher, W. E., III; Roux, B.; Schlenkrich, M.; Smith, J. C.; Stote, R.; Straub, J.; Watanabe, M.; Wiorkiewicz-Kuczera, J.; Yin, D.; Karplus, M., All-hydrogen empirical potential for molecular modeling and dynamics studies of proteins using the CHARMM22 force field. *J. Phys. Chem. B* **1998,** *102*, 3586-3616.

4. MacKerell, A. D., Jr., In *Computational Biochemistry and Biophysics*
Becker, O. M.; MacKerell, A. D., Jr.; Roux, B.; Watanabe, M., Eds. Marcel Dekker: New York, 2001; pp 7-38.

5. Iliff, H. A.; Lynch, D. L.; Kotsikorou, E.; Reggio, P. H., Parameterization of Org27569: An allosteric modulator of the cannabinoid CB(1) G protein-coupled receptor. *J Comput Chem* **2011**.

6. Vanommeslaeghe, K.; Hatcher, E.; Acharya, C.; Kundu, S.; Zhong, S.; Shim, J.; Darian, E.; Guvench, O.; Lopes, P.; Vorobyov, I.; Mackerell, A. D., Jr., CHARMM general force field: A force field for drug-like molecules compatible with the CHARMM all-atom additive biological force fields. *J Comput Chem* **2009,** *31* (4), 671-90.

7. Guvench, O.; MacKerell, A. D., Jr., Automated conformational energy fitting for force-field development. *Journal of molecular modeling* **2008,** *14* (8), 667-79.

APPENDIX A

BOND, ANGLE, AND TORSION PARAMETERS FOR NALOXONE

BOND	K_b	b_o	Source
C61 C61	305.00	1.3750	PROT benzene, JES 8/25/89
C61 CC0	300.00	1.3600	INDO/TRP
C61 O11	334.30	1.4110	PROT MeOH, EMB 10/10/89,
C61 H61	340.00	1.0800	PROT phe,tyr JES 8/25/89
CC0 CC0	360.00	1.3850	INDO/TRP
CO5 OD3	700.00	1.2150	ACO, acetone adm 11/08
CO5 C21	330.00	1.5000	COMPDS PEDRO re-initialized from ACO adm 11/08-TAKEN FROM CO5 C11 4/26/10
C01 C21	222.50	1.5380	RETINOL TMCH/MECH
C01 O31	360.00	1.4150	AMOL, alpha-methoxy-lactic acid, og all34_ethers_1a CG32A OG30A
C14 HG1	309.00	1.1110	PROT alkane update, adm jr., 3/2/92
C14 C21	222.50	1.5380	PROT alkane update, adm jr., 3/2/92
C14 NP1	200.00	1.4900	2MRB, Alpha benzyl gamma 2-methyl piperidine, chayan--TAKEN FROM C14/NP2 4/26/10
C21 C21	222.50	1.5300	PROT alkane update, adm jr., 3/2/92
C21 C24	222.50	1.5300	FLAVOP PIP1,2,3
C21 HG2	309.00	1.1110	PROT alkane update, adm jr., 3/2/92
C21 O31	360.00	1.4150	diethylether, alex
C24 NP1	200.00	1.4800	FLAVOP PIP1,2,3
C24 HG2	284.50	1.1000	FLAVOP PIP1,2,3
CD1 HG4	360.50	1.1000	LIPID propene, yin,adm jr., 12/95
CD2 HG5	365.00	1.1000	LIPID propene; from ethene, yin,adm jr., 12/95
CD1 CD2	500.00	1.3420	LIPID propene, yin,adm jr., 12/95
NP1 HP2	403.00	1.0400	PROT new stretch and bend; methylammonium (KK 03/10/92)
O11 HP1	545.00	0.9600	PROT EMB 11/21/89 methanol vib fit; og tested on MeOH EtOH,...
CC0 O31	450.00	1.3700	ZFUR, benzofuran, kevo--USED CC0-O50 4/28/10
C01 C14	222.50	1.5000	PROT alkane update, adm jr., 3/2/92--USED C11-C14 4/28/10
CC0 C21	230.00	1.4900	PROT phe,tyr, JES 8/25/89--USED C61-C21 4.28.10

Bond	K_b	b_o	Source
CD1 C24	365.00	1.5020	LIPID butene; from propene, yin,adm jr., 12/95--used CD1-C21
CC0 C01	230.00	1.4900	NAMODEL difluorotoluene--USED C61-C11 4/29/10
C11 HG1	309.00	1.1110	PROT alkane update, adm jr., 3/2/92
C01 O11	428.00	1.4200	AMOL, alpha-methoxy-lactic acid, og par22 OH1 CT1
CO5 C11	330.00	1.5000	COMPDS PEDRO re-initialized from ACO adm 11/08
C11 O31	450.00	1.3710	FURA, furan--USED C51-O50 4/28/10
C01 C11	222.50	1.5000	CA, CHOLIC ACID, chayan, 03/06
C01 C01	222.50	1.5000	CA, CHOLIC ACID, chayan, 03/06--USED C01-C11 4/30/10
C61 C21	230.00	1.4900	PROT phe,tyr, JES 8/25/89
C3C1 O351	350.00	1.4250	THF, nucleotide CSD/NDB survey, 5/30/06,viv
C61 C3C1	230.00	1.4900	NAMODEL difluorotoluene--USED C61-C11 5/3/10
CO5 C3C1	330.00	1.5000	COMPDS PEDRO re-initialized from ACO adm 11/08--USED CO5-C11 5/3/10
CC0 O351	450.00	1.3700	ZFUR, benzofuran, kevo--USED CC0-O50 5/4/10
C3C1 C3C1	222.50	1.5230	CARBOCY carbocyclic sugars
C01 C3C1	222.50	1.5240	CARBOCY carbocyclic sugars--USED C11-C3C1 5/4/10
C21 C3C1	222.50	1.5240	CARBOCY carbocyclic sugars
C3C1 HG1	309.00	1.1110	CARBOCY carbocyclic sugars

Angle	K_Θ	Θ_0	Source
CD2 CD1 HG4	42.00	118.00	LIPID propene, yin,adm jr., 12/95
HG5 CD2 HG5	19.00	119.00	LIPID propene, yin,adm jr., 12/95
C24 CD1 HG4	40.00	116.00	LIPID 1-butene; propene, yin,adm jr., 12/95--taken from C21-CD1-HG4 4/27/10
CD2 CD1 C24	48.00	126.00	LIPID 1-butene; propene, yin,adm jr., 12/95--taken from CD2-CD1-C21 4/27/10
CD1 CD2 HG5	45.00	120.50	LIPID propene, yin,adm jr., 12/95
C61 C61 C61	40.00	120.00	PROT JES 8/25/89
C61 C61 CC0	50.00	120.00	adm,dec06 113.20 ! INDO/TRP
C61 C61 H61	30.00	120.00	PROT JES 8/25/89 benzene
CC0 C61 H61	30.00	120.00	122 INDO/TRP
C61 C61 O11	45.20	120.00	PYRIDINE phenol
CC0 C61 O11	45.20	120.00	PYRIDINE phenol--taken from C61-C61-O11 4/27/10
C61 CC0 CC0	50.00	120.00	adm,dec06 110.00 ! INDO/TRP
C61 CC0 O31	100.00	129.40	ZFUR, benzofuran, kevo--taken from C61-CC0-O50 4/27/10
HG2 C21 HG	35.50	109.00	PROT alkane update, adm jr., 3/2/92
C21 C21 HG2	26.50	110.10	PROT alkane update, adm jr., 3/2/92
C01 C21 C21	58.35	113.50	RETINOL TMCH/MECH
C01 C21 HG2	26.50	110.10	RETINOL TMCH/MECH
CO5 C11 HG1	50.00	109.50	BIPHENYL ANALOGS from PROT Alanine Dipeptide ab initio calc's (LK) consistent with adm 11/08
O31 C11 HG1	60.00	109.50	all34_ethers_1a HCA2 CC32A OC30A, gk or og (not affected by mistake)
C11 CO5 OD3	95.00	121.30	BIPHENYLS BF6, C36 new init guess by Kenno based on ACO adm 11/08 ==> re-optimize
C21 CO5 C11	35.00	116.00	ACO, acetone adm 11/08--taken from C31-CO5-C31 4/27/10
CC0 CC0 CC0	50.00	120.00	adm,dec06 110.00 ! INDO/TRP--taken from C61-CC0-CC0 4/27/10
C21 C01 O11	75.70	110.10	AMOL, alpha-methoxy-lactic acid, og--USED C31-C01-O11 4/28/10
C11 C01 C21	58.35	113.50	CA, CHOLIC ACID, chayan, 03/06
C11 C01 C01	58.35	113.50	CA, CHOLIC ACID, chayan, 03/06--USED C11-C01-C11 4/27/10
C01 C14 HG1	34.50	110.10	PROT alkane update, adm jr., 3/2/92

Angle	K_Θ	Θ_0	Source
C01 C14 NP1	67.70	110.00	PROT new aliphatics, adm jr., 2/3/92--used C11-C14-NP3 4/27/10
NP1 C14 HG1	45.00	102.30	2MRB, Alpha benzyl gamma 2-methyl piperidine, chayan--USED NP2-C14-HG1 4/27/10
CO5 C21 C21	60.00	113.80	ALDEHYDE propionaldehyde unmodified--USED CO4-C21-C31 4/27/10
C24 C21 HG2	26.50	110.10	FLAVOP PIP1,2,3
C14 C21 HG2	33.43	110.10	PROT alkanes
NP1 C24 HG2	45.00	102.30	FLAVOP PIP1,2,3
HG2 C24 HG2	35.50	109.00	PIP1,2,3
CC0 O31 C11	65.00	108.00	ETOB, Ethoxybenzene, chayan--USED C61-O31-C21 4/27/10
C01 O11 HP1	50.00	106.00	AMOL, alpha-methoxy-lactic acid, og
C61 O11 HP1	65.00	108.00	PROT JES 8/25/89 phenol
C24 NP1 HP2	30.00	110.80	FLAVOP PIP1,2,3
C14 NP1 HP2	30.00	110.80	FLAVOP PIP1,2,3
C01 C11 HG1	34.60	110.10	CA, CHOLIC ACID, chayan, 03/06
CO5 C11 O31	45.00	109.00	CC321 CC3163 OC3C61 optimize on PROA, gk (not affected by mistake)--used CO3-C11-O31 4/27/10
C61 CC0 C21	45.80	119.00	PYRIDINE pyridines--USED C61-C61-C21 4/28/10
CC0 CC0 C01	45.80	121.00	NAMODEL difluorotoluene--USED C61-C61-C11 4/28/10
CC0 CC0 C21	45.80	119.00	PYRIDINE pyridines
CC0 C21 HG2	49.30	107.50	PYRIDINE pyridines--USED C61-C21-HG2 4/28/10
CC0 C21 C14	51.80	107.50	PROT PARALLH19 (JES)--USED C61-C21-C14 4/28/10
C21 C24 NP1	67.70	110.00	RETINOL SCK1, protonated Schiff's base #eq#
CO5 C11 C01	52.00	108.00	PROT adm jr. 4/05/91, for asn,asp,gln,glu and cters--USED CO3-C11-C11 4/28/10
C01 C11 O31	110.00	120.00	BIPHENYL ANALOGS--USED C61-C61-O31 4/28/10
CC0 C01 C11	51.80	107.50	NAMODEL difluorotoluene--USED C61-C11-C21 4/30/10
C21 C01 C14	58.35	110.50	FLAVOP PIP1,2,3--USED C21-C11-C24 4/30/10

Angle	K_Θ	Θ_0	Source
C01 C01 C21	58.35	113.50	CA, CHOLIC ACID, chayan, 03/06--USED C01-C11-C21 4/30/10
CC0 C01 C01	58.35	113.50	CA, CHOLIC ACID, chayan, 03/06--USED C11-C01-C11 4/30/10
C14 C01 C01	53.35	111.00	PROT alkane update, adm jr., 3/2/92--USED C14-C11-C21 4/30/10
C14 C01 O11	75.70	112.10	FLAVOP PIP1,2,3--USED C24-C11-O11 4/30/10
C01 C01 O11	75.70	110.10	PROT MeOH, EMB, 10/10/89--USED C11-C11-O11 4/30/10
C14 NP1 C24	45.00	115.50	2MRB, Alpha benzyl gamma 2-methyl piperidine, chayan--USED C14-NP2-C24 4/30/10
C24 NP1 C24	45.00	115.50	FLAVOP PIP1,2,3
CC0 CC0 O31	110.00	110.60	ZFUR, benzofuran, kevo--USED CC0-CC0-O50 4/30/10
C21 CO5 OD3	95.00	121.30	BIPHENYLS BF6, C36 new init guess based on ACO adm 11/08 --USED C11-CO5-OD3 4/30/10
CO5 C21 HG2	33.00	109.50	PALD, propionaldehyde from PROT adm jr. 5/02/91, acetic acid pure solvent. Consistent with adm 11/08.
C21 C14 NP1	40.00	110.00	2MRB, Alpha benzyl gamma 2-methyl piperidine, chayan--USED C21-C14-NP2 4/30/10
C01 C14 C21	58.35	113.50	2MRB, Alpha benzyl gamma 2-methyl piperidine, chayan--USED C21-C14-C21 4/30/10
C21 C14 HG1	34.50	110.10	PROT alkane update, adm jr., 3/2/92
CC0 C01 C21	51.80	107.50	NAMODEL difluorotoluene--USED C61-C11-C21 4/30/10
C01 C21 C24	58.35	113.50	RETINOL TMCH/MECH--USED C01-C21-C21 4/30/10
C21 C24 HG2	26.50	111.80	FLAVOP PIP1,2,3
C61 C21 HG2	49.30	107.50	PYRIDINE pyridines
C61 C21 C14	51.80	107.50	PROT PARALLH19 (JES)
C3C1 C21 HG2	34.60	110.10	TF2M viv--USED C351-C21-HG2 5/4/10
C21 C3C1 C3C1	58.00	115.00	TF2M viv--USED C21-C351-C351 5/4/10
O351 C3C1 HG1	70.00	107.30	THF 10/21/05, viv
C3C1 C3C1 O351	45.00	111.10	THF 10/21/05, viv--USED C351-C351-O351 5/4/10

Angle	K_Θ	Θ_0	Source
C3C1 CO5 OD3	95.00	121.30	BIPHENYLS BF6, C36 new init guess by Kenno based on ACO adm 11/08 used c11-co5-od3 5/4/10
C3C1 CO5 C21	35.00	116.00	ACO, acetone adm 11/08--USED C31-CO5-C31 5/4/10
C61 CC0 C61	50.00	120.00	adm,dec06 110.00 ! INDO/TRP--USED C61-CC0-CC0 5/4/10
C61 CC0 O351	100.00	129.40	ZFUR, benzofuran, kevo--USED C51-CC0-O50 5/4/10
C61 C61 C21	45.80	119.00	PYRIDINE pyridines
C61 C61 C3C1	45.80	121.00	NAMODEL difluorotoluene
C21 C11 C3C1	53.35	108.50	BAM1, bile acid steroidal C-D ring, chayan, 02/08--USED C31-C11-C351 5/4/10
C21 C01 C3C1	53.35	103.70	CARBOCY carbocyclic sugars--used C21-C11-C3C1 5/4/10
C3C1 C01 O11	75.70	110.10	CARBOCY ncarbocyclic sugars--USED C3C1-C11-O11 5/4/10
C3C1 C3C1 HG1	34.50	110.10	CARBOCY carbocyclic sugars
C24 C01 C3C1	53.35	111.00	CARBOCY carbocyclic sugars--USED C21-C21-C3C1 5/4/10
C14 C01 C3C1	53.35	103.70	CARBOCY carbocyclic sugars--USED C11-C11-C3C1 5/4/10
C01 C3C1 C3C1	53.35	108.00	CARBOCY carbocyclic sugars--USED C11-C3C1-C3C1 5/4/10
C61 C3C1 C01	51.80	107.50	NAMODEL difluorotoluene--USED C61-C11-C21 5/4/10
C61 C3C1 C21	51.80	107.50	NAMODEL difluorotoluene--USED C61-C11-C21 5/4/10
C61 C3C1 C3C1	51.80	107.50	NAMODEL difluorotoluene--USED C61-C11-C21 5/4/10
C3C1 O351 CC0	95.00	111.00	THF 10/21/05, viv--USED C351-O351-C351 5/4/10
O351 C3C1 CO5	52.00	112.30	TAKEN FROM CO1 C351 C352 P=64 EAP 3/9/12
C3C1 C3C1 CO5	70.00	113.70	TAKEN FROM C3C1 C3C1 N61 P=48 EAP 3/9/12
CO5 C3C1 HG1	50.00	109.50	BIPHENYL from PROT Alanine Dipeptide consistent with adm 11/08--USED CO5-C11-HG1 5/5/10

Angle	K_θ	θ_0	Source
C01 C3C1 C21	53.35	111.00	CARBOCY carbocyclic sugars--USED C11-C3C1-C21 5/5/10
C3C1 C21 C24	58.35	110.50	FLAVOP PIP1,2,3--USED C11-C21-C24 5/5/10
CC0 C61 C3C1	45.80	121.00	NAMODEL difluorotoluene--USED C61-C61-C11 5/5/10

Dihedral	K	n	δ	Source
OD3 CO5 C21 HG2	0.0000	1	0.00	PROT Alanine Dipeptide ab initio calc's (LK) unmodified--USED OD3-CO5-C11-HG1 4/28/10
OD3 CO5 C21 C21	1.0500	1	180.00	ALDEHYDE propionaldehyde unmodified--USED OD1-CO4-C21-C31 4/28/10
OD3 CO5 C11 C01	0.0500	6	180.00	PROT For side chains of asp,asn,glu,gln, (n=6) from KK(LK)--USED OD2-CO3-C21-C11 4/28/10
OD3 CO5 C11 HG1	0.0000	1	0.00	PROT Alanine Dipeptide ab initio calc's (LK) unmodified
OD3 CO5 C11 O31	0.5500	2	180.00	og amop mp2/ccpvtz--USED OD2-C03-C11-O31 4/28/10
C11 CO5 C21 HG2	0.0000	1	180.00	BIPHENYL ANALOGS unmodified--USED C61-CO5-C11-HG1 4/28/10
C11 CO5 C21 C21	1.5850	2	180.00	BIPHENYL ANALOGS unmodified--USED C11-CO5-C61-C61 4/28/10
C21 CO5 C11 C01	1.5850	2	180.00	BIPHENYL ANALOGS unmodified--USED C11-CO5-C61-C61 4/28/10
C21 CO5 C11 HG1	0.0000	1	180.00	BIPHENYL ANALOGS unmodified--USED C61-CO5-C11-HG1 4/28/10
C21 CO5 C11 O31	0.0000	2	180.00	BIPHENYL ANALOGS unmodified--USED C61-CO5-C11-O11 4/28/10
CC0 C61 C61 H61	3.0000	2	180.00	INDO/TRP
C61 C61 C61 H61	4.2000	2	180.00	PROT JES 8/25/89 benzene
H61 C61 C61 H61	2.4000	2	180.00	PROT JES 8/25/89 benzene
O11 C61 C61 H61	2.4000	2	180.00	PROT JES 8/25/89 phenol Kenno: 4.2 -> 2.4
C61 C61 CC0 O31	0.0000	2	180.00	ZFUR, benzofuran, kevo--USED C61-C61-CC0-O50 4/28/10
C61 C61 CC0 C21	3.1000	2	180.00	PROT JES 8/25/89 toluene and ethylbenzene-USED C61-C61-C61-C21 4/28/10
H61 C61 CC0 CC0	3.0000	2	180.00	INDO/TRP
C61 C61 C61 O11	3.1000	2	180.00	PYRIDINE phenol--USED C61-C61-C61-O11 4/28/10
O11 C61 CC0 O31	2.4000	2	180.00	PROT JES 8/25/89 phenol Kenno: 4.2 -> 2.4--USED O11-C61-C61-H61 4/28/10

Dihedral	K	n	δ	Source
C21 CC0 C61 H61	2.4000	2	180.00	PROT JES 8/25/89 toluene and ethylbenzene Kenno: 4.2 -> 2.4--USED C21-C61-C61-H61 4/29/10
C61 C61 CC0 CC0	3.0000	2	180.00	INDO/TRP
C61 C61 O11 HP1	0.9900	2	180.00	PROT phenol OH rot bar, 3.37 kcal/mole, adm jr. 3/7/92
CC0 C61 O11 HP1	0.9900	2	180.00	PROT phenol OH rot bar, 3.37 kcal/mole, adm jr. 3/7/92--USED C61-C61-011-HP1 4/29/10
C61 CC0 CC0 CC0	3.0000	2	180.00	INDO/TRP--USED C61-CC0-CC0-C61 4/29/10
CC0 CC0 CC0 O31	0.0000	2	180.00	ZFUR, benzofuran, kevo--USED C61-CC0-CC0-O50 4/29/10
C61 CC0 CC0 C01	3.1000	2	180.00	NAMODEL difluorotoluene--USED C61-C61-C61-C11 4/29/10
CC0 CC0 C01 C11	0.2300	2	180.00	NAMODEL difluorotoluene--USED C61-C61-C11-C11 4/29/10
CC0 CC0 C01 C01	0.2300	2	180.00	NAMODEL difluorotoluene--USED C61-C61-C11-C11 4/29/10
C61 CC0 C21 C14	0.2300	2	180.00	PROT ethylbenzene ethyl rotation, adm jr. 3/7/92--USED C61-C61-C21-C14 4/29/10
C61 CC0 C21 HG2	0.0000	2	0.00	3ALP, nicotinaldehyde (PYRIDINE pyr-CH2OH)--USED C61-C61-C21-HG2 4/29/10
CC0 CC0 C21 C14	0.2300	2	180.00	PROT ethylbenzene ethyl rotation, adm jr. 3/7/92--USED C61-C61-C21-C14 4/29/10
CC0 CC0 C21 HG2	0.0000	2	0.00	3ALP, nicotinaldehyde (PYRIDINE pyr-CH2OH)--USED C61-C61-C21-HG2 4/29/10
C61 CC0 O31 C11	1.6200	2	180.00	ETOB, Ethoxybenzene, chayan--USED C61-C61-O31-C21 4/29/10
C61 CC0 O31 C11	0.1900	4	180.00	ETOB, Ethoxybenzene, chayan--USED C61-C61-O31-C21 4/29/10
CC0 CC0 O31 C11	1.6200	2	180.00	ETOB, Ethoxybenzene, chayan--USED C61-C61-O31-C21 4/29/10
CC0 CC0 O31 C11	0.1900	4	180.00	ETOB, Ethoxybenzene, chayan--USED C61-C61-O31-C21 4/29/10

Dihedral	K	n	δ	Source
C01 C01 C11 HG1	0.2000	3	0.00	CA, Cholic Acid, chayan, 03/06--USED C01-C11-C11-HG1 4/29/10
C21 C01 C11 O31	0.8000	3	180.00	NA, sugar--USED C21-C11-C11-O33 4/29/10
C21 C01 C11 O31	0.2000	4	0.00	NA, sugar--USED C21-C11-C11-O33 4/29/10
CO5 C11 C01 C21	0.2000	3	0.00	--USED CO2-C11-C11-C21 4/29/10
CO5 C11 C01 C01	0.2000	3	0.00	--USED CO2-C11-C11-C21 4/29/10
C01 C01 C11 O31	2.0000	3	180.00	NA, sugar--USED C11-C11-C11-O33 4/29/10
C01 C01 C11 O31	0.4000	5	0.00	NA, sugar--USED C11-C11-C11-O33 4/29/10
C01 C01 C11 O31	0.8000	6	0.00	NA, sugar--USED C11-C11-C11-O33 4/29/10
C11 C01 C01 O11	0.1400	3	0.00	PROT, hydroxyl wild card--USED C11-C11-C11-O11 4/29/10
C11 C01 C01 C14	0.5000	4	180.00	NA bkb--USED C11-C11-C11-C21 4/29/10
C11 C01 C01 C21	0.5000	4	180.00	NA bkb--USED C11-C11-C11-C21 4/29/10
CC0 C01 C11 HG1	0.1500	3	0.00	CARBOCY carbocyclic sugar--USED CC1-C11-C11-HG1 4/29/10
C21 C01 C11 HG1	0.1950	3	0.00	NA, sugar--USED C21-C11-C11-HG1 4/29/10
CO5 C11 C01 CC0	0.0400	3	0.00	deleteme DELETEME (we want to use wildcarting)--USED CO2-C11-C21-C61 4/29/10
CC0 C01 C01 O11	0.6000	1	0.00	CARBOCY carbocyclic sugars--USED CC1-C11-C11-O11 4/29/10
CC0 C01 C01 O11	0.7000	3	0.00	CARBOCY carbocyclic sugars--USED CC1-C11-C11-O11 4/29/10
CC0 C01 C11 O31	0.0000	2	180.00	ZFUR, benzofuran, kevo--USED C61-CC0-CC0-O50 4/29/10
CC0 C01 C01 C21	0.0000	3	0.00	NAMODEL difluorotoluene--USED C61-C11-C21-C11 4/29/10
CC0 C01 C01 C14	0.1500	3	0.00	CARBOCY carbocyclic sugars
C01 C01 C14 NP1	0.2000	3	0.00	PROT alkane update, adm jr., 3/2/92--USED C21-C11-C14-NP3 4/29/10
C01 C01 C14 HG1	0.1950	3	0.00	NA, sugar--USED C21-C11-C14-HG1 4/29/10

Dihedral	K	n	δ	Source
NP1 C14 C01 C21	0.1950	3	0.00	3MRB, Gamma-3 methyl piperidine, alpha-benzyl GA CDCA amide, chayan--USED NP2-C14-C21-C21 4/29/10
C21 C14 C01 C01	0.2000	3	0.00	3MRB,Gamma-3 methyl piperidine, alpha-benzyl GA CDCA amide, chayan--USED C21-C14-C21-C21 4/29/10
C21 C01 C14 HG1	0.1950	3	0.00	NA, sugar--USED C21-C11-C14-HG1 4/29/10
C21 C14 C01 C21	0.2000	3	0.00	3MRB,Gamma-3 methyl piperidine, alpha-benzyl GA CDCA amide, chayan--USED C21-C14-C11-C21 4/29/10
NP1 C14 C01 O11	0.2000	3	0.00	PROT alkane update, adm jr., 3/2/92--USED NP3-C14-C21-O11 4/29/10
HG1 C14 C01 O11	0.1950	3	0.00	NA, sugar--USED HG1-C14-C21-O11 4/29/10
C21 C14 C01 O11	0.2000	3	0.00	PROT alkane update, adm jr., 3/2/92--USED CO3-C14-C21-O11 4/29/10
C01 C01 C21 C21	0.2000	3	0.00	DCA, Deoxycholic Acid, chayan, 03/06--USED C01-C11-C21-C21 4/29/10
C01 C01 C21 HG2	0.2000	3	0.00	CA, Cholic Acid, chayan, 03/06--USED C01-C11-C21-HG2 4/29/10
C11 C01 C21 C24	0.1000	3	0.00	NA--USED C11-C11-C21-C21 4/29/10
C11 C01 C21 C24	0.5000	4	0.00	NA--USED C11-C11-C21-C21 4/29/10
C11 C01 C21 HG2	0.1950	3	0.00	NA, sugar--USED C11-C11-C21-HG2 4/29/10
O11 C01 C21 HG2	0.1950	3	180.00	NA, sugar--USED O11-C11-C21-HG2 4/29/10
O11 C01 C21 C21	0.5000	1	180.00	NA elevates energy at 0 (c3'endo), adm--USED O11-C11-C21-C21 4/29/10
O11 C01 C21 C21	0.7000	2	0.00	NA elevates energy at 0 (c3'endo), adm--USED O11-C11-C21-C21 4/29/10
O11 C01 C21 C21	0.4000	3	0.00	NA abasic nucleoside--USED O11-C11-C21-C21 4/29/10
O11 C01 C21 C21	0.4000	5	0.00	NA abasic nucleoside--USED O11-C11-C21-C21 4/29/10
C14 C01 C21 C21	0.2000	3	0.00	PROT alkane update, adm jr., 3/2/92--USED C14-C11-C21-C31 4/29/10

Dihedral	K	n	δ	Source
C14 C01 C21 HG2	0.1950	3	0.00	NA, sugar--USED C14-C11-C21-HG2 4/29/10
C01 C01 O11 HP1	1.3300	1	0.00	PROT 2-propanol OH hf/torsional surface, adm jr., 3/2/93--USED C11-C11-O11-HP1 4/29/10
C01 C01 O11 HP1	0.1800	2	0.00	PROT 2-propanol OH hf/torsional surface, adm jr., 3/2/93--USED C11-C11-O11-HP1 4/29/10
C01 C01 O11 HP1	0.3200	3	0.00	PROT 2-propanol OH hf/torsional surface, adm jr., 3/2/93--USED C11-C11-O11-HP1 4/29/10
C14 C01 O11 HP1	0.5000	1	0.00	FLAVOP PIP3--USED C24-C11-O11-HP1 4/29/10
C14 C01 O11 HP1	0.7000	2	0.00	FLAVOP PIP3--USED C24-C11-O11-HP1 4/29/10
C21 C01 O11 HP1	0.3000	1	0.00	CARBOCY carbocyclic sugars--USED C21-C11-O11-HP1 4/29/10
C21 C01 O11 HP1	0.3000	3	0.00	CHOLEST cholesterol--USED C21-C11-O11-HP1 4/29/10
NP1 C14 C21 HG2	0.2000	3	0.00	PROT alkane update, adm jr., 3/2/92--USED NP3-C14-C21-HG2 4/29/10
C01 C14 NP1 HP2	0.1000	3	0.00	PROT 0.715->0.10 METHYLAMMONIUM (KK)--USED C11-C14-NP3-HP2 4/29/10
C21 C14 NP1 HP2	0.1000	3	0.00	3MRB, Gamma-3 methyl piperidine, alpha-benzyl GA CDCA amide, chayan--USED C21-C14-NP2-HP2 4/29/10
HG1 C14 NP1 C24	0.1000	3	0.00	3MRB, Gamma-3 methyl piperidine, alpha-benzyl GA CDCA amide, chayan--USED HG1-C14-NP2-C24 4/29/10
HG1 C14 NP1 HP2	0.1000	3	0.00	3MRB, Gamma-3 methyl piperidine, alpha-benzyl GA CDCA amide, chayan--USED HG1-C14-NP2-HP2 4/29/10
C01 C14 NP1 C24	0.1000	3	0.00	G3P(R/S), Gamma-3-Piperidine Glu Acid CDCA Amide, chayan--USED C11-C24-NP2-C24 4/29/10
HG1 C14 C21 HG2	0.1950	3	0.00	NA, sugar

Dihedral	K	n	δ	Source
C21 C14 NP1 C24	0.1000	3	0.00	3MRB, Gamma-3 methyl piperidine, alpha-benzyl GA CDCA amide, chayan--USED C21-C14-NP1-C24 4/29/10
CO5 C21 C21 HG2	0.1950	3	0.00	deleteme DELETEME (we want to use wildcarting)--USED CO2-C21-C21-HG2 4/29/10
CO5 C21 C21 C01	0.2100	1	180.00	LIPID methylbutyrate--USED CO2-C21-C21-C31 4/29/10
CO5 C21 C21 C01	0.3900	2	0.00	LIPID methylbutyrate--USED CO2-C21-C21-C31 4/29/10
CO5 C21 C21 C01	0.3500	3	180.00	LIPID methylbutyrate--USED CO2-C21-C21-C31 4/29/10
CO5 C21 C21 C01	0.1100	4	0.00	LIPID methylbutyrate--USED CO2-C21-C21-C31 4/29/10
CO5 C21 C21 C01	0.0900	6	180.00	LIPID methylbutyrate--USED CO2-C21-C21-C31 4/29/10
HG2 C21 C21 HG2	0.2200	3	0.00	LIPID alkanes
C01 C21 C21 HG2	0.1950	3	0.00	PROT alkane update, adm jr., 3/2/92
HG2 C21 C24 HG2	0.1950	3	0.00	FLAVOP PIP1,2,3
HG2 C21 C24 NP1	0.1950	3	0.00	FLAVOP PIP1,2,3
C21 C24 NP1 HP2	0.1000	3	0.00	FLAVOP PIP1,2,3
HG2 C24 NP1 C14	0.1000	3	0.00	3MRB, Gamma-3 methyl piperidine, alpha-benzyl GA CDCA amide, chayan--USED HG2-C24-NP2-C14 4/30/10
C21 C24 NP1 C14	0.1000	3	0.00	3MRB, Gamma-3 methyl piperidine, alpha-benzyl GA CDCA amide, chayan--USED C21-C24-NP2-C14 4/30/10
HG2 C24 NP1 C24	0.1000	3	0.00	FLAVOP PIP1,2,3
C61 C61 C61 CC0	3.0000	2	180.00	INDO/TRP
C01 C14 C21 HG2	0.1950	1	0.00	3MRB,Gamma-3 methyl piperidine, alpha-benzyl GA CDCA amide, chayan--USED C21-C14-C21-HG2 4/30/10
HG4 CD1 CD2 HG5	5.2000	2	180.00	LIPID propene, yin,adm jr., 12/95
OD3 CO5 C3C1 HG1	0.0000	1	0.00	PROT Alanine Dipeptide ab initio calc's (LK) unmodified--USED OD1-CO5-C11-HG1 5/4/10

Dihedral	K	n	δ	Source
C3C1 CO5 C21 HG2	0.1000	3	0.00	ketone, RIMP2/cc-pVTZ//MP2/6-31G(d), adm 11/08--USED C31-CO5-C31-HG3 5/4/10
C3C1 CO5 C21 C21	0.1000	3	0.00	ketone, RIMP2/cc-pVTZ//MP2/6-31G(d), adm 11/08--USED C31-CO5-C31-HG3 5/4/10
OD3 CO5 C3C1 C3C1	0.0000	1	0.00	PROT Alanine Dipeptide ab initio calc's (LK) unmodified--USED OD3-CO5-C11-HG1 5/4/10
OD3 CO5 C3C1 C3C1	0.0000	1	0.00	PROT Alanine Dipeptide ab initio calc's (LK) unmodified--USED OD3-CO5-C11-HG1 5/4/10
C61 C61 CC0 O351	0.0000	2	180.00	ZFUR, benzofuran, kevo--USED C61-C61-CC0-O351 5/5/10
C61 C61 C3C1 C01	0.2300	2	180.00	NAMODEL difluorotoluene--USED C61-C61-C11-C11 5/5/10
C61 C61 C3C1 C3C1	0.2300	2	180.00	NAMODEL difluorotoluene--USED C61-C61-C11-C11 5/5/10
C61 C61 C3C1 C21	0.2300	2	180.00	NAMODEL difluorotoluene--USED C61-C61-C11-C21 5/5/10
C61 C61 C21 C14	0.2300	2	180.00	PROT ethylbenzene ethyl rotation, adm jr. 3/7/92
C61 C61 C21 HG2	0.0000	2	0.00	3ALP, nicotinaldehyde (PYRIDINE pyr-CH2OH)
C61 C61 C61 C61	3.1000	2	180.00	PROT JES 8/25/89
C61 C61 C61 C21	3.1000	2	180.00	PROT JES 8/25/89 toluene and ethylbenzene
C61 C61 C61 C3C1	3.1000	2	180.00	NAMODEL difluorotoluene--USED C61-C61-C61-C11 5/5/10
C21 C61 C61 H61	2.4000	2	180.00	PROT JES 8/25/89 toluene and ethylbenzene Kenno: 4.2 -> 2.4
C21 C61 C61 C3C1	2.4000	2	180.00	OXYL, o-xylene, kevo for gsk/ibm--USED C31-C61-C61-C31 5/5/10
C61 C61 CC0 C61	3.0000	2	180.00	INDO/TRP--USED C61-C61-CC0-CC0 5/5/10
C61 CC0 C61 O11	3.1000	2	180.00	PYRIDINE phenol--USED C61-C61-C61-O11 5/5/10
C61 CC0 C61 C3C1	3.1000	2	180.00	NAMODEL difluorotoluene

Dihedral	K	n	δ	Source
CC0 C61 C3C1 C01	0.2300	2	180.00	NAMODEL difluorotoluene--USED C61-C61-C11-C11 5/5/10
CC0 C61 C3C1 C11	0.2300	2	180.00	NAMODEL difluorotoluene--USED C61-C61-C11-C11 5/5/10
C3C1 C01 C21 C21	0.1580	3	0.00	CA, Cholic Acid, chayan, 03/06--USED C11-C01-C21-C21 5/5/10
C3C1 C01 C21 HG2	0.1580	3	0.00	CA, Cholic Acid, chayan, 03/06--USED C11-C01-C21-HG2 5/5/10
C14 C01 C3C1 C21	0.0500	3	0.00	CA, Cholic Acid, chayan, 03/06--USED C11-C01-C11-C21 5/5/10
HG1 C14 C21 C61	0.0400	3	0.00	PROT 2.7 kcal/mole CH3 rot in ethylbenzene, adm jr, 3/7/92
NP1 C14 C21 C61	0.2000	3	0.00	PROT alkane update, adm jr., 3/2/92--USED NP3-C14-C21-C61 5/5/10
C61 C3C1 C21 HG2	0.0000	3	0.00	NAMODEL difluorotoluene--USED C61-C11-C21-HG2 5/5/10
C01 C3C1 C21 HG2	0.2000	3	0.00	CA, Cholic Acid, chayan, 03/06--USED C01-C11-C21-HG2 5/5/10
C01 C3C1 C21 C24	0.2000	3	0.00	DCA, Deoxycholic Acid, chayan, 03/06--USED C01-C11-C21-C21 5/5/10
C01 C3C1 C3C1 HG1	0.1500	3	0.00	CARBOCY carbocyclic sugars--USED C11-C3C1-C3C1-HG1 5/5/10
C21 C3C1 C3C1 HG1	0.1500	3	0.00	CARBOCY carbocyclic sugars
C61 C3C1 C3C1 HG1	0.0400	3	0.00	NAMODEL difluorotoluene--USED C61-C11-C11-HG1 5/5/10
O11 C01 C3C1 C21	0.4500	2	0.00	CARBOCY carbocyclic sugars--USED O11-C11-C3C1-C21 5/5/10
C21 C01 C3C1 C21	2.2000	2	180.00	CARBOCY carbocyclic sugars--USED C21-C11-C3C1-C21 5/5/10
C21 C01 C3C1 C21	4.0000	3	0.00	CARBOCY carbocyclic sugars--USED C21-C11-C3C1-C21 5/5/10
C21 C01 C3C1 C21	0.5500	6	180.00	CARBOCY carbocyclic sugars--USED C21-C11-C3C1-C21 5/5/10
C21 C01 C3C1 C3C1	0.1500	3	0.00	CARBOCY carbocyclic sugars--USED C21-C11-C3C1-C3C1 5/5/10
O11 C01 C3C1 C3C1	0.4500	2	0.00	CARBOCY carbocyclic sugars

Dihedral	K	n	δ	Source
C14 C01 C3C1 C3C1	0.1500	3	0.00	CARBOCY carbocyclic sugars--USED C11-C11-C3C1-C3C1 5/5/10H
HG2 C21 C3C1 C3C1	0.1500	3	0.00	CARBOCY carbocyclic sugars
C24 C21 C3C1 C3C1	0.1500	3	0.00	CARBOCY carbocyclic sugars--USED C21-C21-C3C1-C3C1 5/5/10
CC0 C61 C61 C21	3.1000	2	180.00	PROT JES 8/25/89 toluene and ethylbenzene--USED C61-C61-C61-C21 5/5/10
C21 CO5 C3C1 O351	0.7500	1	0.00	TAKEN FROM C21 CO5 C21 C21 EAP 3/9/12
C21 CO5 C3C1 O351	0.1800	2	180.00	TAKEN FROM C21 CO5 C21 C21 EAP 3/9/12
C21 CO5 C3C1 O351	0.0650	3	0.00	TAKEN FROM C21 CO5 C21 C21 EAP 3/9/12
C21 CO5 C3C1 O351	0.0300	6	0.00	TAKEN FROM C21 CO5 C21 C21 EAP 3/9/12
C21 CO5 C3C1 C3C1	0.7500	1	0.00	TAKEN FROM C21 CO5 C21 C21 EAP 3/9/12
C21 CO5 C3C1 C3C1	0.1800	2	0.00	TAKEN FROM C21 CO5 C21 C21 EAP 3/9/12
C21 CO5 C3C1 C3C1	0.0650	3	0.00	TAKEN FROM C21 CO5 C21 C21 EAP 3/9/12
C21 CO5 C3C1 C3C1	0.0300	6	0.00	TAKEN FROM C21 CO5 C21 C21 EAP 3/9/12
C21 CO5 C3C1 HG1	0.1000	3	0.00	TAKEN FROM C21 CO5 C21 HG2 EAP 3/9/12
C3C1 C61 CC0 O351	6.0000	2	180.00	TAKEN FROM C352 CC0 CC0 N351 EAP 3/9/12
CC0 C61 O351 C3C1	0.3000	2	180.00	TAKEN FROM CC0 CC0 O351 C352 EAP 3/9/12
C14 C01 C3C1 C61	0.5000	4	180.00	TAKEN FROM C21 C11 C3C1 C352 (CC0) EAP 3/9/12
O11 C01 C3C1 C61	0.1580	3	0.00	TAKEN FROM O11 C11 C3C1 C3C1(CC0) EAP 3/9/12
C21 C01 C3C1 C61	0.5000	4	180.00	TAKEN FROM C21 C11 C3C1 C352(CC0) EAP 3/9/12
C3C1 C01 C14 NP1	0.2000	3	0.00	TAKEN FROM C21 C11 C14 NP3 EAP 3/9/12

Dihedral	K	n	δ	Source
C3C1 C01 C14 C21	0.1500	3	0.00	TAKEN FROM C21 C11 C11 C3C1 EAP 3/9/12
C3C1 C01 C14 HG1	0.1500	3	0.00	TAKEN FROM C3C1 C11 C11 HG1 EAP 3/9/12
C3C1 C01 O11 HP1	1.5000	1	0.00	TAKEN FROM C3C1 C11 O11 HP1 EAP 3/9/12
C3C1 C01 O11 HP1	0.3000	2	180.00	TAKEN FROM C3C1 C11 O11 HP1 EAP 3/9/12
C3C1 C01 O11 HP1	0.5000	3	0.00	TAKEN FROM C3C1 C11 O11 HP1 EAP 3/9/12
C01 C14 C21 C61	0.0400	3	0.00	TAKEN FROM C31 C11 C21 C61 EAP 3/9/12
C24 C21 C3C1 C61	0.2000	3	0.00	TAKEN FROM C21 C21 C3C1 C352(CC0) EAP 3/9/12
C3C1 C21 C24 NP1	1.0000	3	0.00	TAKEN FROM C21 C21 C24 NP1 EAP 3/9/12
C3C1 C21 C24 HG2	0.1950	3	0.00	TAKEN FROM C3C1 C21 C21 HG2 EAP 3/9/12
C61 C3C1 C3C1 O351	1.2000	3	0.00	TAKEN FROM C352(CC0) C3C1 C3C1 O351 EAP 3/9/12
C61 C3C1 C3C1 CO5	0.1500	3	0.00	TAKEN FROM C352(CC0) C3C1 C3C1 N61 EAP 3/9/12
C3C1 C3C1 O351 CC0	0.0000	3	0.00	TAKEN FROM C3C1 C3C1 O351 C352 EAP 3/9/12
C01 C3C1 C3C1 O351	1.2000	3	0.00	TAKEN FROM C352 C3C1 C3C1 O351 EAP 3/9/12
CC0 O351 C3C1 HG1	0.3000	3	0.00	TAKEN FROM CC0 O351 C352 HG2 EAP 3/9/12
O11 C61 CC0 O351	2.5800	2	180.00	TAKEN FROM N11 C61 C61 O60 4 EAP 3/9/12
O351 C3C1 C3C1 C21	1.2000	3	0.00	TAKEN FROM C352 C3C1 C3C1 O351 EAP 3/9/12
C61 CC0 O351 C3C1	0.3000	2	0.00	TAKEN FROM C61 CC0 O351 C352 EAP 3/9/12
CC0 C61 C3C1 C3C1	1.0300	3	180.00	TAKEN FROM CC0 CC0 C352 C352 EAP 3/9/12
CC0 C61 C3C1 C21	1.0300	3	180.00	TAKEN FROM CC0 CC0 C352 C351 EAP 3/9/12

Dihedral	K	n	δ	Source
O351 C3C1 CO5 OD3	0.0000	2	0.00	TAKEN FROM OD3 CO5 C11 C11 EAP 3/13/12
CO5 C3C1 C3C1 C01	4.0000	3	0.00	TAKEN FROM C11 C3C1 C3C1 C21 EAP 3/13/12
CO5 C3C1 C3C1 C21	0.1500	3	0.00	TAKEN FROM C21 C3C1 C3C1 C21 EAP 3/13/12
CC0 O351 C3C1 CO5	0.7300	3	0.00	TAKEN FROM C352 C352 O351 C51 EAP 3/13/12
C14 NP1 C24 CD1	0.4700	1	0.00	TAKEN FROM CD1 C24 NP1 C24 PIPA EAP 3/13/12
CD1 C24 NP1 C24	0.4700	1	0.00	CNCC_1_100000_2nd_round PIPA EBP 5/18/10
CD1 C24 NP1 HP2	0.7000	3	0.00	CNCC_2_003000_1st_round PIPA EBP 5/13/10
CD2 CD1 C24 NP1	0.8400	2	0.00	NCCC_1_023000_1st_ROUND PIPA EBP 10/5/10
CD2 CD1 C24 NP1	1.3500	3	180.00	NCCC_1_023000_1st_ROUND PIPA EBP 10/5/10
HG4 CD1 C24 NP1	0.4100	4	180.00	NCCC_2_000450_1st_round PIPA EBP 10/13/10
HG4 CD1 C24 NP1	0.1100	5	0.00	NCCC_2_000450_1st_round PIPA EBP 10/13/10
CD2 CD1 C24 HG2	0.0200	5	180.00	NCCC_3_000050_2nd_round PIPA EBP 10/18/10
HG4 CD1 C24 HG2	1.2800	1	0.00	NCCC_4_100400_1st_round PIPA EBP 10/15/10
HG4 CD1 C24 HG2	0.2300	4	180.00	NCCC_4_100400_1st_round PIPA EBP 10/15/10
C24 CD1 CD2 HG5	5.2000	2	180.00	TAKEN FROM C21-CD1-CD2-HG5 3/9/12